Aus dem
Institut für Immunologie
Institut der Ludwig-Maximilians-Universität München
Vorstand: Prof. Dr. Thomas Brocker

Targeting antigens to phosphatidylserine triggers rapid T- and B-cell responses

Dissertation
zum Erwerb des Doktorgrades der Naturwissenschaften
an der Medizinischen Fakultät der
Ludwig-Maximilians-Universität München

vorgelegt von
Wenbo Hu

aus
Qinghai, China

Jahr
2024

Mit Genehmigung der Medizinischen Fakultat
der Ludwig-Maximilians-Universitat Munchen

Betreuer:	Prof. Dr. Thomas Brocker
Zweitgutachterin:	PD Dr. Anneli Peters
Dekan:	Prof. Dr. med. Thomas Gudermann
Tag der mundlichen Prufung:	15/04/2025

LMU LUDWIG-MAXIMILIANS-UNIVERSITÄT MÜNCHEN

Dekanat Medizinische Fakultät
Promotionsbüro

Confirmation of congruency between printed and electronic version of the doctoral thesis

Hu, Wenbo

name, first name

I hereby declare that the electronic version of the submitted thesis, entitled:

Targeting antigens to phosphatidylserine triggers rapid T- and B-cell responses

is congruent with the printed version both in content and format.

Shanghai. China 18/04/2025

Place, Date

Wenbo Hu

Signature doctoral candidate

Affidavit

Hu, Wenbo

Surname, first name

I hereby declare, that the submitted thesis entitled

Targeting antigens to phosphatidylserine triggers rapid T- and B-cell responses

is my own work. I have only used the sources indicated and have not made unauthorised use of services of a third party. Where the work of others has been quoted or reproduced, the source is always given.

I further declare that the dissertation presented here has not been submitted in the same or similar form to any other institution for the purpose of obtaining an academic degree.

Shanghai. China 18/04/2025

Place, Date

Wenbo Hu

Signature doctoral candidate

List of publications

1. Kaiser, R., Escaig, R., Kranich, J., Hoffknecht, M. L., Anjum, A., Polewka, V., Mader, M., Hu, W., Belz, L., Gold, C., Titova, A., Lorenz, M., Pekayvaz, K., Kääb, S., Gaertner, F., Stark, K., Brocker, T., Massberg, S., & Nicolai, L. (2022). Procoagulant platelet sentinels prevent inflammatory bleeding through GPIIBIIIA and GPVI. *Blood*, *140*(2), 121–139.

2. Hu, W., Flaskamp, L., Kranich, J., Brocker, T. Targeting Antigen to extracellular vesicles accelerates and broadens humoral responses. (Manuscript in preparation)

Table of Contents

List of tables I
List of figures III
Abbreviations V
1. Abstract 1
2. Zusammenfassung 2
3. Introduction 3
3.1 The immune responses. 3
3.1.1 Innate immune responses. 3
3.1.2 Adaptive immune responses. 4
3.1.2.1 Cellular immunity. 4
3.1.2.2 Humoral immunity 6
3.1.3 Vaccine induced immune response. 11
3.2 Extracellular vesicles (EVs). 14
3.2.1 Biogenesis of EVs. 14
3.2.2 EVs in immune system. 15
3.2.3 EVs as drug delivery platform. 20
3.3 Milk fat globule epidermal growth factor 8 (Mfge8) 21
3.3.1 Mfge8 in apoptotic cell clearance. 22
3.3.2 Mfge8 as a tool to study EVs. 24
4. Aim of the thesis 25
5. Materials and methods 26
5.1 Buffers, reagents and chemicals 26
5.1.1 Self-prepared buffers and media 26
5.1.2 Purchased reagents and kits 29
5.2 Chemicals 30
5.3 Devices 31
5.4 Staining antibodies 32
5.5 Mouse strains 35
5.6 Protocols and assays 37
5.6.1 Serum collection 37
5.6.2 Indirect enzyme-linked immunosorbent assay (ELISA) 37
5.6.3 Protein expression and purification 38
5.6.3.1 Cultivation of bacterial expression system with kanamycin resistance. 38
5.6.3.2 Cultivation of bacterial expression system with ampicillin resistance. 38
5.6.3.3 Cultivation of bacterial expression system with kanamycin + ampicillin + tetracycline resistance. 39
5.6.3.4 Purification of proteins with polyhistidine tag (His-tag). 39
5.6.3.5 Purification of proteins with glutathione-s-transferase tag (GST-tag). 41
5.6.3.6 Mfge8-EGFP and C1C2-EGFP purification. 41
5.6.4 Biotinylation by sortase-mediated transpeptidation reaction. 42
5.6.5 SA-OVA conjugation 43
5.6.6 mC1 tetramer formation 43
5.6.7 Fluorochrome labelling 44

5.6.8 Cell isolation and prepare of single cell suspension. 44
5.6.8.1 Isolation of splenocytes. 44
5.6.8.2 Bone marrow cells isolation. 45
5.6.9 Staining of cells for flow cytometry. 45
5.6.10 T cell in vitro re-stimulation assay. 46
5.6.11 CD8 T cell memory recall assay. 46
5.6.12 CTL in vivo killing assay. 47
5.6.13 Western blot (SDS-PAGE) 47
5.6.14 Cell sorting 48
5.6.14.1 Magnetic cell sorting 48
5.6.14.2 Fluorescence-activated cell sorting (FACS). 49
5.6.15 Full length BCR and targeted mRNA library preparation. 49
5.6.16 EV isolation 59
5.6.17 Immunofluorescence microscopy 60
5.7 Statistics and analysis software 61
6. Results 63
6.1 Targeting EGFP to EVs promotes humoral immune response. 63
6.1.1 Mfge8-EGFP accumulates in the marginal zone. 63
6.1.2 PS-targeting antigen strongly accumulates on FDCs. 67
6.1.3 Mfge8-EGFP promotes anti-EGFP antibody responses. 68
6.2 PS-targeting antigen is transported to FDCs independently of C3. 71
6.3 CD169^{+} microvesicles can be found on FDCs. 74
6.3.1 Mfge8-EGFP colocalized with CD169^{+} microvesicles in the FDC area 74
6.3.2 Approx. 15% of Mfge8-EGFP are transported by CD169+ microvesicles. 75
6.4 PS-targeting antigen enhances germinal center reactions. 76
6.5 Immunization with increasing EGFP doses promotes antibody production but not GC reactions 78
6.6 PS-targeting antigens do not prolong GC reactions. 79
6.7 Immunization with PS-targeting antigen promotes GC B cell class switching. 80
6.8 Immunization with PS-targeting antigen promotes GC B cell somatic hypermutation. 82
6.9 Immunization with PS-targeting antigen increases the selection strength. 83
6.10 Immunization with PS-targeting antigen induces a more diverse GC B cell repertoire. 84
6.11 Immunization with EGFP and Mfge8-EGFP show similar long-term antibody titers. 86
6.12 Secondary immunization with PS-targeting antigen induces faster antibody memory recall responses. 88
6.13 PS-targeting antigen enhances T cell responses. 89
6.13.1 PS-targeting antigen induces more T follicular helper cells. 89
6.13.2 PS-targeted antigen induces more effector CD4 and CD8 T cells. 91
6.14 RGD motif is not required for the immune-boosting effect of Mfge8-EGFP. 93
6.15 Antigens conjugated to multimerized mC1 domains promote B cell responses. 95
6.16 Immunization with OVA-SA-mC1 tetramer generates robust B cell memory. 98
6.17 PS-targeting antigens elicit strong CTL responses. 99
6.17.1 OVA-SA-mC1 induces more activated CD8 T cells. 99
6.17.2 OVA-SA-mC1 immunization induces more efficient CTL killing of target cells. 100
6.18 Immunization with OVA-SA-mC1 tetramer generates robust CD8 T cell memory. 102

6.19 OVA-SA-mC1 tetramer immunization induces more Tfh cells.....103

7. Discussion..... 105

7.1 PS-targeting antigens are transferred to FDCs in unimmunized naïve mice.....105

7.1.1 PS-targeting antigens are transferred to FDCs independent of C3. 105

7.1.2 CD169+ microvesicles transport PS-targeting antigens to FDCs. 106

7.2 PS-targeting antigens induce fast serum immune responses. 109

7.2.1 PS-targeting antigens induce rapid IgG production. 109

7.2.2 PS-targeting antigens promote GC reactions. 110

7.2.3 PS-targeting antigens induce a more diverse GC B cell repertoire. 113

7.2.4 Immunization with PS-targeting antigens improves the quality of antibodies. 114

7.3 PS-targeting antigens induce robust T cell responses.....116

8. Conclusions 119

9. References 120

10. Acknowledgements 137

List of tables

Table Nr.	Name	Page
Table 1	Self-prepared buffers and medium	26
Table 2	Purchased reagents and kits	29
Table 3	Chemicals	30
Table 4	Devices and suppliers	31
Table 5	Antibodies used for flow cytometry	32
Table 6	Antibodies used for histology	34
Table 7	Antibodies used for ELISA	35
Table 8	Gitocher buffer mix	35
Table 9	Primers for genotyping	36
Table 10	Genotyping reaction mix	36
Table 11	PCR program for genotyping	36
Table 12	Sortase reaction mix	42
Table 13	CASY TT cell counter settings	45
Table 14	Separating gel recipe	47
Table 15	Stacking gel recipe	47
Table 16	cDNA / template switching mix	50
Table 17	TSO mix	50
Table 18	BCR extension mix	51
Table 19	Exonuclease I mix	51
Table 20	Sample Tag PCR1 reaction mix	51
Table 21	PCR1 program for Sample Tag	52
Table 22	BCR panel PCR1 reaction mix	52
Table 23	PCR1 program for BCR panel	52
Table 24	Targeted mRNA panel PCR1 reaction mix	53
Table 25	PCR1 program for Targeted mRNA panel	53
Table 26	BCR panel PCR2 reaction mix	54
Table 27	Targeted mRNA panel PCR2 reaction mix	54
Table 28	Sample Tag PCR2 reaction mix	54
Table 29	PCR2 program for BCR panel	55
Table 30	PCR2 program for Targeted mRNA panel	55
Table 31	PCR2 program for Sample Tag	56
Table 32	Random primer mix	56
Table 33	BCR random priming program	56
Table 34	Primer extension enzyme mix	57
Table 35	Random priming extension program	57
Table 36	Index PCR reaction mix for BCR RPE product	57

Table 37	Index PCR reaction mix for Targeted mRNA and Sample Tag PCR2 products	58
Table 38	Index PCR program for BCR and Targeted mRNA libraries	58
Table 39	Index PCR program for Sample Tag libraries	58
Table 40	Mouse B cell PCR1 primers	59
Table 41	Mouse B cell PCR2 primers	59
Table 42	R packages	61

List of figures

Figure Nr.	Name	Page
Figure 1	Initiation of GC reaction.	8
Figure 2	Transportation of immune complexes to FDCs.	9
Figure 3	Biogenesis of EVs.	15
Figure 4	Presentation of peptide-MHC complex to T cells.	18
Figure 5	Schematic diagram of Mfge8 structure.	22
Figure 6	Plasma membrane in live cells and apoptotic cells.	22
Figure 7	Mfge8-EGFP accumulates in the marginal zone.	64
Figure 8	Mfge8-EGFP binding on different cell types.	65
Figure 9	Mfge8-EGFP co-localizes with EVs.	66
Figure 10	Mfge8-EGFP accumulates on FDCs.	68
Figure 11	Mfge8-EGFP immunization promotes anti-EGFP antibody responses.	69
Figure 12	Subcutaneous immunization.	71
Figure 13	EGFP is transported to FDCs in pre-immunized mice.	71
Figure 14	C3 KO negatively affects GC formation.	72
Figure 15	Mfge8-EGFP deposition on FDCs is independent of C3.	73
Figure 16	Mfge8-EGFP colocalizes with CD169+ microvesicles in the FDCs area.	75
Figure 17	Quantification of CD169 co-localization on Mfge8-EGFP+ cells.	76
Figure 18	Mice immunized with Mfge8-EGFP generate larger GCs.	77
Figure 19	Mfge8-EGFP immunization promotes GC reactions.	78
Figure 20	Mfge8-EGFP immunization out-competes 8x molar excess of EGFP.	79
Figure 21	Mfge8-EGFP immunization does not prolong the GC reaction.	80
Figure 22	Mfge8-EGFP immunization promotes class switch recombination.	82
Figure 23	Mfge8-EGFP immunization promotes GC B cell somatic hypermutation.	83
Figure 24	Mfge8-EGFP immunization increases the selection strength on day 14.	84
Figure 25	Mfge8-EGFP immunization induces more diverse GC B cell repertoire.	85
Figure 26	Immunization with EGFP and Mfge8-EGFP shows similar long-term antibody titers.	87
Figure 27	Secondary immunization with Mfge8-EGFP induces faster antibody memory recall responses.	88
Figure 28	Mfge8-EGFP induces more T follicular helper cells.	90
Figure 29	Mfge8-EGFP induces more effector CD4 T cells.	91
Figure 30	Mfge8-EGFP induces more effector CD8 T cells.	92
Figure 31	C1C2-EGFP is transported to FDCs.	93

Figure 32	RGD motif is not required for the immune-boosting effect of Mfge8-EGFP.	94
Figure 33	OVA-SA-mC1 tetramers are transported to FDCs.	96
Figure 34	OVA-SA-mC1 tetramer immunization promotes antibodies production.	97
Figure 35	OVA-SA-mC1 tetramer immunization promotes GC reactions.	98
Figure 36	OVA-SA-mC1 tetramer immunization generates robust B cell memory.	99
Figure 37	OVA-SA-mC1 induces more activated CD8 T cells.	100
Figure 38	OVA-SA-mC1 induces more efficient CTL killing.	101
Figure 39	OVA-SA-mC1 immunization generates robust CD8 T cell memory.	103
Figure 40	OVA-SA-mC1 tetramer immunization induces more Tfh cells.	104

Abbreviations

ACK	Ammonium-chloride-potassium
ADCC	Antibody-dependent cell-mediated cytotoxicity
AID	Activation-induced cytidine deaminase
APCs	Antigen presenting cells
APS	Ammonium persulfate
ARRDC1	Arrestin domain containing protein 1
ASCs	Antibody-secreting cells
BASELINe	Bayesian estimation of antigen-driven selection
BCR	B cell receptor
BDS	Bright detail similarity
BMDC	Bone marrow-derived dendritic cell
CAE	Convolutional autoencoder
CDR	Complementarity-determining region
CFSE	Carboxyfluorescein succinimidyl ester
CMP	Cardiomyocyte targeting peptide
CR	Complement receptor
CSR	Class-switch recombination
CTLs	Cytotoxic T lymphocytes
DAMPs	Damage-assocaited molecular patterns
DC	Dendritic cell
ddH_2O	Double distilled water
DSBs	Double-strand breaks
DTT	Dithiothreitol
DZ	Dark zone
ECL	Enhanced chemiluminescence
EDTA	Ethylenediaminetetraacetic acid
EF	Extrafollicular
EGF	Epidermal growth factor
EGFP	Enhanced green fluorescent protein
ELISA	Enzyme-linked immunosorbent assay
ESCRT	Endosomal sorting complex required for transport
EVs	Extracellular vesicles
FACS	Flow cytometry
FCS	Fetal bovine serum
FDCs	Follicular dendritic cell
FWR	Framework region
Gas6	Growth arrest specific 6
GC	Germinal center
GM-CSF	Granulocyte-macrophage colony-stimulating factor

HRP	Horseradish peroxidase
HSP	Heat shock protein
ICs	Immune complexes
IFN-γ	Interferon-γ
Ig	Immunoglobulin
IL	Interleukin
ILVs	Intra luminal vesicles
IPTG	Isopropyl β-D-1-thiogalactopyranoside
IV	Intravenous
LB	Lysogeny broth
LLPCs	Long-lived plasma cells
LNPs	Lipid nanoparticles
LPS	Lipopolysaccharides
LZ	Light zone
MACS	Magnetic-activated cell sorting
MBCs	Memory B cells
MBL	Mannose-binding lectin
Mfge8	Milk fat globule-EGF factor 8
MHC	Major histocompatibility complex
MPLA	Monophosphoryl lipid A
mRNA	Messenger RNA
MVEs	Multi-vesicular endosomes
MVs	Microvesicles
MW	Molecular weight
MZ	Marginal zone
NA	Neuraminidase
Neo	Neomycin
Ni-NTA	Nickel-nitrilotriacetic acid
OSB	Optimized stabilizing buffer
OVA	Ovalbumin
PAMPs	Pathogen-associated molecular patterns
PBs	Plasmablasts
PBS	Phosphate-buffered saline
PCR	Polymerase chain reaction
PCs	Plasma cells
PE	Phosphatidylethanolamine
PMA	Phorbol 12-myristate 13-acetate
PRRs	Pattern-recognition receptors
PS	Phosphatidylserine
RPE	Random priming extension
S1PR1	Sphingosine-1-phosphate receptor 1
SA	Streptavidin
SC	Subcutaneous

SCS	Subcapsular sinus
SDS	Sodium dodecyl sulfate
SDS-PAGE	Sodium dodecyl sulfate – polyacrylamide gel electrophoresis
SE	Standard error
SHM	Somatic hypermutation
SLE	Systemic lupus erythematosus
SRBC	Sheep red blood cells
SS	Similarity score
STED	Stimulated emission depletion
TBMs	Tingible body macrophages
TCR	T cell receptor
TD	T cell dependent
TEMED	Tetramethylethylenediamine
Tfh	T follicular helper
TGF-β	Transforming growth factor-β
Th	T helper
TI	T cell independent
TLRs	Toll-like receptors
TNF-α	Tumor necrosis factor-α
Tris	Trisaminomethane
TSO	Template switch oligo
UNG	Uracil DNA glycosylase
VLPs	Virus-like particles

1. Abstract

Phosphatidylserine (PS) is a phospholipid that is abundant in cell membranes. In live cells, PS is asymmetrically restrained to the inner leaflet of membrane. In dying cells, activated platelets and extracellular vesicles (EVs), PS is exposed on the membrane surface and it can be bound by PS-binding proteins, such as Milk fat globule epidermal growth factor 8 (Mfge8). In previous studies, we have established use of fluorescent Mfge8 to label and characterize EVs *in vivo*. Here in this study, we explored the possibility of using Mfge8 as an antigen carrier to load antigens onto PS+ EVs. PS-targeting antigens were created by conjugating antigens to Mfge8 or the tetramerized PS-binding C1 domains of Mfge8. We found that compared with non-targeting conventional antigens, PS-targeting antigens accumulated in the marginal zone of lymphoid follicles soon after injection. Hours later, they were transferred onto the follicular dendritic cell (FDC) network without the need of previous primary immunization. We measured the antigen-specific immune responses elicited by these PS-targeting antigens and found that germinal center (GC) B cell proliferation and somatic hypermutation were significantly enhanced. As a result, serum antigen specific IgG titers were significantly higher than mice immunized with conventional antigens, and antibody isotype switching was greatly accelerated. PS-targeting antigens also induced increased number of T follicular helper cells (Tfh cells) to support GC reaction, as well as more activated CD8 T cells that eliminated target cells more efficiently. Therefore, targeting antigens to PS promoted both B- and T- cell responses, which make it a promising novel vaccination platform.

2. Zusammenfassung

Phosphatidylserin (PS) ist ein Phospholipid, das in der Zellmembran vorhanden ist. In lebenden Zellen ist PS asymmetrisch verteilt und kommt ausschließlich auf der Membraninnenseite vor. In sterbenden Zellen, aktivierten Blutplättchen und extrazellulären Vesikeln (EVs) flippt PS auf die Membranaussenseite und kann somit durch PS-bindende Proteine wie Milk fat globule-EGF-Faktor 8 (Mfge8) nachgewiesen werden. In früheren Studien haben wir fluoreszentes Mfge8 für die *in vivo* Detektion und Charakterisierung von EV verwendet. Hier in dieser Studie haben wir die Möglichkeit untersucht, Mfge8 als Antigenträger zu verwenden, um Antigene auf PS+-EVs zu laden. Antigene mit PS-Bindedomäne wurden durch Konjugation an Mfge8 oder die tetramerisierten PS-bindenden C1-Domänen von Mfge8 erzeugt. Wir fanden, dass PS-bindende Antigene im Vergleich zu herkömmlichen Antigenen kurz nach der Injektion in der Marginalzone der Lymphfollikel akkumulieren. Stunden später wurden sie auf follikulären dendritischen Zellen (FDCs) abgelagert, ohne dass eine vorherige Primärimmunisierung erforderlich war. Wir haben die antigenspezifischen Immunantworten gemessen, die durch diese PS-bindenden Antigene hervorgerufen werden, und fanden heraus, dass die Proliferation von B-Zellen im Keimzentrum (GC) und die somatische Hypermutation signifikant erhöht waren. Infolgedessen waren die Antigen-spezifischen IgG-Titer im Serum im ersten Monat nach der Immunisierung signifikant höher als bei Mäusen, die mit herkömmlichen Antigenen immunisiert wurden. Auch der Antikörper-Isotypwechsel wurde stark beschleunigt. PS-bindende-Antigene induzierten außerdem eine erhöhte Anzahl von follikulären T-Helferzellen (Tfh), um die GC-Reaktion zu unterstützen und förderten die Aktivierung von CD8-T-Zellen, wodurch die Zielzellen effizienter eliminiert wurden. Daher förderten PS-bindende Antigene sowohl humorale als auch zelluläre Immunantworten, was diese Strategie zu einer vielversprechenden neuartigen Impfplattform macht.

3. Introduction

3.1 The immune responses.

The immune system consists of lymphoid organs, various cells and cytokines, forming a complex closely interactive network. The main role of the immune system is to recognise and eliminate pathogenic invaders, such as bacteria, viruses and fungi as well as to surveil malignancy. The incident of a disease is a result of dysregulation of host immune system and increased pathogenicity (virulence) of the pathogen (Pulendran and Ahmed, 2011). According to the specificity, mode of action and the speed of response onset, the immune responses are classified into two categories: innate and adaptive immune response.

3.1.1 Innate immune responses.

Innate immunity consists of physical barriers (such as skin, mucosal epithelia) and innate immune cells (including phagocytic cells, mast cells, NK cells, basophils and eosinophils) as well as other antimicrobial substances, cytokines and complement system (Abbas, 2005).

Innate immunity is highly conserved and exists in all the multicellular organisms and is crucial for survival. It provides the host with a rapid first line protection against pathogens. These protective mechanisms, either physically, chemically or biologically, exist before exposure to pathogens. The innate immune responses are induced by pattern-recognition receptors (PRRs), which recognize structures shared by microbes. Due to the lack of specificity, the effector mechanisms of innate immune responses sometimes damage normal tissues, however, the general sensing of pathogen-associated molecular patterns (PAMPs) enables innate immune cells to rapidly recognize and eliminate invading pathogens, and subsequently activate specific adaptive immune responses by providing second costimulatory signals and cytokines (Pulendran and Ahmed, 2011, Odenwald and Turner, 2017, Abbas, 2005).

3.1.2 Adaptive immune responses.

Development of adaptive immune responses usually takes several days after exposure to pathogens, and it requires previous activation of an innate immune response. In contrast to innate immune responses, adaptive immune responses recognize infected pathogens by antigen-specific receptors expressed on T and B cells. This is achieved by random rearrangement and splicing of multiple DNA segments (V, D, J and C segments) that code for the antigen-binding receptors during the early T and B cell development. It results in approximately 10^8 different T cell receptors (TCRs) and 10^{12} different B cell receptors (BCRs), which are adequate to cover the majority of pathogens in the accessible environment (Arstila et al., 1999, Briney et al., 2019). The antigen-specific recognition provides hosts with more precise and specific protection and causes little damage to normal tissues. In addition to the specificity, adaptive immunity can establish immunological memory, to provide more rapid and vigorous protection against the same pathogens that have been encountered previously (Janeway et al., 2001).

Adaptive immune responses are divided into two categories: The humoral immunity mediated by B cells and their secreted antibodies, function in eliminating extracellular pathogens and toxins. The cellular immunity performed by T cells, which plays a key role in defending against intracellular viruses and some bacteria, as well as malignant cells in cancer (Abbas, 2005, Sun et al., 2023). I will discuss the two immune responses separately.

3.1.2.1 Cellular immunity.

As soon as a T cell meets its specific antigen peptide-MHC complex presented on antigen presenting cells (APCs), and co-stimulatory factors such as CD80, CD86 (bind to CD28 and CTLA-4), and CD40 (binds to CD40L) are provided, this specific T cell is activated and starts to proliferate and differentiate into effector and memory cells. The effector T cells leave the peripheral lymphoid organs and migrate to the site of inflammation, where CD4 and CD8 effector T cells perform distinct functions: CD4 effector T cells are also called T helper (Th) cells, upon recognition of target antigen, they do not eliminate pathogens directly, they rather act as a conductor to orchestrate the immune responses. Their major function is to produce cytokines, and according to

the cytokines they produce, Th cells can be classified into Th1, Th2, Th17 and other subsets (Saravia et al., 2019, Parkin and Cohen, 2001).

Follicular T helper cells (Tfh cells) are a specialized subset of T helper cells, they express the chemotactic receptor CXCR5, which responds to CXCL13 and enables Tfh cells to reside in B cell follicles of lymph nodes and the spleen (Ansel et al., 1999, Gunn et al., 1998), to assist B cell activation and antibody production. Tfh cells provide CD40L signal and cytokines such as IL-4, IL-21, and IFN-γ that initiate both germinal center (GC) reaction and extrafollicular antibody response. Tfh cells' migration into the GCs is crucial in supporting GC B cell proliferation, class-switch recombination (CSR) and affinity maturation (Crotty, 2019, Vinuesa et al., 2016). The procedure of GC reaction and Tfh cells' functions are discussed in more detail in the "Humoral immunity" section.

CD8 T cells play important roles in eliminating intracellular pathogens and immune surveillance. After activation by cognate antigenic peptide-MHC I complexes and co-stimulators, naive CD8 T cells proliferate and differentiate into effector or memory cells. Effector CD8 T cells, also known as cytotoxic T lymphocytes (CTLs) are the major effector cells that directly kill target cells expressing foreign peptides on MHC I molecules. CTLs are characterized by their perforin and granzyme containing granules, and secretion of cytokines including IFN-γ and TNF-α. CTL-mediated cell killing is dependend on the physical contact with the target cells, immediately after recognition of specific peptide-MHC I complexes, CTLs form an immunologic synapses or highly dynamic kinapses with target cells (de la Roche et al., 2016, Halle et al., 2016), then rapidly trigger degranulation and release perforin and granzymes into the synapses, perforin creates pores on the target cells' membrane, enabling granzymes to enter the target cells. Caspases are activated by granzymes, which cause DNA fragmentation and induce apoptosis. In addition, TCR activation leads to the expression of Fas ligands (FasL) on the CTLs, FasL binds Fas on target cells and induce apoptosis directly (Halle et al., 2017, Sun et al., 2023). Other mechanism including ferroptosis and pyroptosis are identified in recent studies, by which CTLs suppress tumor growth (Koh et al., 2023, Tang et al., 2020b). Moreover, secreted cytokines IFN-γ and TNF-α activate phagocytes and repress virus replication, play complementary roles to the cytotoxic activity of CTLs (Sun et al., 2023).

3.1.2.2 Humoral immunity

Humoral immunity is mediated by antibodies and B cells. According to the character of antigen and whether T cell help is needed, humoral immunity is classified into T cell independent (TI) responses and T cell dependent (TD) responses.

The TI response is elicited by many non-protein antigens, including polysaccharides, glycolipids and nucleic acids. Most of these antigens are polyvalent, contain many identical repeating epitopes that cross link multiple BCRs, which leads to a strong BCR signal that directly activates B cells to rapidly produce IgM antibodies without T cell help (Parkin and Cohen, 2001). In addition, some TI antigens activate the alternative pathway of the complement system and bind C3d, or activate innate pattern-recognition receptors like TLRs, which provide a second activation signal for B cells. TI responses are mostly mediated by B1 cells and marginal zone (MZ) B cells, these B cells differ from the majority of B cells and have limited BCR diversity, the antibodies produced by them are mainly low affinity IgM, with few isotype switching and poor specificity. Although high affinity IgG antibodies are usually preferred in defense against infections, many TI antigens, such as polysaccharides, are common components of bacterial cell walls and viral capsids, rapid production of IgM in TI response still plays an important role in defense against infections and prevent penetration of commensal bacteria (He et al., 2004, Bonilla and Oettgen, 2010, Abbas, 2005, Fagarasan and Honjo, 2000).

Antibody responses against protein antigens require the assistance from helper T cells, this TD responses are mediated by the majority of conventional follicular B cells (B2 cells) in two steps. The first step is initiated by the encounter of B cells with their specific cognate antigen. Then the Ag-specific B cells internalize the BCR-antigen complex and are primed. The primed B cell present antigenic peptides-MHC II complex as well as costimulatory molecules, and then migrate to the border of the B cell zone and T cell zone, where they interact with Tfh cells. Tfh cells are firstly primed by dendritic cell (DC) presenting specific antigen. After the T-B interaction, Tfh cells are fully activated, while B cells in turn receive CD40L signals from Tfh cells and are activated as well (Okada et al., 2005, Qi et al., 2008). A fraction of the activated B cells stay in extrafollicular (EF) sites, they proliferate and differentiate into short-lived plasmablasts that secret the first wave of antibodies (Jacob and Kelsoe, 1992). The

antibodies produced in the extrafollicular response exhibit little class-switch recombination (CSR) and somatic hypermutation (SHM), therefore the affinity is relatively low, however, they provide precious early protection during an infection (Nutt et al., 2015).

Concurrently, other activated B cells (with relatively high affinity BCR) and Tfh cells re-enter the B cell follicle (Shih et al., 2002, De Silva and Klein, 2015), wherein they start the second step named germinal center (GC) reaction (Figure 1). GC precursor B cells undergo vigorous proliferation within the follicle and form the GCs. GC B cells gradually expand and displace the surrounding naïve B cells, which form a mantle zone around the GC. One distinct histological feature of GC is that it polarizes into two functional different zones named dark zone (DZ) and light zone (LZ). The DZ contains densely packed proliferating GC B cells within an interconnected FDC-like reticular cell network (Rodda et al., 2015), the LZ consists of sparse GC B cells, Tfh cells, FDCs and tingible body macrophages (TBMs). GC B cells in the DZ rapidly proliferate and SHM takes place. SHM is a process that activation-induced cytidine deaminase (AID) deaminates deoxycytosines to deoxyuracils, which are then removed by uracil DNA glycosylase (UNG), introducing U:G point mutations in the immunoglobulin V regions of both heavy and light chain. Additionally, DNA polymerases that participate in mismatch repair, such as Polη, is error-prone and can cause other mutations around the AID target sites. Taken together, the mutation frequency (0.001 mutation per base pair in every cell division) is around 10^6 times higher than the spontaneous somatic mutation frequency. As a result, it creates a large and diverse GC B cell repertoire that differ in the antigen binding capability (Di Noia and Neuberger, 2007, Odegard and Schatz, 2006, Peled et al., 2008).

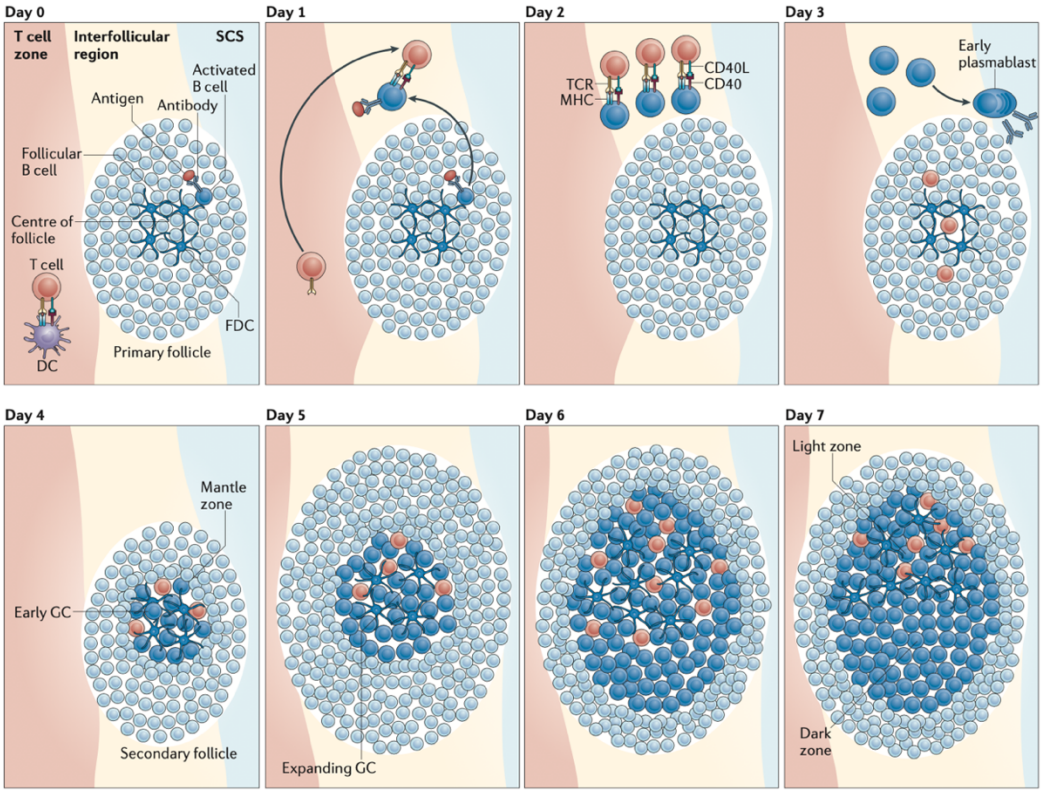

Figure 1 : Initiation of GC reaction.

B cells and T cells are primed by recognising cognate antigens or antigenic peptide- MHC complexes presented on DCs, respectively. Then on day 1-2, primed B and T cells interact at the T-B border (interfollicular region), where they receive stimulatory signals reciprocally and are fully activated. A group of activated T cells differentiate to Tfh cells and migrate into the B cell follicle. Some of the activated B cells differentiate into early plasmablasts and stay in the extrafollicular sites, while the rest of the activated B cells migrare to the centre of the follicle and start proliferation to form the GC since day 4. On day 7, DZ and LZ are formed and are histologically distinguishable. The DZ mainly consists of proliferating GC B cells, while LZ contains Tfh cells, FDCs , TBMs and GC B cells undergo positive selection. Figure is taken from (De Silva and Klein, 2015).

Newly generated GC B cells bearing mutated BCRs migrate to the LZ, where they compete for antigens deposited on FDCs (Figure 2) and present the processed antigenic peptide-MHC II complexes to Tfh cells. GC B cells expressing high affinity BCRs are more likely to capture antigens (or capture more antigens) from FDCs, and Tfh cells preferentially provide help (including IL-21, IL-4, CD40L and CXCL13) to GC B cells expressing high level of peptide-MHC II complexes. GC B cells that successfully receive Tfh cells' help survive (positive selection) and upregulate c-Myc expression, then they reenter the DZ and undergo more rounds of proliferation and SHM (cyclic reentry). On the contrary, GC B cells that don't receive survival signals from Tfh cells, die by apoptosis and are cleared by TBMs (Crotty, 2019, Vinuesa et

al., 2016). This iterative proliferation, hypermutation and preferential survival of high-affinity mutants leads to the selection of GC B cells that produce high affinity antibodies. This process is therefore termed “affinity maturation” (Victora and Nussenzweig, 2012, Victora and Nussenzweig, 2022).

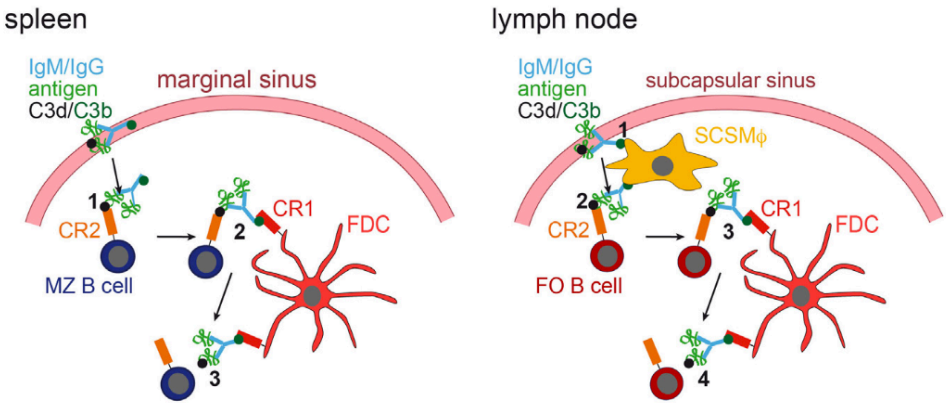

Figure 2 : Transportation of immune complexes to FDCs.

Immune complexes, which contain antigen, specific antibody and complement component 3 (C3) cleavage products (C3d and C3b), are captured by MZ B cells in the spleen or subcapsulary sinus (SCS) macrophages and follicular (FO) B cells in the lymph nodes via complement receptor 2 (CR2). Those Immune complexes are then transferred onto FDCs via CR1. Figure is taken from (Kranich and Krautler, 2016).

AID and UNG create double-strand breaks (DSBs) and cause DNA recombination between the switch (S) regions in the heavy chains (IgH) constant regions (C_H). As a result, the originally expressed Cμ (IgM), is replaced by either Cα(IgA), Cε(IgE) or Cγ (IgG), while the antigen-binding variable region is unchanged. This process is named class-switch recombination (CSR), and it contributes to the generation of antibodies with distinct tissue distribution and protection efficacy against different pathogen types. Tfh cells play critical roles in regulating CSR, especially CD40 and CD40L engagement is required in inducing expression of AID. Cytokines from Tfh cells determine the S regions that will undergo recombination, for example: strong CD40 signal induce switching to IgG1, however, the existence of IL-4 skews the switching to IgE, IFN-γ guides switching to IgG2a, transforming growth factor-β (TGF-β) and IL-5 induce switching to IgA. The antibody isotypes generated and the cytokines produced depend on the anatomic site of the lymphoid organs, stimulation by pathogenic components and TLR activation, which maximize the protection efficiency of antibodies (Xu et al., 2012, Chaudhuri and Alt, 2004).

GC B cells terminally differentiate into either antibody-secreting cells (ASCs) or memory B cells (MBCs). ASCs can be further classified into plasmablasts (PBs) and plasma cells (PCs). High affinity GC B cells preferentially differentiate into proliferative PBs, then some of PBs further differentiate into non-proliferative PCs that continuously secrete antibodies. Tfh-help during positive selection plays an important role in determining the PB and PC fate. Studies have found that Tfh-derived IL-21 induces expression of primary PC fate transcription regulator Blimp-1, and together with stromal cell-derived IL-6, induce generation of early PBs (Zhang et al., 2018, Crotty, 2019), in addition, CD40L-CD40 interaction is also a PC fate regulator, as demonstrated in a CD40 haploinsufficiency mouse model. $CD40^{+/-}$ mice show similar GC B cell number, but significantly fewer PBs. In the same study, the authors also found that a strong CD40 signal can induce intercellular adhesion molecule 1 (ICAM-1), signalling lymphocytic activation molecule (SLAM) and CD40 expression on LZ GC B cells. These adhesion molecules help to establish stable and extended GC cell-Tfh cell conjugates, which favor PB differentiation (Ise et al., 2018). Besides this, the BCR isotype can also affect PB differentiation, especially in the case of IgE expressing GC B cells, which show an antigen-independent bias towards PC differentiation, but a reduced GC response. This could be potentially due to the difference in the capability of the isotype to capture antigens from FDCs (Cyster and Allen, 2019, Erazo et al., 2007, Yang et al., 2012, Yang et al., 2016, Victora and Nussenzweig, 2022). Differentiated ASCs express sphingosine-1-phosphate receptor 1 (S1PR1) and egress from secondary lymphoid organs, then the chemokine receptor CXCR4 interacts with CXCL12 and mediates ASCs homing to the bone marrow, where a part of ASCs mature to long-lived plasma cells (LLPCs), which produce antibodies for years or even a lifetime (Nutt et al., 2015).

In contrast to this, a small population of GC B cells expresses relatively low or intermediate affinity BCRs that receive moderate help from Tfh cells, differentiate into MBCs in a Bach2 dependent way (Suan et al., 2017, Viant et al., 2020b, Wong et al., 2020), while strong Tfh cells' help inhibits the MBCs differentiation through downregulation of Bach2 and upregulation of mTORC1 (Inoue et al., 2021, Victora and Nussenzweig, 2022, Shinnakasu et al., 2016, Crotty, 2019). Recent studies also have shown that restricting the availability of IL-21 or IL-4 by decoy receptors on FDCs could promote MBCs generation (Quast et al., 2022, Duan et al., 2021). The majority

of MBCs reside closely with memory Tfh cells in the subcapsular sinus (SCS) of the lymph node, where $CD169^+$ macrophages constantly monitor and capture circulating particulate antigens, facilitating the activation of MBCs. Upon re-activation by subsequent antigen exposure, MBCs rapidly differentiate into secondary PCs or GC B cells (together with naïve B cells) for further proliferation and affinity maturation. MBCs are found to be more clonally diverse than PCs, which provide significant protection, because the MBC repertoire may contain non-immunodominant clones that cross-react with potential pathogen variants (Tas et al., 2016, Victora and Nussenzweig, 2022). Therefore, a new concept of “memory compartment” has been proposed, including LLPCs and MBCs, as they cooperate in protection against re-infection: LLPCs continually secrete high affinity antibodies that protect against re-infection with the same pathogen, while MBCs expressing cross-reactive BCRs re-enter the GCs and re-shape their BCRs through SHM, enabling binding of new variants with small structural changes (Inoue and Kurosaki, 2024).

3.1.3 Vaccine induced immune response.

Vaccines are biological products that contain weakened or inactive pathogenic microorganisms or their components. Upon vaccination, they induce immunity without causing the clinical manifestations of the disease, and confer long-lasting protection on subsequent exposure to the specific pathogen (Pollard and Bijker, 2021). Vaccines can be generally classified into two groups according to whether they contain live pathogens or not. The first group contains live attenuated pathogen with replication capability. The other group contains non-live vaccines, including inactivated vaccines that consist of killed whole pathogens, and subunit vaccines which contain purified or synthetically produced antigenic components of a pathogen, such as proteins, polysaccharides or conjugate vaccines (Pollard and Bijker, 2021).

The live and non-live vaccines differ in the mechanisms by which they induce immune responses. Live attenuated vaccines replicate controllably in an immunocompetent individual. Therefore, they mimic natural infections that induce strong immune responses and lifelong memory. Upon injection, live microorganisms activate several PRRs in the innate immune response, including TLRs, RIG-I and MDA5, leading to synergistic activation of DCs (Querec et al., 2009, Pulendran and Ahmed, 2011,

Napolitani et al., 2005). On the contrary, non-live antigenic components of subunit vaccines are inefficient in inducing innate immune responses. Therefore, they are normally combined with adjuvants that provide danger signals required to activate PRRs.

For a long period of time, alum was the only licensed adjuvant. It is an aluminium hydroxide wet gel suspension that has positively charged particles which can absorb negatively charged antigenic proteins at pH 5-7. Following injection, antigens gradually elute from the particles after exposure to interstitial fluid and are internalized by DCs through macropinocytosis or phagocytosis (Morefield et al., 2005). Aluminum hydroxide particles themselves act as stress-inducing agents and create pro-inflammatory environment, which recruits neutrophils, monocytes and DCs to the injected site and facilitate antigen presentation (Reed et al., 2013, De Gregorio et al., 2008). Besides this, aluminium salts activate IL-4 producing eosinophils which prime B cells for optimal antibody production (Wang and Weller, 2008). Moreover, although controversial, some studies report that aluminium salts stimulate DCs through activation of the NALP3 inflammasomes and thereby enhancing antigen uptake (Hornung et al., 2008, Reed et al., 2013). Alum containing vaccines mainly induce Th2 responses, however its mechanisms remain to be further elucidated (Reed et al., 2013, Zhao et al., 2023). Novel adjuvants, such as oil-in-water emulsion adjuvants MF59 and AS03, TLR agonist molecule-based adjuvants AS04 (TLR4) and CpG ODN 1018 (TLR9), and liposomal particulate adjuvant AS01 have been approved for use in a variety of vaccines. However, their complex action mechanisms are not completely known. Current understanding includes: sustained antigen release or protection of the antigen from degradation, thus prolongated antigen interaction with the immune system; activation of innate immune cells through various PRRs and increased antigen presentation; promotion of cytokine and chemokine release by macrophages to recruit other immune cells (Zhao et al., 2023).

The goal of the vaccination and its protective effects have long been attributed to the induction of persistent antibodies. Neutralizing antibodies (nAbs), which only account for a small population of all induced antibodies, are able to bind the active site of pathogens, interfere receptor-ligand binding, thus directly block the entry of pathogens into the host cells and prevent infections or limit viral burden (Gruell et al., 2022). Other

antibody subsets function in the clearance of the blood-borne pathogens or infected cell, by either antibody-mediated opsonization, or antibody-dependent cell-mediated cytotoxicity (ADCC) (Pulendran and Ahmed, 2011).

Recently, more and more researches have shown the importance of vaccine induced T cell responses in preventing infections. For example, one study found influenza-specific T cell responses are positively correlated with vaccine-induced protection in the elderly, rather than the antibody titers (McElhaney et al., 2006). Similar results are also found in vaccination against varicella virus and mycobacterium tuberculosis (Levin et al., 2008, Eisenhut et al., 2009). Besides, many vaccines are expected to induce effective T cell responses for complete protection, such as HIV and malaria (Pulendran and Ahmed, 2011). As discussed earlier, activated T cells differentiate into different effector subsets to handle different types of pathogens: Th1 and CTLs control intracellular pathogens, while Th2 and Th17 assist humoral responses and control extracellular bacteria, fungi and helminths. Therefore, understanding the mechanisms by which T cells differentiate into different subsets will greatly help vaccine development. T cell fate is determined by DC subsets activated by different PRRs and in cooperation with local environmental stimuli (Pulendran et al., 1999, Maldonado-López et al., 1999, den Haan et al., 2000). These results indicate that the use of different adjuvants that target specific PRRs on different DC subsets can direct the T cell response towards the most favorable subset. Among the classical adjuvants, alum, MF59 and AS03 induce Th2 responses; CPG ODN1018 induces strong Th1 responses and CTLs production; AS01 contains immunostimulant monophosphoryl lipid A (MPLA) and an active ingredient QS-21, which can activate both Th1 (MPLA) and Th2 (QS-21) responses. Besides, AS01 is found to promote antigen cross presentation to CD8 T cells and induce CTLs generation; AS04 is also a mixed adjuvant, consisting of alum and MPLA and therefore is able to induce both Th2 and Th1 response (Zhao et al., 2023). In conclusion, T cell mediated cellular immunity is critical for the protective effect of vaccines. By using specific adjuvants, T cell differentiation and responses can be preferentially manipulated.

3.2 Extracellular vesicles (EVs).

3.2.1 Biogenesis of EVs.

Extracellular vesicles (EVs) are membrane-bound particles derived from cells, they encapsulate distinct proteins, lipids and nucleic acids signatures reflecting their cell origin (van Niel et al., 2018, Yates et al., 2022b). EVs are evolutionary conserved, all cell types, ranging from bacteria to plant and human cells can secrete various types of EVs (Deatherage and Cookson, 2012, Robinson et al., 2016, van Niel et al., 2018). EVs are highly heterogeneous, to ease the characterization, EVs are generally classified into two groups: exosomes and microvesicles (MVs, also known as ectosomes), according to their size, morphology and biogenesis (Figure 3). Exosomes (30-100nm in diameter) are initially formed as intra luminal vesicles (ILVs) in multi-vesicular endosomes (MVEs) by inward budding of MVE membranes. ILVs are secreted as exosomes into the extracellular space after MVEs fuse with the cell membrane (Harding et al., 1984, Pan et al., 1985, van Niel et al., 2018). This process is mostly regulated by the endosomal sorting complex required for transport (ESCRT), however, ESCRT independent pathway also exists, which requires the generation of ceramide by neutral type II sphingomyelinase (Trajkovic et al., 2008, Yates et al., 2022b). In contrast, MVs are larger in size with a diameter ranging from 50-1000nm. Cancer cell derived oncosomes are even larger with diameters up to 10um. MVs are generated by directly outward budding of the cell membrane, therefore contain more plasma membrane proteins (Tricarico et al., 2017, Raposo and Stoorvogel, 2013, van Niel et al., 2018). In some reviews, the concept of EVs also includes apoptotic bodies (1-5um), which are released after programmed cell death (Yates et al., 2022b). Considering apoptotic bodies are very distinct from exosomes and MVs in regard of their contents and functions, here I will mainly focus on exosomes and MVs.

EVs contain common structural components such as membrane lipids (including phosphatidylserine (PS), cholesterol, ganglioside, glycosphingolipids and ceramide), additionally, membrane tetraspanin proteins (CD9, CD63 and CD81) are enriched among EVs (Jankovičová et al., 2020, Chen et al., 2019, Yates et al., 2022b). EVs modulate functions of recipient cells through surface proteins, as well as enclosed cargo molecules, including proteins, lipids, extra-chromosomal DNAs, ncRNAs, mRNAs and miRNAs (Robbins and Morelli, 2014). However, the composition of EVs

varies depending on the cell types which they originate from and the physiological state of the donor cell (Colombo et al., 2014). The heterogeneity of EV composition has attracted a lot of research interests, and studies have revealed their important roles in intercellular communication in both pathogenesis as well as maintaining homeostasis.

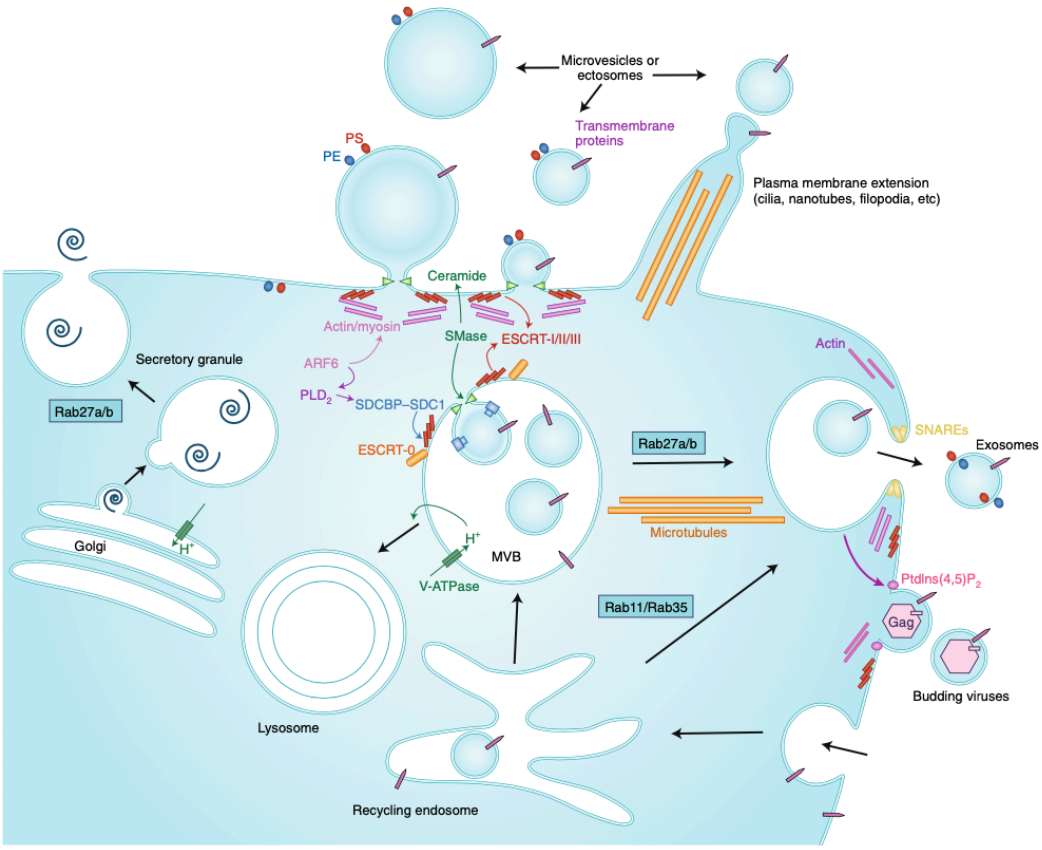

Figure 3 : Biogenesis of EVs.

EVs are generally divided into two groups: microvesicles and exosomes according to their distinct biogensis. Exosomes are initially formed in MVEs, then exosomes are secreted into the extracellular space (this process is mediate by Rab27a/b). Microvesicles are produced by direct outward budding of the cell membrane. Formation of both exsomes and microvesicles require the ESCRT machinery and cytoskeleton rearrangement. Figure is taken from (Mathieu et al., 2019).

3.2.2 EVs in immune system.

Immune responses require frequent cell to cell contact and communication. EVs as additional communication and information exchange mechanisms, are found to be involved in every aspect of immune responses. During the early initaition of innate immune responses, lymphatic endothelial cells at the inflammatory site release large amounts of EVs that are enriched in pro-migratory proteins. The membrane-bound C-

X3-C motif chemokine ligand 1 (CX3CL1) on these EVs interacts with CX3C receptor 1 (CX3CR1) on DCs. This interaction enhances responsiveness of DCs to chemokine gradients such as CCL19 and CCL21, which directs DCs to migrate to the inflammatory site (Brown et al., 2018, Sung et al., 2021). In addition to this, mast cell derived EVs contain concentrated heat shock protein 60 (HSP60) and HSP70. Studies have found that these EVs can promote DC maturation, increase the expression of MHC II and other costimulatory factors including CD40, CD80, and CD86, thereby promoting the antigen presentation to T cells (Skokos et al., 2003). EVs secreted by neutrophils could transfer arachidonic acid to platelets, which in turn metabolise into thromboxane A2 and induce neutrophil extravasation (Rossaint et al., 2016, Buzas, 2023). Besides this, neutrophil derived EVs contain microbicidal toxic oxygen metabolites and are able to restrain bacteria growth and dissemination (Timár et al., 2013, Yates et al., 2022b). Macrophages as one of the most important components of innate immunity are found to secrete EVs that contain pathogenic antigens and PAMPs after infection with intracellular pathogens. These EVs are able to induce TLR-dependent proinflammatory responses in unifected macrophages (Bhatnagar et al., 2007). Moreover, EV-associated cytokines and damage-associated molecular patterns (DAMPs): including HSPs and histones, were able to promote M1 macrophage polarization in a sepsis study (Burgelman et al., 2021, Buzas, 2023). EVs can also serve as a container for various cytokines, either on the surface (TNF, CCL2 and TGF-β) or as enclosed cargo (IL-2, IL-4, IL-17,IL-21, IFN-γ etc.) (Fitzgerald et al., 2018). They function similarly to the free form of cytokines that regulate cell function in either a juxtacrine, autocrine, paracrine or endocrine fashion. One big advantage of EV-associated cytokines is that they are protected from protease degradation on the cell surface and in extracellular environment, increasing their activity allowing them to regulate functions in more distant cells (Lima et al., 2021, Fitzgerald et al., 2018, Robbins and Morelli, 2014, Buzas, 2023).

The most significant function of EVs in adaptive immune response is antigen presentation. Early in the 1990s, studies had found that APC derived EVs contain both MHC I and MHC II complexes, as well as costimulatory factors and adhesion molecules, which indicated these EVs could potentially activate T cells (Robbins and Morelli, 2014, Raposo et al., 1996). Later, evidence was provided in experiments in which mice were immunized with DCs derived EVs containing peptide-MHC II

complexes. The results showed antigen-specific naïve CD4 T cells were activated (Théry et al., 2002), and that tumor peptide loaded DC-derived EVs could prime antigen specific CTLs in vivo (Zitvogel et al., 1998). With much of the knowledge that accumulated in the last two decades, we now know antigen presentation through EVs appears in different forms (Figure 4): APCs derived EVs alone can directly activate primed T cells, or activate naïve T cells with bystander DCs (Segura et al., 2005, Segura et al., 2007, Lindenbergh and Stoorvogel, 2018). Whether EVs alone can activate naïve T cells in the absence of DCs is still controversial, our recent data showed that EVs attached to activated $CD8^+$ effector cells rather than naive $CD8^+$ T cells, and induced antigen specific T cell activation independent of DCs (Rausch et al., 2023). Therefore, EVs alone is unlikely to activate naïve $CD8^+$ T cells, probably due to the lack of LFA-1 expression on naïve $CD8^+$ T cells that unable to recruit EVs (Nolte-'t Hoen et al., 2009). However, Buzas had proposed a different theory that EVs alone can activate naïve T cells but in very low efficiency, existence of DCs can significnatly increase the antigen presentation efficacy and T cell activation (Buzas, 2023).

In addition to the activation by free EVs directly, most released EVs remain attached on the surface of the producing cells and acceptor cells (cross-dressing), those membrane associated peptide-MHC complexes containing-EVs are found to be more potent in activating T cells than free EVs, because acceptor cells (DCs) provide additional and stable costimulation by CD80 and CD86. Another reason could be that DCs recruit large numer of peptide-MHCs through EVs, facilitate formation of immune synapses and TCR crosslinking (Lindenbergh and Stoorvogel, 2018, Wakim and Bevan, 2011, Buzas, 2023). Additionally, cross-dressing by mature DC-derived EVs can even enable those DCs that have not directly contacted the antigen and non-professional APCs to activate naïve T cells (Buzas, 2023, Robbins and Morelli, 2014, Segura et al., 2005). Moreover, cognate interaction between DCs and T cells induces DCs to release peptide-MHC carrying EVs, which may assist T cell activation, one proposed function is that those EVs also carry costimulatory factors, which continuously activate T cells, therefore release burdens of DCs (Buschow et al., 2009, Zhou et al., 2005). Transfer of peptide-MHC complexes from donor cell to the acceptor cell by cross-dressing is also seen when antigen-encountered migratory DCs home to lymph node or spleen, they release peptide-MHC bearing EVs. These EVs are then

efficiently recruited by resident DCs. The cross-dressed resident DCs show higher efficiency in activating T cells than migratory DCs, which indicates the close cooperation between migratory and resident DCs through EVs (Allan et al., 2006, Qu et al., 2009, Montecalvo et al., 2008).

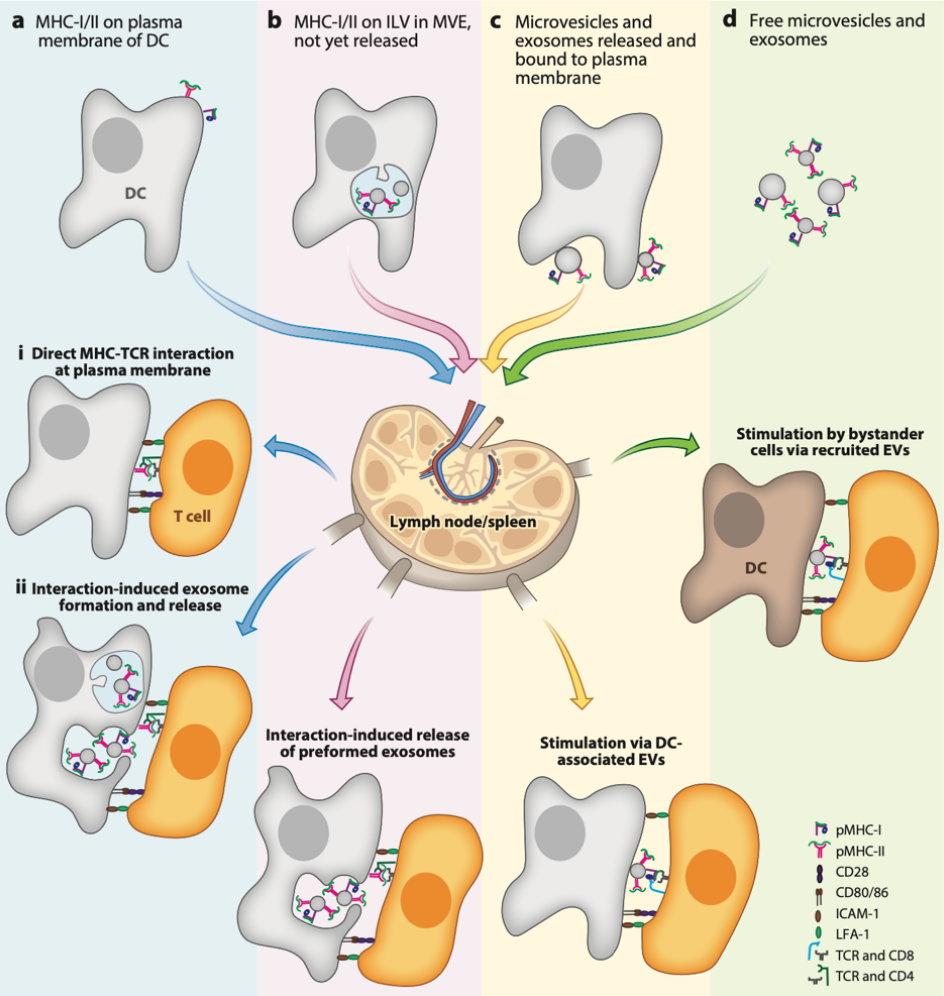

Figure 4 : Presentation of peptide-MHC complexes to T cells.

Peptide-MHC complex can be presented to T cell by direct contact (i). DC and cognate T cell interaction can induce release of EVs that carry peptide-MHC complexes, these EVs either remain attached on DCs or are captured by T cells, they may assist T cell activation (ii). Migratory DCs release EVs that contain peptide-MHC complex in the secondary lymphoid organs, these EVs are then efficiently recruited by resident DCs, the cross-dressed resident DCs can present these peptide-MHC complexes and activate T cells more efficiently (d). Figure is taken from (Lindenbergh and Stoorvogel, 2018).

Apart from T cells, EVs loaded with intact antigen (OVA) can activate B cells and induce antibody production in vivo (Qazi et al., 2009, Lindenbergh and Stoorvogel, 2018). B cells themselves can provide large amount of EVs after activation by cognate CD4 T cells. These EVs contain MHC molecules, complement factor 3 and antigen-

immunoglobulin complexes (Muntasell et al., 2007, Arita et al., 2008, Saunderson et al., 2008, Rialland et al., 2006), therefore these B cell derived EVs are assumed to be preferentially recruited by FDCs through FcR, complement receptors or intergrin α4β1 (Denzer et al., 2000, Wang et al., 2014). EVs captured by FDCs are preserved for prolonged time, and the intact antigen within the EVs may regulate the GC reaction and maintain the phenotype of Tfh cells (Crotty, 2014, Lindenbergh and Stoorvogel, 2018).

In contrast to pro-inflammatory effects, EVs can also have immunosuppressive functions. For example: peptide-MHC complexes cross-dressed CD4 T cells can present them to activated CD4 T cells and then inhibit their further expansion (Helft et al., 2008). Fas ligand on some B cell derived EVs can induce apoptosis of antigen-specific CD4 T cells, therefore function as a negative-feedback loop to reduce T cell response (Lundy and Klinker, 2014, Klinker et al., 2014). Immunosuppressive EVs also play important roles in generating immune tolearance. Intestinal epithelial cells derived EVs collected from OVA-fed mice, can inudce OVA-specific tolerance when transferred to naïve recipient mice (Ostman et al., 2005). Tregs can also release EVs that have immunosuppressive effects, this is mediated by the CD73 and the enclosed miRNAs, including miR155, Let7b and Let7d (Smyth et al., 2013, Okoye et al., 2014).

Although the function of EVs in immune system has drawn more and more attentions and many progresses have been made in the past decade, people should always be aware of the heterogeneousness of EVs, either caused by different cellular origins, or caused by different biological conditions of the same cell type. As well as the limitations in the EVs isolation methods, all these defects hamper the efforts to get conclusive results of EVs' function. Besides, most previous researches used EVs that were produced from cell cultures and tested *in vitro*. Whether these in vitro results could reflect EVs' real functions *in vivo* is still a big question. What's more, many researches did *in vivo* tests by systemic injection of EVs. This could overestimate the function of EVs, because most released EVs remain attched on the surface of the producing cells and nearby cells, they mainly perform their effects locally, only a few EVs enter the circulation.

3.2.3 EVs as drug delivery platform.

EVs have many features that make them an attractive natural delivery system for medical applications. Firstly, EVs are enclosed by biocompatible phospholipid bilayers, and are able to transport various bioactive materials to the recipient cells. Secondly, some studies have found EVs are able to cross biological barriers (Alvarez-Erviti et al., 2011, Cooper et al., 2014, Liu et al., 2015).

To use EVs as carrier systems, various methods to load the therapeutic substances into the EVs have been developed. Isolated EVs can be loaded exogenously by passive incubation with hydrophobic substances (such as curcumin), which enables them to be incorporated onto the EV membrane (Herrmann et al., 2021, Sun et al., 2010). Additionally, temporal permeabilization of EVs by sonication, electroporation or saponin treatment allows hydrophilic substances and large proteins to enter the EV lumen (Haney et al., 2015, Alvarez-Erviti et al., 2011). A recent study uses synthetic liposomes to wrap soluble cargoes, which are then fused with the EV membrane. This method can efficiently load large molecules, either lipophilic or hydrophilic, into the EVs without compromising the EVs membrane (Piffoux et al., 2018, de Jong et al., 2019, Herrmann et al., 2021). Alternatively, EVs that contain desired cargo can also be generated endoegnously by utilizing the sorting and packaging mechanisms of the EVs biogenesis. For example, cells can be genetically engineered to express desired cargo molecule fused with molecules that are naturally sorted and enriched in EVs (such as Nedd4, Lamp2a and ARRDC1). As a result, the desired molecule is also loaded into the EVs before their secretion (Elsharkasy et al., 2020, Sutaria et al., 2017, Wang et al., 2018).

EVs also show some degree of intrinsic targeting capability, due to the different expression pattern of integrins on EVs, which increase their accumulation in some specific organs, as integrins α6β4 and α6β1 direct EVs to home to the lung, while integrin αvβ5 favour liver accumulation (Hoshino et al., 2015). In addition, EVs targeting capability can be conferred through the cargo-loading techniques as described above. For example, fusing Lamp2b with neuron-specific rabies viral glycoprotein (RVG) peptide could increase EVs uptake by neurons, microglia, and oligodendrocytes in the brain (Alvarez-Erviti et al., 2011). Lamp2b fused with a cardiomyocyte targeting peptide (CMP) could target EVs to cardiomyocytes and

improved cardic retention (Mentkowski and Lang, 2019). Moreover, by fusing Lamp2b with αvβ3 integrin-specific iRGD peptide, EVs showed increased accumulation in tumors, which could potentially improve cancer therapies (Tian et al., 2014, Liu et al., 2008).

3.3 Milk fat globule epidermal growth factor 8 (Mfge8)

Milk fat globule epidermal growth factor 8 (Mfge8, also known as lactadherin) is a glycoprotein that has bivalent binding capability to integrins and phospholipids. A variety of cells can secrete Mfge8, including epithelial cells of mammary glands, activated macrophages, immature DCs, FDCs, astrocytes, pancreatocytes and epidermal keratinocytes (Aziz et al., 2011, Elliott and Ravichandran, 2010, Watanabe et al., 2005, Kranich et al., 2008, Kranich et al., 2010). Mouse Mfge8 mainly consists of two epidermal growth factor (EGF)-like domains in the N-terminus, and on the second EGF repeat, there is a conservative arginine-glycine-aspartic acid (RGD) motif. The EGF-like domains are followed by two tandem F5/8-type C domains in the C-terminus (Figure 5). The C domains are common among species, whereas the number of EGF-like domains differs, for example human Mfge8 only has one EGF-like domain with an RGD motif, while bird, amphibian and fish Mfge8 has three EGF-like domains. Those structures contribute to the bivalent binding capability of Mfge8: the RGD motif binds to αVβ3 and αVβ5 integrins, and the C domains bind to phosphatidylserine (PS). Mfge8 is involved in many physiological and pathological processes, including maintaining immune homeostasis, angiogenesis, regulation of haemostasis, as well as pathogenesis of atherosclerosis (Oshima et al., 2014, Kamińska et al., 2018). In this introduction, I will focus on it's role in apoptotic cell clearance and haemostasis.

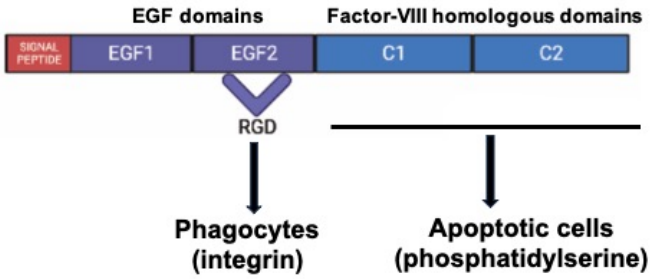

Figure 5 : Schematic diagram of Mfge8 structure.

Mfge8 mainly contains two F5/8-type C domains and two EGF-like domains. Physiologically, Mfge8 binds to PS on apoptotic cells through C domains, and bridges to integrins on phagocytes through the RGD motif on the second EGF domain. Diagram is created in biorender.

3.3.1 Mfge8 in apoptotic cell clearance.

Phosphatidylserine (PS) and phosphatidylethanolamine (PE) are the most abundant phospholipids in plasma membrane (O'Donnell et al., 2014, Encinar et al., 1996). In live healthy cells, PS and PE are asymmetrically confined to the inner membrane leaflet by scramblases (TMEM16 and XKR families), which unspecifically transport PS and PE between the inner and outer leaflets according to the lipid gradient or through ATP dependent specific translocation from the outer to the inner leaflet by flippases (ATP11A and ATP11C), regardless of the lipid concentration gradient (Nagata, 2018, Segawa et al., 2014, Segawa et al., 2016). When cells undergo apoptosis, ATP11A and ATP11C are inactivated by caspase 3 cleavage, while scramblases are activated by caspase 3 and caspase 7, as a result, PS and PE are exposed on the outer surface of membranes in apoptotic cells (Figure 6) (Suzuki et al., 2013, Suzuki et al., 2014).

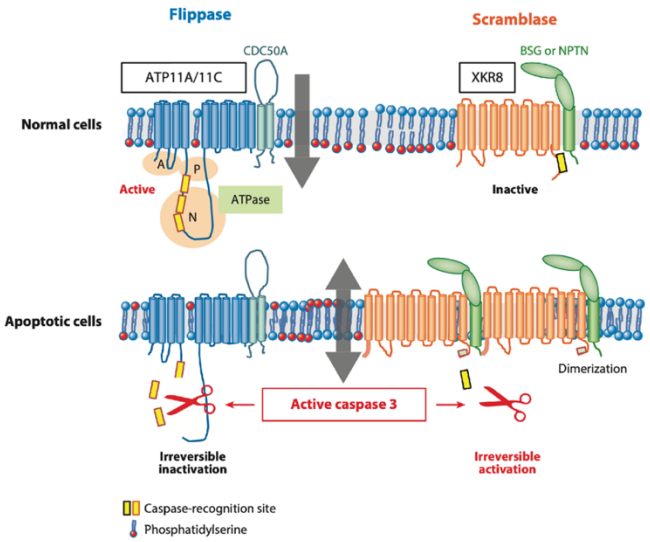

Figure 6 : Plasma membrane in live cells and apoptotic cells.

In live cells, membrane asymmetry is maintained, PS and PE are confined to the inner leaflet by flippases in an ATP dependent manner. The cytoplasmic region of flippases contains actuator (A), nucleotide-binding (N) and phosphorylation (P) domains, N domain contains caspase-recognition sites. When cells undergo apoptosis, caspase 3 irreversibly inactivate flippases but activate scramblases. As a result, PS is translocated to the membrane surface accoding to the concentration gradient. Figure is taken from (Nagata, 2018).

The externalised PS serves as an “eat me” signal for phagocytosis. Macrophages express various receptors to either directly recognise PS^+ apoptotic cells, such as TIM4, or indirectly bind them trough bridging proteins, such as TAM receptors (including Tyro3, Axl and Mer), which require growth arrest specific 6 (Gas6) and Protein S (Pros1) to bridge TAM^+ macrophages to PS^+ apoptotic cells (Lemke, 2019). Mfge8 is aslo a bridging protein, it bind to the PS on apoptotic cells via the C domains, meanwhile the RGD motif binds to integrins on macrophages, thereby facilitating clearance of apoptotic cells (Hanayama et al., 2002, Hanayama et al., 2004).

Mfge8 not only plays an important role in labeling apoptotic cells and maintaining homeostasis, its role is especially important during the GC reaction, where GC B cells that express dysfunctional BCRs or low affinity BCRs that don’t receive survival signals from Tfh cells, will undergo apoptosis. FDCs derived Mfge8 will label those apoptotic GC B cells and license TBMs to eliminate these dying cells (Kranich et al., 2008, Hanayama et al., 2006).

Eliminating apoptotic cells is an important mechanism to prevent development of autoimmune disease. This was demonstrated in Mfge8-deficient mice, in which apoptotic cells clearance was impaired. These mice showed that apoptotic cells accumulated on the surface of TBMs in the spleen and lymph nodes (Hanayama et al., 2004). Incapable of cleaning apoptotic cells resulted in secondary necrosis of the cells. Intracellular contents and autoantigens were exposed to the immunse system, causing the development of a systemic lupus erythematosus (SLE)- like autoimmune disease. In line with this, large amount of anti-double stranded DNA and anti-nuclear antibodies are observed in Mfge8-deficient mice. As a consequence, immune complexes were dopsited in the glomeruli of the kidney, causing glomerulonephritis and proteinuria (Hanayama et al., 2004, Peng and Elkon, 2011, Gaipl et al., 2005). Besides this, Mfge8-deficient mice show reduced IL-10 but increased IFN-γ production, demonstrating the important role of Mfge8 in maintaining peripheral tolerance (Neutzner et al., 2007, Kamińska et al., 2018).

3.3.2 Mfge8 as a tool to study EVs.

Mfge8 is a promising tool to label PS^+ apoptotic cell and other PS^+ membrane products, such as EVs and cell debris. Traditionally, PS binding annexin V is used to stain apoptotic cells, now Mfge8 shows great potential to be a powerful substitute. Compared with annexin V, Mfge8 binds to PS in a Ca^{2+} independent manner (Kamińska et al., 2018, Neutzner et al., 2007, Kranich et al., 2020), which extends its application to *in vivo* labeling of apoptotic cells. Besides this, Mfge8 shows greater sensitivity in binding PS than annexin V (Hu et al., 2008, Shi et al., 2006), and Mfge8 preferentially binds to small PS^+ membranes particles with higher curvature, such as EVs (Shi et al., 2004, Dasgupta and Thiagarajan, 2014). These features make Mfge8 a powerful tool to assist EVs researches. Our lab has created several fluorescent Mfge8 fusion proteins and fluorescent PS-binding C domain tetramers that can be used for *in vivo* PS binding, and in cooperation with Prof. Dr. Fabian J. Theis and Dr. Nikolaos-Kosmas Chlis, we created a deep learning based convolutional autoencoder (CAE) to identify apoptotic cells and EVs-attached cells based on their surface exposure of PS (Mfge8 binding pattern) and other parameters of the images taken from imaging flow cytometry (Kranich et al., 2020). This tool has been proved to be valid in various studies: it helped to characterize EVs and EVs-attached CD8 T cells in viral infection, we showed that activated $CD8^+$ effector cells preferentially bind EVs. These EVs induced antigen specific T cell activation, and the nuclear translocation of the Nuclear factor of activated T-cells (NFATc1) was increased (Rausch et al., 2023). We also applied this method to human COVID-19 patients and found platelet-derived EVs show strong positive correlation with disease severity (Rausch et al., 2021).

4. Aim of the thesis

In addition to its use as a staining reagent, we wanted to exploit Mfge8 as PS-targeting tool to target antigens onto EVs *in vivo*. As it has been shown that EVs accumulate in lymphoid follicles, we wanted to assess whether EV-associated antigens can activate B cells or modulate B cell responses. In this study, EGFP and OVA were fused or conjugated with Mfge8 or mouse C1 (mC1) tetramer, respectively. These PS-targeting antigens were used to immunize mice. We targeted naturally occurring, circulating EVs to enrich antigens in lymphoid organs, and tested if this method could boost immune responses. With this study, we aim to develop a new vaccination strategy.

5. Materials and methods

5.1 Buffers, reagents and chemicals

5.1.1 Self-prepared buffers and media

Buffers and media are prepared in double distilled water (ddH_2O) unless otherwise specified.

Table 1. Self-prepared buffers and medium.

Buffer name	Composition and concentration
Phosphate-buffered saline (PBS) pH 7.4	137 mM NaCl 2.7 mM KCl 10 mM Na_2HPO_4 2 mM KH_2PO_4
Optimized stabilizing buffer (OSB) pH 7.4	500 mM NaCl 25 mM HEPES 18 mM L-arginine 3.5 mM L-leucine 5.7 mM L-glutamic acid 8 % Glycerol
Arg-Glu injection buffer pH 7.4	150 mM NaCl 25 mM HEPES 200 mM L-arginine 200 mM L-glutamic acid 2 % Glycerol
Flow cytometry (FACS) buffer	PBS 2 % Fetal bovine serum (FCS)
Ammonium-chloride-potassium (ACK) lysing buffer pH 7.4	154.4 mM NH_4Cl 10 mM $KHCO_3$ 97.3 µM $Na_4EDTA{\cdot}4H_2O$
Magnetic-activated cell sorting (MACS) buffer	PBS 2 % FCS 2 mM Ethylenediaminetetraacetic acid (EDTA)
5x sodium dodecyl sulfate (SDS) loading buffer	250 mM Trisaminomethane (Tris) 500 mM Dithiothreitol (DTT) 0.5 % Bromophenol blue 50 % Glycerol 10 % SDS
Sodium dodecyl sulfate – polyacrylamide gel electrophoresis (SDS-PAGE) running buffer (10x) pH 8.3	250 mM Tris 1.92 M Glycine 1 % SDS

Buffer name	Composition and concentration
Western blot transfer buffer pH 8.3	25 mM Tris 192 mM Glycine 20% Methanol 0.1 % SDS
Coomassie blue G-250 staining buffer	0.12 % Coomassie blue G-250 10 % $(NH_4)_2SO_4$ 10 % H_3PO_4 20% Methanol
Bacterial lysis buffer (for mC1) pH 7.4	300 mM NaCl 20 mM HEPES 20 mM Imidazole 1x Protease inhibitor cocktail (add before use)
Wash buffer for mC1 purification pH 7.4	300 mM NaCl 20 mM HEPES 20 mM Imidazole 0.1% Triton x-100
Elution buffer for mC1 purification pH 7.4	500 mM NaCl 25 mM HEPES 18 mM L-arginine 3.5 mM L-leucine 5.7 mM L-glutamic acid 8 % Glycerol 200 mM Imidazole
Sortase reaction buffer pH 7.4	500 mM NaCl 25 mM HEPES 18 mM L-arginine 3.5 mM L-leucine 5.7 mM L-glutamic acid 8 % Glycerol 10 mM $CaCl_2$
Sortase reaction stop buffer pH 7.4	500 mM NaCl 25 mM HEPES 18 mM L-arginine 3.5 mM L-leucine 5.7 mM L-glutamic acid 8 % Glycerol 7 mM EDTA 2x Protease inhibitor cocktail (add before use)
Enzyme-linked immunosorbent assay (ELISA) coating buffer pH 9.6	70 mM $NaHCO_3$ 30 mM Na_2CO_3

Buffer name	Composition and concentration
ELISA blocking/sample buffer	1x Casein blocking buffer (final working concentration) 0.1% Tween-20
ELISA washing buffer	PBS 0.1% Tween-20
ELISA stopping buffer	0.5 M H_2SO_4
Lysogeny broth (LB) medium	25 g Complete LB powder 1 L ddH_2O
T cell culture medium	500 ml RPMI 1640 10% FCS 1% Penicillin 1% Streptomycin 5 µM 2-mercaptoethanol
10 x Gitocher buffer pH 8.8	670 mM Tris 166 mM Ammonium sulfate 65 mM $MgCl_2$ 0.1 % Gelatin
Lysis / wash buffer for sortase purification pH 7.5	50 mM Tris 150 mM NaCl 5 mM $MgCl_2$ 10 % Glycerol 10 mM Imidazole
Elution buffer for sortase purification pH 7.5	50 mM Tris 150 mM NaCl 10 % Glycerol 500 mM Imidazole
GeFi buffer for sortase purification pH 7.5	50 mM Tris 150 mM NaCl 10 % Glycerol
Lysis buffer for GST-senp2 purification pH 7.6	20 mM Tris 350 mM NaCl 1 mM DTT
Wash buffer for GST-senp2 purification pH 7.6	20 mM Tris 350 mM NaCl 1 mM DTT 0.1% Triton x-100
Elution buffer for GST-senp2 purification pH 7.6	20 mM Tris 350 mM NaCl 1 mM DTT 10 mM Glutathione (reduced)
Storage buffer for GST-senp2 purification pH 8.0	20 mM Tris 150 mM NaCl 1 mM DTT 20 % Glycerol

Buffer name	Composition and concentration
Lysis buffer for EGFP purification pH 7.4	300 mM NaCl 50 mM Na_2HPO_4 5 mM Imidazole 10 % Glycerol 1x Protease inhibitor cocktail (add before use)
Elution buffer for EGFP purification pH 7.4	300 mM NaCl 50 mM Na_2HPO_4 500 mM Imidazole
Bone marrow-derived dendritic cell (BMDC) differentiation medium	500 ml RPMI 1640 medium with GlutaMAX ™ Supplement 1% Penicillin 1% Streptomycin 10 % FCS 0.05 mM 2-mercaptoethanol
BMDC stimulation medium	500 ml RPMI 1640 medium with GlutaMAX ™ Supplement 1% Penicillin 1% Streptomycin 10 % FCS (EVs free) 20 ng/ml Granulocyte-macrophage colony-stimulating factor (GM-CSF) 30 ng/ml LPS 0.05 mM 2-mercaptoethanol

5.1.2 Purchased reagents and kits

Table 2. Purchased reagents and kits.

Name	Supplier	Catalog number
0.5 M EDTA, pH 8.0	Invitrogen	15575020
1 M HEPES Solution	Sigma-Aldrich	SRE0065-100ML
2-Mercaptoethanol 50 mM	Gibco	31350010
Alexa Fluor™ 488 Protein Labelling Kit	Invitrogen	A10235
Alexa Fluor™ 555 Protein Labelling Kit	Invitrogen	A20174
Alexa Fluor™ 647 Protein Labelling Kit	Invitrogen	A20173
Alhydrogel® Adjuvant 2% Aluminum Hydroxide Gel	InvivoGen	Vac-alu-50
AMPure XP reagent	Beckman Coulter	A63880
B Cell Isolation Kit (mouse)	Miltenyi Biotec	130-090-862
BD Cytofix/Cytoperm™ Fixation/Permeabilization Kit	BD Biosciences	554714
BD Rhapsody™ cDNA Kit	BD Biosciences	633733

BD Rhapsody™ Enhanced Cartridge Reagent Kit	BD Biosciences	664887
BD Rhapsody™Cartridge Kit	BD Biosciences	633733
BupH™ Carbonate-Bicarbonate Buffer Packs	Thermo Scientific	28382
Calcein, AM, cell-permeant dye	Invitrogen	C1430
Casein Blocking Buffer 10x	Sigma-Aldrich	B6429-500ML
CF680R succinimidyl ester Protein Labelling Kit	Biotium	92226
DRAQ7™ Dye	Invitrogen	D15106
Dulbecco's Phosphate Buffered Saline	Sigma-Aldrich	D8537 -500ML
EDTA-free Protease Inhibitor Cocktail	Roche	4693159001
Ex-Cell 293 Serum-free Medium for HEK 293 Cells	Sigma-Aldrich	24571C -1L
Fetal Bovine Serum	Gibco	A5256701
Germinal Center B Cell (PNA) MicroBead Kit (mouse)	Miltenyi Biotec	130-110-479
Glutathione Sepharose™ 4B	GE Healthcare	17-0756-01
KPL TMB Microwell Peroxidase Substrate System	SeraCare Life Sciences	5120-0037
Ni-NTA Agarose	InvivoGen	R90110
Pierce™ Antibody Clean-up Kit	Thermo Scientific	44600
Proteinase K	Sigma-Aldrich	P2308-100MG
Qubit™ dsDNA Quantification Assay Kits	Invitrogen	Q32851
ROTIPHORESE®Gel 30 (37.5:1)	Carl Roth	3029.1
RPMI 1640 Medium GlutaMAX™ Suppplement	Gibco	61870-010
Streptavidin Conjugation Kit	Abcam	Ab102921-1MG
TEMED	Carl Roth	2367.3
Western Lightning Plus-ECL, Chemiluminescent Substrate	PerkinElmer	NEL103001EA

5.2 Chemicals

Table 3. Chemicals

Name	Supplier	Catalog number
1,4-Dithiothreit (DTT)	Carl Roth	6908.1
Aceton	Carl Roth	9372.1
Agarose, universal	VWR International	9012-36-6
Albumin Fraction V	Carl Roth	8076.3
Albumin from chicken egg white	Sigma-Aldrich	A7641-250MG
Calcium chloride	Sigma-Aldrich	10043-52-4
Coomassie Brilliant Blue R-250	ITW Reagents	6104-59-2
di-Sodium hydrogen phosphate dihydrate	Carl Roth	4984.1
EDTA	Carl Roth	8043.1

Ethanol absolute	Th. Geyer	2273.1000
Glycerol	Carl Roth	3783.1
Glycine	Th. Geyer	9366.1000
HEPES	Carl Roth	9105.4
Hydrochloric acid	Carl Roth	4625.1
Imidazole	Carl Roth	X998.4
IPTG, dioxane-free	Thermo Scientific	R0392
L- Glutamic acid	Sigma-Aldrich	G1251-500G
L-Arginine monohydrochloride	Sigma-Aldrich	A5131-100G
L-Glutathione reduced	Carl Roth	6382.2
L-Leucine	Sigma-Aldrich	L8000-100G
LB Broth	Carl Roth	X968.3
Methanol	Th. Geyer	1462.2511
SDS pellets	Carl Roth	8029.3
Sodium carbonate	Carl Roth	8563.1
Sodium chloride	Th. Geyer	1367.5000
Sodium hydrogen carbonate	Merck	144-55-8
Sodium hydroxide	Merck	1310-73-2
Sulphuric acid	Carl Roth	4623.1
Tris	Carl Roth	4855.3
TWEEN-20	Sigma-Aldrich	P1379-500ML

5.3 Devices

Table 4. Devices and suppliers.

Name	Supplier
AccuSpin Micro 17R	Fisher Scientific
Adventurer™ Analytic Scale	Ohaus Corporation
ÄKTA Pure 25 L1 Chromatography System	GE Healthcare Life Sciences (Cytiva)
Avanti JXN-26 Centrifuge	Beckman Coulter
BD FACSAria™ Fusion	BD Biosciences
BD FacsCanto™ II Flow Cytometer	BD Biosciences
BD Rhapsody™ HT Xpress System	BD Biosciences
BD Rhapsody™ Scanner	BD Biosciences
BioPhotometer	Eppendorf
CASY TT Cell Counter	OLS OMNI Life Science GmbH & Co. KG
Comfort Refrigerator (4 °C)	Liebherr
Cryostat CM1950	Leica
Cytek Amnis ImageStream X Mark II	Cytek Biosciences
Electrophoresis Power Supply	Bio Rad
Fluorescence Microscope BX41	Olympus
Galaxy 170S CO_2 Incubator	Eppendorf New Brunswick
Heraeus Multifuge X3R Centrifuge	Thermo Scientific
HiLoad 26/600 Superdex 200 pg	GE Healthcare Life Sciences (Cytiva)
Inverted Confocal Microscope (SP8X WLL)	Leica

Labfors 5 Bioreactor	Infors HT
Magnetic Stirrer	Ika Labortechnik
Microbiological Safety cabinet FlowSafe B-[MaxPro]^2-160	Berner International GmbH
Multi-Channel Pipette	Labsystems
NanoDrop Spectrophotometer	Peqlab Biotechnologie GmbH
Particle Metrix	Zeta View
pH Meter (pH level 1)	Inolab
Pipette Controller	Intergra Biosciences
Premium Nofrost Freezer (-20 °C)	Liebherr
Protec X-ray Imager	Barowi Med GmbH
Scale	Kern
Single Channel Pipettes (10ul, 200ul, 1000ul)	Axypet
Thermocycler	Biometra
Thermocycler	Biometra
Thermocycler	Analytik Jena
Thermomixer compact	Eppendorf
TSX Series Freezer (-80 °C)	Thermo Scientific
Ultrasonic Cell Disruptors	Branson Ultrasonics Corporation
Versa max microplate reader	Molecular Devices
Vortex-Genie 2	Scientific Industries

5.4 Staining antibodies

Antibodies listed below were anti - mouse unless otherwise specified. AF stood for Alexa Fluor Dyes. BV stood for Brilliant Violet Dyes.

Table 5. Antibodies used for flow cytometry.

Reactivity	Conjugate	Clone	Supplier	Catalog Nr.
Bcl-6	BV421	K112-91	BD Biosciences	563363
CD107a	PE	1D4B	Biolegend	121612
CD11b	PE-Cy7	M1/70	Biolegend	101216
CD11c	eFluor 450	N418	eBioscience	48-0114-82
CD138	PE	281-2	Biolegend	142504
CD16/32 (Fc Block)	N. A	93	Biolegend	101320
CD169	AF594	3D6.112	Biolegend	142416
CD169	BV421	3D6.112	Biolegend	142421
CD169	AF647	3D6.112	Biolegend	142408
CD19	AF594	6D5	Biolegend	115552
CD19	APC	1D3	Biolegend	152510
CD19	eFluor 450	1D3	eBioscience	48-0193-82
CD19	PE-Cy7	6D5	Biolegend	115520
CD19	Percp-Cy5.5	eBio1D3	eBioscience	45-0194-82
CD21/35	APC	7G6	BD Biosciences	558658

CD21/35	FITC	7G8	BD Biosciences	553818
CD21/35	PE	7G6	BD Biosciences	552957
CD23	Pacific Blue	B3B4	Biolegend	101616
CD23	PE-Cy7	B3B4	Biolegend	101614
CD38	PE-Cy7	90	Biolegend	102718
CD3e	AF647	145-2C11	Biolegend	100322
CD3e	PE	145-2C11	Biolegend	100308
CD3e	PE-Cy7	145-2C11	Biolegend	100320
CD4	BV421	GK1.5	Biolegend	100438
CD4	FITC	GK1.5	Biolegend	100406
CD4	PE-Cy7	GK1.5	Biolegend	100422
CD4	Percp	RM4-5	Biolegend	100538
CD40	N. A	FGK4.5	Bio X Cell	BE0016-2
CD44	FITC	IM7	Biolegend	103006
CD44	PE-Cy7	IM7	Biolegend	103030
CD44	PE-Cy5	IM7	BD Biosciences	553135
CD45.1	FITC	A20	BD Biosciences	553775
CD45.2	PE-Cy7	104	Biolegend	109830
CD62L	APC	MEL-14	BD Biosciences	553152
CD62L	Pacific Blue	MEL-14	Biolegend	104424
CD62L	PE	MEL-14	eBioscience	12-0621-82
CD63	PE	NVG-2	Biolegend	143904
CD63	Percp-Cy5.5	NVG-2	Biolegend	143912
CD63	APC	NVG-2	Biolegend	143905
CD81	AF594	431301	R&D Systems	FAB4865T
CD86	FITC	GL-1	Biolegend	105006
CD8a	APC	53-6.7	eBioscience	17-0081-83
CD8a	eFluor 450	53-6.7	eBioscience	48-0081-82
CD8a	PE-Cy7	53-6.7	Biolegend	100722
CD8a	Percp	53-6.7	Biolegend	100734
CD9	AF594	479608	R&D Systems	FAB5218T
CD90.1	Percp	OX-7	Biolegend	202516
CD95	FITC	Jo2	BD Biosciences	561979
CD95	PE-Cy7	Jo2	BD Biosciences	557653
CD95	Percp-eF710	15A7	eBioscience	46-0951-82
CD98	BV421	H202-141	BD Biosciences	744831
CXCR3 (CD183)	PE-Cy7	CXCR3-173	Biolegend	126516
CXCR4 (CD184)	AF647	L276F12	Biolegend	146504
CXCR4 (CD184)	PE	L276F12	Biolegend	146506

CXCR5 (CD185)	PE	SPRCL5	eBioscience	12-7185-82
EpCAM (CD326)	BV421	G8.8	Biolegend	118225
Fixable Viability Dye	eFluor780	N. A	eBioscience	65-0865-14
GL7	eFluor 450	GL-7	eBioscience	48-5902-82
IFN-γ	APC	XMG1.2	Biolegend	505810
IgD	PE	11-26c.2a	Biolegend	405706
IgD	PE-Cy7	11-26c.2a	Biolegend	405720
IL-2	PE-Cy7	JES6-5H4	eBioscience	25-7021-82
IL-21	PE	149204	R&D Systems	IC594P-100
IL-4	AF488	11B11	BD Biosciences	557728
MHC II (IA/IE)	PE	M5/114.15.2	eBioscience	12-5321-82
PD-1 (CD279)	APC	J43	eBioscience	17-9985-82
PD-1 (CD279)	BV421	29F-1A12	Biolegend	1335217
SIGN-R1 (CD209b)	APC	eBio22D1	eBioscience	17-2093-82
TCR β chain	APC-Cy7	H57-597	Biolegend	109220
TNF-a	PE	MP6-XT22	eBioscience	12-7321-82

Table 6. Antibodies used for histology.

Reactivity	Conjugate	Clone	Supplier	Catalog Nr.
CD 21/35	CF680R (Self conjugated)	eBio8D9	eBioscience	14-0211-81
CD169	AF594	3D6.112	Biolegend	142416
CD169	APC	SER-4	eBioscience	50-5755-82
CD169	BV421	3D6.112	Biolegend	142421
CD21/35	PE	7G6	BD Biosciences	552957
CD4	APC	RM4-5	Biolegend	100516
CD68	AF647	FA-11	Biolegend	137004
CD68	PE	FA-11	Biolegend	137014
CD81	AF594	431301	R&D Systems	FAB4865T
EGFP	Abberior Star 635p	WJ45	Creative Biolabs	MDWJ15
EGFP	FITC	polyclonal	Abcam	Ab6662
GL7	AF647	GL7	Biolegend	144606
GL7	FITC	GL7	Biolegend	144604
IgD	eF450	11-26c	eBioscience	48-5993-82
OVA	FITC	polyclonal	Rockland Immunochemicals	200-4233
PD-1 (CD279)	PE	RMPI-30	Biolegend	109130
PNA	AF488	N. A	Invitrogen	L21409
SIGN-R1	APC	eBio22D1	eBioscience	17-2093-82
Streptavidin	FITC	polyclonal	LSBio	LS-C195991

Table 7. Antibodies used for ELISA.

Reactivity	Conjugate	Clone	Supplier	Catalog Nr.
Donkey anti-mouse IgG	HRP	Polyclonal	Jackson ImmunoResearch	715-035-150
Donkey anti-rabbit IgG	HRP	Polyclonal	Jackson ImmunoResearch	711-035-152
Goat anti-mouse IgG1	HRP	Polyclonal	SouthernBiotech	1070-05
Goat anti-mouse IgG2b	HRP	Polyclonal	SouthernBiotech	1090-05
Goat anti-mouse IgM	HRP	Polyclonal	SouthernBiotech	1021-05
OVA	HRP	Polyclonal	Invitrogen	
Streptavidin	HRP		Abcam	Ab191338

5.5 Mouse strains

C57BL/6 wild-type mice were either purchased from Core facility Animal Models, Biomedizinisches Centrum, Ludwig-Maximilians- Universität München (LMU) or from JANVIER LABS (France).

Transgenic B6.129S4-C3^{tm1Crr}/J mice (C3-KO in short, JAX stock #029661) were purchased from Jackson Laboratory (USA). B6.129S4-C3^{tm1Crr}/J mice contain a deletion of around 600nt and an insertion of neomycin (Neo) resistance cassette into the exon of the C3 gene, resulting in the deletion of the β chain and the N-terminal region of the α chain, including the site for processing the pro-C3 molecule into the two-chain structure (Wessels et al., 1995).

For genotyping the B6.129S4-C3^{tm1Crr}/J mice left-over ear tissue from ear-marking the mice was used. Genomic DNA was isolated by incubating tail tips with Gitocher buffer mix for 6h at 55°C. The reaction was stopped by incubating mixture at 95°C for 5 minutes (proteinase K was inactivated). After digestion, 75ul H_20 was added to the mixture and then centrifuged for a short time.

Table 8. Gitocher buffer mix.

10x Gitocher	5 ul
Triton-X	2.5 ul
β -Mercaptoethanol	0.5 ul
Proteinase K (10 mg/ml)	2 ul

H_2O	40ul

To genotype B6.129S4-C3^{tm1Crr}/J mice by standard polymerase chain reaction (PCR), 1 µL of isolated genomic DNA was used in PCR master mix.

Table 9. Primers for genotyping.

Primer names	Sequence 5´ → 3´	Primer type
oIMR1325	ATC TTG AGT GCA CCA AGC C	Common
oIMR1326	GGT TGC AGC AGT CTA TGA AGG	Wild type
oIMR7415	GCC AGA GGC CAC TTG TGT AG	Mutant

Table 10. Genotyping reaction mix.

PCR reaction components	Final concentration
ddH2O	
Kapa 2G HS buffer	1.30 X
$MgCl_2$	2.60 mM
dNTP KAPA	0.26 mM
oIMR1325	0.50 uM
oIMR1326	0.50 uM
oIMR7415	0.50 uM
Glycerol	6.50 %
Dye	1.00 X
Kapa 2G HS taq polymerase	0.03 U/ul
DNA	1ul

Table 11. PCR program for genotyping.

Step	Temperature °C	Time	Note
1	95.0	3 minutes	
2	95.0	1 minute	
3	64.0	30 seconds	
4	72.0	1 minute	Repeat steps 2-4 for 33 cycles
5	72.0	10 minutes	
6	4.0	--	Pause

PCR products were separated by 1% agarose gel (added with 0.5 g/mL ethidium bromide) electrophoresis. Agarose gel images were taken from Gel Doc XR+ Molecular Imager.

Possible DNA bands:
Mutant = ~500 bp
Heterozygte = ~500 bp and 350 bp
Wild type = 350 bp

B6129SF1/J mice were purchased from Jackson Laboratory (JAX stock #101043). B6129SF1/J mice were F1 hybrid mice from a cross between 129S1/SvImJ males (129S) and C57BL/6J females (B6). B6129SF1/J mice were to provide approximate wild type controls for B6.129S4-C3^{tm1Crr}/J mice that were generated with genetically engineered 129S-derived embryonic stem cells and further backcrossed to C57BL/6J mice for many generations.

All animals were kept according to the corresponding animal welfare regulations and laws. All animal experiments were approved by the Ethics Committee of the Regierung Oberbayern, Bavaria, Germany.

5.6 Protocols and assays

5.6.1 Serum collection

Blood samples were collected either from mouse tail veins, the retro-orbital sinus or by cardiac puncture using a 1ml Omnican®-F syringe immediately from euthanised mice. Blood samples were transferred into individual Micovette® 500 Z-Gel tubes and then centrifuged at 10000 x g for 5 minutes at 20°C. Serum samples were collected above the gels, and stored in -80°C.

5.6.2 Indirect enzyme-linked immunosorbent assay (ELISA)

Indirect ELISA was used to measure serum anti-EGFP or anti-OVA antibody levels. Thermo Scientific™ Clear Flat-Bottom Immuno Nonsterile 96-Well Plates were coated with 100ul per well 10ug/ml desired antigen (EGFP or OVA) in coating buffer overnight at 4°C. On the following day, the plates were washed 6 times by immersing them in ELISA washing buffer. The residual liquid was removed by tapping the plates on tissue towels. Then the plates were blocked with 100ul per well blocking buffer for 2h. During

the incubation period, serum samples were prediluted 1:100. Then 1:2 serial dilutions were performed. After 2h of incubation, blocking buffer was discarded and to each well 100ul sample dilution was added. The plates were incubated for 2h, followed by 6 washes with washing buffer. Next, to each well 100ul 1:2500 diluted horseradish peroxidase (HRP) conjugated secondary antibodies specific for different isotypes was added. The plates were incubated for 1h, afterwards, the plates were washed with washing buffer for 4 times and twice with PBS. Finally, 100ul per well KPL TMB Peroxidase Substrates were added and incubated for 10 minutes, the reaction was stopped by applying 100ul ELSA stopping buffer. The absorbance at A450nm was measured by VersaMax Microplate Reader.

5.6.3 Protein expression and purification

5.6.3.1 Cultivation of bacterial expression system with kanamycin resistance.

This protocol applies to BL21(DE3) + pTK32 Sortase A expression and BL21(DE3) + pTK77 GST-Senp2 expression.

Bacterial glycerol stock was inoculated in 50 ml LB-Kan medium (50 ug/ml kanamycin) and cultured overnight at 37°C, shaken in 140 rpm in 250 ml Erlenmeyer flask. On the next day, 15 ml of the overnight culture was transferred into 1.5L fresh LB-Kan medium, shaken in 2 L Erlenmeyer flasks with baffles at 37°C, 100 rpm, until the OD_{600} reached 0.4 - 0.6. The cell culture was then induced with 0.5 mM isopropyl β-D-1-thiogalactopyranoside (IPTG) and subsequently cultured at 25°C, 100 rpm overnight (16h) to induce T7 promoter-controlled protein expression. On day3, the overnight culture was transferred into 250 ml buckets and centrifuged in Beckmann cooling centrifuge at 4000 x g, 10 min, 4°C. The cell pellet was collected into a 50 ml Falcon tube. After centrifuging the 50 ml Falcon tube at 4000 x g, 10 min, 4°C, supernatant was discarded and the cell pellet was weighted and collected into a 50 ml Falcon tube, then the cell pellet was stored in -80°C.

5.6.3.2 Cultivation of bacterial expression system with ampicillin resistance.

This protocol applies to BL21(DE3) + pTK108 Enhanced Green Fluorescent Protein (EGFP) expression.

Bacterial glycerol stock was inoculated in 50 ml LB medium supplied with 100 ug/ml ampicillin (LB-Amp) and grown at 37°C overnight, 140 rpm in a 250 ml Erlenmeyer flask. On the second day, 5 ml of the overnight culture was transferred into fresh 500 ml LB-Amp medium in 1 L Erlenmeyer flasks with baffles. The cells were cultured at 37°C and 100 rpm, until the OD_{600} reached 0.4-0.6. Then, the cell culture was centrifuged at 4000g x 15 min, 25ºC to remove the supernatant. The cell pellet was resuspended in 1.5 L fresh LB-Amp medium and cultured for 1h at 37ºC. In the last 30 minutes, the temperature was reduced to 20ºC, followed by induction with 0.2 mM IPTG overnight (16h) at 140 rpm, 20°C. On day 3, cells were harvested by centrifugation at 4000 x g, 10 min, 4°C. Cell pellet was collected into a 50 ml Falcon tube and was stored in -80°C.

5.6.3.3 Cultivation of bacterial expression system with kanamycin + ampicillin + tetracycline resistance.

This protocol applies to Origami B + pTK85 mC1-LPETG expression.

Bacterial glycerol stock was inoculated in 50 ml LB medium (supplied with 50 ug/ml kanamycin + 100 ug/ml ampicillin + 10 ug/ml tetracycline) and grown at 37°C, 120 rpm in 250 ml Erlenmeyer flask overnight. On the second day, overnight culture was centrifuged at 4100 x g, 8 min, 25°C, the supernatant was discarded and the cell pellet was resuspended in 500 ml fresh LB-Kan-Amp-Tet medium in 1 L Erlenmeyer flask with baffles. The culture was grown at 37°C, 120 rpm until OD_{600} reached between 3 - 4. The culture was spun down again (4000 x g, 15 min, 25°C) and the cell pellet was resuspended in 1 L fresh LB-Kan-Amp-Tet medium in a 2 L Erlenmeyer flask with baffles. Then cells were grown at 37°C for 30 minutes, followed by culturing at 25°C for 30 minutes. The cell culture was subsequently induced with 1mM IPTG overnight (15-16h) at 120 rpm, 25°C. On the third day, the overnight culture was centrifuged at 4000 x g, 15 min, 4°C. Cell pellet was collected into a 50 ml Falcon tube and was stored in -80°C.

5.6.3.4 Purification of proteins with polyhistidine tag (His-tag).

This protocol applies to Sortase A, EGFP and mC1-LPETG purification.

Cell pellet was resuspended in 10 ml lysis buffer per gram and then transferred into a metal beaker, placed in ice-cooled water bath. Cells were lysed by using a Branson

sonicator: ½ inch tip, output control: 7, 40% duty cycle. Sonication was performed in six 5min cycles. To cool down the lysate, a 1.5-minute break was added between cycles. Cell lysates were centrifuged at 30000 x g, 30 min, 4°C. The supernatant was incubated with 5 ml Ni-NTA (nickel-nitrilotriacetic acid) agarose at 4°C and rotated for 1h. The beads that captured His-tagged proteins, were transferred into a 35 ml chromatography column, then His-tagged proteins were eluted by adding 50 ml elution buffer in 5 elution steps (each step 10 ml). Protein concentration of the eluates was determined by NanoDrop (setting 1 Abs = 1 mg/ml). Then the eluates were diluted with the same volume of lysis buffer to decrease imidazole to approximate 250 mM. Next, the pooled eluates were concentrated to a total of 5 ml by Sartorius VIVASPIN 20, 10 KDa MWCO (Molecular weight cut-off) protein concentrators. The concentrated proteins were centrifuged at 30000 x g, 30 min, 4°C to remove aggregates, and then loaded on HiLoad 26/600 Superdex 200 pg column, run "HiLoad 26_600_with fractionation" program.

After the program ended, fractions that contained the desired proteins (Sortase A: fraction 55-74, mC1-LPETG: fraction 69-84, EGFP: fraction 58-74) were pooled and then concentrated by Sartorius VIVASPIN 20, 10 KDa MWCO protein concentrators. The final concentration was measured by NanoDrop, sample type: other protein (E & MW).

NanoDrop settings for Sortase A: molecular weight: 23.46 KDa, molar extinction coefficient: 17420 M^{-1} cm^{-1}).

NanoDrop settings for mC1-LPETG: molecular weight: 19.35 KDa, molar extinction coefficient: 27180 M^{-1} cm^{-1}).

NanoDrop settings for EGFP: molecular weight: 26.94 KDa, molar extinction coefficient: 21890M^{-1} cm^{-1}).

Protein aliquots were prepared and stored at -80°C.

*Extra steps for mC1-LPETG purification: The beads that captured the His-tag on GST-SUMO3-mC1-LPETG-His_6 were transferred into a 35 ml chromatography column. Cleavage of the GST-SUMO3 was performed by incubating beads with 30 ml

lysis buffer supplemented with 250 µg GST-Senp2 protease for 1.5h on a rotator at room temperature. Then, the column was drained by gravity flow and the cleavage was repeated with fresh lysis buffer and protease for another 1.5 h. The beads were thoroughly washed by 50 ml wash buffer and 50 ml OSB buffer after cleavage, then proteins were eluted from the beads.

*Extra steps for EGFP purification: The beads that captured His_6-SUMO3-EGFP were transferred into a 35 ml chromatography column. Next, two steps of SUMO3 cleavage were performed by adding 250 ug His_6-senp2, rotated for 3h at room temperature. EGFP was cleaved off the beads, therefore, the flow-through was collected and concentrated to a total of 5 ml.

5.6.3.5 Purification of proteins with glutathione-s-transferase tag (GST-tag).

This protocol applies to GST-Senp2 purification.

Cells were resuspended in 10 ml lysis buffer per gram of wet cell weight, then the cells were lysed by a sonicator (½ inch tip, output control: 7, 60% duty cycle). 4 cycles of sonication were performed, with 1.5-minute breaks between sonication cycles. Cell lysate was centrifuged at 30000 x g, 20 min, 4°C, and then the supernatant was incubated with 1 ml Pierce™ glutathione agarose and rotated for 2h at 4°C. The beads that captured GST-tagged Senp2 were separated from cell lysate by a 14 ml chromatography column, followed by washing with 30 ml wash buffer and 20 ml lysis buffer. Next, GST-Senp2 was eluted by adding 4 x 1 ml elution buffer. Pooled eluates were dialyzed against 500 ml storage buffer overnight at 4°C.

On the following day, dialyzed proteins were collected and centrifuged at 22000 x g, 20 min, 4°C to remove aggregates. Concentration was measured by NanoDrop (setting 1 Abs = 1 mg/ml), Aliquots were prepared and stored at -80°C.

5.6.3.6 Mfge8-EGFP and C1C2-EGFP purification.

HEK293 cells stably transfected with respective constructs (pcDNA3.1 Mfge8-EGFP-FLAG or pcDNA3.1 C1C2-EGFP-FLAG) were cultured in Ex-Cell 293 serum-free medium added with 1 % penicillin/streptomycin and 2 mM HEPES. 300 ml cells with a

viability > 85% and density of 1.5 - 2.5 x 10^6 cells/ml were used to inoculate 3 L of fresh in Ex-Cell 293 serum-free medium in the Labfors Bioreactor, the fermentation took 5 days (pH 7.4, pCO_2: 5%). Supernatant was collected by centrifugation at 300 x g, 10 minutes to remove cells. Supernatant was incubated with , 5.7 mM L-Glutamic acid, 350 mM NaCl, 3.5 mM L-Leucine, 18mM L-Arginine and 0.5% Triton X for 1 hour at 4°C. Followed by a high-speed centrifugation at 20000 x g, 90 minutes and filtration (0.2 um) to remove cell debris. Clarified supernatant was then purified by using FLAG affinity chromatography (M2-FLAG-agarose beads, which captured FLAG-tag on the C-terminal of Mfge8-EGFP and C1C2-EGFP). The bead- bound proteins were eluted by incubating and rotating with an excess of FLAG-peptide (30 mL Arg-Glu buffer mixed with 5 mg of FLAG-peptides) for 1h at 4°C. The eluted proteins were then concentrated to approximate 1 - 2 mg/ml. Mfge8-EGFP and C1C2-EGFP absorbance at wavelength of 488 nm (EGFP absorbance) were measured by NanoDrop. Concentrations (mg/ml) were calculated respectively:

C(Mfge8-EGFP) = Absorbance at 488nm / 56000 $M^{-1}cm^{-1}$ (EGFP molar extinction coefficient) x 81200 g/mol (Mfge8-EGFP molecular weight)

C(C1C2-EGFP) = Absorbance at 488nm / 56000 $M^{-1}cm^{-1}$ (EGFP molar extinction coefficient) x 65000 g/mol (C1C2-EGFP molecular weight)

Purification was performed by PD. Dr. Jan Kranich, Christine Ried, Beatrice Rauter, Tijana Kandic and Dr. Pallavi Pranita, protocol described in previous publication (Trautz et al., 2017).

5.6.4 Biotinylation by sortase-mediated transpeptidation reaction.

Method was adopted from (Guimaraes et al., 2013).

Table 12. Sortase reaction mix

mC1-LPETG	50 uM
Sortase A	50 uM
GGG-TEVcs-K(biotin)	1 mM
1x Sortase reaction buffer (dilute from 5x stock)	
H_2O	

The sortase reaction mix was left at room temperature (RT) for at least 1h. Then 3x the reaction-volume of sortase stop buffer was added and incubated on ice for 20

minutes to stop the reaction. Next, the reaction mix with stop buffer was concentrated to a total of 5 ml, followed by centrifugation at 22000 x g, 30 min, 4°C to remove aggregations. Then the supernatant was loaded on HiLoad 26/600 Superdex 200 pg column that was pre-equilibrated with OSB buffer and gel-filtration was performed ("HiLoad 26_600_with fractionation" program). After the purification, fractions that contained mC1-biotin (fraction: 69-83) were collected and then concentrated to at least 3 mg/ml. Aliquots were prepared and stored at -80°C.

5.6.5 SA-OVA conjugation

Streptavidin Conjugation Kit - Lightning-Link® was used to conjugate OVA with streptavidin (SA). Lyophilized SA provided in the kit was dissolved in 1ml PBS (c=1 mg/). In parallel, 200 ul modifier was added to another 1ml 1 mg/ml OVA. Then, dissolved SA and OVA with modifier were mixed together and incubated at 25 °C, 500 rpm overnight. On the next day, 200 ul quencher was added to the mix and incubated for 1h to stop the reaction. The conjugation mix was then centrifuged at 30000 x g, 30 min, 4°C to remove aggregates and afterwards loaded on HiLoad 26/600 Superdex 200 pg column and gel-filtration was performed ("HiLoad 26_600_with fractionation" program).

After the purification, all fractions were collected and samples of each peak were run on the SDS-PAGE. Fractions 32-39 were shown to contain OVA-SA 1:1 conjugation. These fractions were pooled and concentrated to a volume of 1 ml. Concentration of the purified protein was measured by ELSA (anti-OVA). Aliquots were prepared and stored at -80°C.

5.6.6 mC1 tetramer formation

Streptavidin has four biotin binding sites, but to ensure sufficient tetramer formation, a 5x molar excess of mC1-biotin was mixed with 1 mol SA. The mix was incubated for 30 minutes on ice. Then the mix was centrifuged at 30000 x g, 30 min, 4°C to remove aggregations. Concentration of the tetramer was measured by ELSA. Aliquots were prepared and stored at -80°C.

5.6.7 Fluorochrome labelling

Fluorescent proteins (OVA) were used to detect antigen specific B cells. Alexa Fluor™ 647 and Alexa Fluor™ 488 Protein Labelling Kits were used to label OVA. 1ml x 2 mg/ml PBS dissolved OVA was mixed with 100 ul 1 M bicarbonate buffer provided in the kits. Then the protein solution was mixed with one vial of reactive dye and incubated at RT for 1h. Next, the reaction mix was added to a Dye Removal Spin Column provided in the kits. The column was placed in a collection tube and centrifuged together at 1000 x g for 2 minutes. Fluorochrome-labelled proteins collected in the tube were measured the absorbance at 280 nm (A_{280}) and at the maximum absorbance wavelengths (A_{dye}) by NanoDrop.

The concentration of labelled protein was calculated according to the formula:

Protein concentration (M) = [A_{280} – (A_{dye} x CF_{280})] x dilution factor / molar extinction coefficient at 280 nm ($cm^{-1}M^{-1}$).

*CF_{280} is a correction factor for the fluorochrome's contribution to the absorbance at 280 nm (Alexa Fluor™ 488: 0.11, Alexa Fluor™ 647: 0.03).

Labelled proteins were stored as small aliquots in -80°C.

5.6.8 Cell isolation and prepare of single cell suspension.

5.6.8.1 Isolation of splenocytes.

Mice were euthanized by cervical disloaction or CO2, then moistened and disinfected with 70% ethanol. Spleen was removed and kept in FACS buffer on ice until use. Single splenocyte suspension was generated by squeezing the spleen between two coarse nylon meshes using tweezers in a petri dish. Cells were collected in a 15ml Falcon tube, the nylon meshes and petri dish were washed three times to collect residual cells. The cell suspension was centrifuged at 1500 rpm at 4 °C for 5 minutes to pellet the cells. Cells were resuspended in 1ml red blood cell lysis buffer (ACK buffer), then cell suspension was incubated for 5 minutes at RT. The lysis was stopped by adding 12ml FACS buffer and then centrifuged at 1500 rpm at 4 °C for 5 minutes,

supernatant was discarded, the cell pellet was resuspended in 5ml FACS buffer and filtered through 40um mesh.

5.6.8.2 Bone marrow cells isolation.

Mice were euthanized by cervical disloaction or CO_2, then moistened and disinfected with 70% ethanol. The rear legs were cut and the flesh removed with a scalpel. Bones were kept in FACS buffer on ice until use. Bone marrow was collected by cutting below and above the knee, then flushed out the bone marrow with FACS buffer from femur and tibia using a 25-27G syringe. Bone marrow was collected and resuspended in a 15ml Falcon tube and centrifuged at 1500 rpm for 5 minutes at 4 °C. The cell pellet was resuspended in 1ml ACK buffer and incubated for 5 minutes at RT. The lysis was stopped by adding 12ml FACS buffer and then centrifuged at 1500 rpm at 4 °C for 5 minutes, supernatant was discarded and the cell pellet resuspended in 5ml FACS and filtered through 40um mesh.

5.6.9 Staining of cells for flow cytometry.

Single cell suspension was firstly counted using a CASY TT cell counter: 10ul of the single cell suspension was gently resuspended with 10ml CASYton buffer in a CASY cup (1:1000 dilution). Counting parameters are shown in Table 13.

Table 13. CASY TT cell counter settings.

CASY TT cell counter program 1 for measuring mouse splenocytes.	
Capillary	150 um
Sample volume	400 ul
X - axis	15 um
Cycles	2
Evaluation cursor	5.14–15 um
Normalization cursor	1.01–15 um
Debris	On
Aggregation correction	Off

Around 2 x 10^6 cells from each sample were transferred into one well of a 96-well round-bottom plate. The plate was centrifuged at 1500 rpm at 4°C for 5 minutes, then the supernatant was discarded, the cells pellet was dissociated by vertexing and stained with 10ul Fc-block (1:1000 diluted) for 10 minutes on ice. Followed by staining with 100ul antibody mix for 20 minutes on ice. Next, 100ul FACS buffer was added and the plate was centrifuged for 2 minutes at 1500rpm at 4 °C. The supernatant was

discarded and the cells were washed with 200ul FACS buffer twice. Finally, cells were resuspended in 200ul FACS buffer (40ul for image flow cytometry) and filtered into FACS tubes. Samples were kept on ice until FACS analysis.

Intracellular staining for cytokines was performed after surface markers staining. Cells were fixed with 100ul per well Fixation/Permeabilization solution from BD Cytofix/Cytoperm^{TM} kit. After fixation at 4°C for 20 minutes, cells were washed twice with 250ul per well 1× BD Perm/Wash™ buffer. Then the cells were stained with 100ul intracellular staining antibodies mixed in 1× Perm/Wash™ buffer. After 30 minutes incubation at 4°C, cells were washed twice with 250ul per well 1× Perm/Wash™ buffer and finally resuspended in FACS buffer for analysis.

5.6.10 T cell in vitro re-stimulation assay.

Mice were intravenously immunized with either 0.7 nmol OVA, OVA-SA or OVA-SA-mC1 tetramer + 50 ug anti-CD40 antibodies. On day 7 splenocytes were isolated, 2 x 10^6 cells in 100 ul T cell culture medium were plated into a 96-well plate. Next, 50 ul 20 ug/ml OVA peptides (OVA_{55}, OVA_{107} and OVA_{257}) and 25 ul 1:38 diluted PE conjugated anti-CD107a antibodies were mixed with cells. Negative controls and positive controls were prepared by substituting OVA peptide with 50 ul fresh medium or 50 ul mixture of 1:250 diluted PMA (phorbol 12-myristate 13-acetate) + 1:125 diluted ionomycin, respectively. Cells were cultured at 37°C for 1h. Then, 25 ul 1:125 diluted monensin was added to block secretion of cytokines. Cells were then cultured for another 3h at 37°C. Next, cells were collected and intracellularly stained for cytokines (IFN-γ and CD107a for CD8 T cells, IFN-γ and IL-2 for CD4 T cells), and subsequently acquired on a BD FACSCanto™ II Flow Cytometer.

5.6.11 CD8 T cell memory recall assay.

Mice were intravenously injected with either 0.7 nmol of OVA or OVA-SA-mC1 tetramer mixed with 50 ug CPG as primary immunization. 27 days later, all mice were boosted with OVA peptides (mixture of 50 ug OVA_{55}, 50 ug OVA_{107}, 50 ug OVA_{257} peptides, 100 ug PolyI:C and 50 ug anti-CD40 antibodies). 4 days later, splenocytes were isolated and in vitro re-stimulated with OVA peptides as described in “5.6.10 T cell in vitro restimulation assay”.

5.6.12 CTL in vivo killing assay.

Two groups of mice were intravenously immunized with either 0.7 nmol OVA-SA or OVA-SA-mC1 tetramer + 50 ug anti-CD40 antibodies for 7 days. On the last day, another group of naïve mice were used to isolate splenocytes. Half of the naïve splenocytes were pulsed with 10 uM (10 ug/ml) OVA_{257} peptides for 1.5 h, cultured in T cell culture medium at 37°C. Then these peptides pulsed splenocytes were labelled with 5 uM carboxyfluorescein succinimidyl ester (CFSE), noted as $CFSE^{hi}$ cells. In parallel, the other half of naïve solenocytes were labelled with 0.5 uM CFSE, noted as $CFSE^{lo}$ cells. $CFSE^{hi}$ and $CFSE^{lo}$ cells were mixed 1:1, then these mixtures of cells were injected intravenously into the immunized mice (each mouse received around 4 x 10^7 cells). 2-8h later, blood samples from these immunized mice were collected into 15 ml falcon tubes containing 1 drop of heparin and 5 ml PBS. Cells were centrifuged at 1500 rpm, 4 °C for 5 minutes and supernatant was carefully discarded. Red blood cells were lysed by incubating with 3 ml ACK buffer for 7 minutes, followed by two washes with 10 ml PBS and centrifugation at 1500 rpm for 5 minutes. Cells were acquired on a BD FACSCanto™ II Flow Cytometer. CTL killing efficiency was calculated by the ratio of $CFSE^{hi}$ to $CFSE^{lo}$ cells (r). A lower r represented higher CTL killing efficiency.

5.6.13 Western blot (SDS-PAGE)

12 % SDS gels were prepared according to the following recipe:

Table 14. Separating gel recipe

Acrylamide (30%)	10 ml
1.5 M Tris-HCl (pH 8.8)	6.25 ml
10 % SDS	250 ul
10 % Ammonium persulfate (APS)	250 ul
H_2O	8.25 ml
Tetramethylethylenediamine (TEMED)	25 ul

Table 15. Stacking gel recipe

Acrylamide (30%)	1.04 ml
1 M Tris-HCl (pH 6.8)	0.79 ml
10 % SDS	62.5 ul
10 % APS	62.5 ul
H_2O	4.25 ml
TEMED	6.25 ul

Separating gels were prepared first in glass plates with a 1 mm spacer. After the separating gels were solidified, stacking gels were poured on the top of separating gels, 15-well combs were inserted between the glass plates on the top to create sample loading wells.

After loading the samples into the wells, gels were placed in a Mini-PROTEAN® 3 Electrophoresis System and run at 80 V until protein samples crossed the stacking gels. Then the voltage was changed to 130 V and run until the excessive bromophenol blue ran out of the separating gel from the bottom.

After the electrophoresis, gels were either stained with Coomassie blue G-250 staining buffer for 1h and washed with H_2O for a assessment of protein expression, otherwise, the gels were assembled with a nitrocellulose blotting membrane, filter papers and sponges on both sides in a transfer cassette. The protein transferring took 90 minutes at 90 V in cold room (4°C). Then the membranes were blocked with 5 % BSA in PBS + 0.1% Tween-20 (PBST buffer) for 2h at RT, followed by incubation with primary antibodies overnight in the cold room. On day 2, membranes were washed with PBST buffer 3 x 15 minutes. Then the membranes were incubated with HRP conjugated secondary antibodies for 1h at RT. After washing with PBST buffer 3 x 15 minutes, enhanced chemiluminescence (ECL) western blot substrates were applied to the membrane. The images were acquired with a Sapphire Biomolecular Imager.

5.6.14 Cell sorting

5.6.14.1 Magnetic cell sorting

The Germinal Center B Cell (PNA) MicroBead Kit (Miltenyi Biotec) was used to isolate PNA+ GC B cells. Single-cell suspensions of splenocytes were prepared from immunized mice. After centrifugation at 300 × g for 10 minutes, cells were resuspended in 40ul MACS buffer per 10^7 cells then 10 ul PNA-biotin per 10^7 cells were added. Cells were incubated for 5 minutes at 4°C. Next, 30 ul MACS buffer and 20 ul anti-biotin microbeads were added per 10^7 cells. Followed by another incubation for 10 minutes at 4°C. After incubation, cells were washed with 1 ml (per 10^7 cells) MACS buffer and centrifuged at 300 × g, 10 minutes. The cell pellets were resuspended in 500 ul MACS buffer and then applied to the MACS columns placed in a magnetic field (MACS separator). Flow-throughs were discarded and the columns

were washed with 3 ml MACS buffer for 3 times. Then the columns were removed from the magnetic field and put onto collection tubes. 5 ml MACS buffer was added to the columns and magnetically labelled PNA+ GC B cells were flushed out by firmly pushing the plunger into the column.

5.6.14.2 Fluorescence-activated cell sorting (FACS).

Surface makers were stained on isolated PNA+ GC B cells (see "5.6.9 Staining of cells for flow cytometry") In addition to this, each sample was stained with a unique sample tag antibody (anti MHC-I) from the BD™ Single-Cell Multiplexing Set. All stained cells were pooled together and transferred into PBS + 0.5 % BSA + 2 mM EDTA to prevent formation of aggregates. Additionally, 25 mM HEPES was added to maintain a neutral pH during cell sorting. Cells were diluted to 10^6 cells/ml, and a BD FACSAria™ Fusion Flow Cytometer with a 100um nozzle was used to sort EGFP specific GC B cells. Sorting precision mode was set to "Purity" and the event rate was adjusted to 600 – 1500 evts/sec. Cells were collected in 1.5 ml Eppendorf LoBind tubes that had been precoated with 100% FCS for 1h and filled with 500 ul PBS + 50 % FCS for collection.

5.6.15 Full length BCR and targeted mRNA library preparation.

Sorted EGFP specific GC B cells were centrifuged at 400 × g for 5 minutes, the supernatant was discarded and the cell pellet was resuspended in 620 ul cold Sample Buffer provided in the BD Rhapsody™ Enhanced Cartridge Reagent Kit. Cell viability was measured by staining cells with 3.1 µL of 0.3 mM DRAQ7™ and 3.1 uL of 2 mM Calcein AM. 10 ul cells were loaded into the INCYTO™ disposable hemocytometer and cells were counted using the BD Rhapsody™ Scanner. Cells that showed viability > 70 % were loaded onto the BD Rhapsody™ Cartridge that had been primed by 100 % ethanol and cartridge wash buffer 1 and 2. After 15 minutes incubation, 630 ul BD Rhapsody™ Enhanced Cell Capture Beads were loaded onto the cartridge, placed in the BD Rhapsody™ Express System and incubated for 3 minutes at room temperature, followed by 2 washes with 700 ul cold Sample Buffer. Next, the left slider on the Express System was moved to "LYSIS", 550 ul Lysis Buffer with DTT was added to the cartridge and incubated for 2 minutes at RT. After the incubation, the front slider of Express System was moved to "BEADS", while the left slider was moved to "RETRIEVAL" to place the retrieval magnet lid on the top of the cartridge for 30s. Then the left slider was moved to "0" and the cartridge was immediately loaded with

4950 ul Lysis Buffer with DTT. Beads that captured mRNA molecules from single-cell lysates were retrieved into a 5 mL LoBind tube placed in the drawer of the Express System. The 5 mL LoBind tube containing retrieved beads was placed on a large magnet with the 15 mL tube adapter for 1 minute. The supernatant was carefully discarded, beads were transferred into a new 1.5 ml LoBind tube and washed with 1 ml cold Bead Wash Buffer, the tube was subsequently placed on a 1.5 ml magnet and the supernatant was discarded. The beads were then stored in 1 ml cold Bead Wash Buffer on ice.

The reagents for cDNA synthesis and template switching were provided in the BD Rhapsody™ cDNA Kit. cDNA / template switching mix was prepared as follows:

Table 16. cDNA / template switching mix.

Component	Volume (ul) with 20% overage
RT Buffer	48.0
dNTP	24.0
RT 0.1 M DTT	12.0
Bead RT/PCR Enhancer	14.4
RNase Inhibitor	12.0
Reverse Transcriptase	12.0
Nuclease-Free Water	117.6

The supernatant of the beads was removed on the magnet, subsequently 200 ul of cDNA / template switching mix was added. The beads were incubated on the ThermoMixer at 1200 rpm, 42 °C for 30 minutes. Then, 8 ul of template switch oligo (TSO) mix was added to the reaction and incubated at 1200 rpm, 42 °C for another 30 minutes.

Table 17. TSO mix.

Component	Volume (ul) with 20% overage
TSO	7.2
1M $MgCl_2$	2.4

After reverse transcription and template switching, the tube was placed on a magnet and the supernatant was removed. The beads were subsequently added with 75 ul Elution Buffer and incubated at 95 °C for 5 minutes to denature. The tube was centrifuged and then placed on a magnet. The supernatant contained sample tags and was collected in a new 1.5 ml LoBind tube, stored at 4 °C. The beads were

resuspended in 1 ml Hybridization Buffer and incubated at 1200 rpm, 25 °C for 2 minutes.

For BCR extension, the tube was placed on a magnet and the supernatant was removed. Then 200 ul BCR extension mix was added to the beads and incubated at 1200 rpm, 37 °C for 30 minutes. The supernatant was discarded on the magnet.

Table 18. BCR extension mix.

Component	Volume (ul) with 20% overage
BCR Extension Buffer	24
dNTP	24
BCR Extension Enzyme	12
Nuclease-free water	180

To remove surplus reverse transcription primers, 200 ul exonuclease I mix was added to the beads and incubated at 1200 rpm for 30 minutes, 37 °C. Then the exonuclease I was inactivated by incubation for 20 minutes at 80°C. The supernatant was removed and the beads were stored in 200 ul cold Bead Resuspension Buffer at 4 °C.

Table 19. Exonuclease I mix.

Component	Volume (ul) with 20% overage
10x Exonuclease I Buffer	24.0
Exonuclease I	12.0
Nuclease-Free Water	204.0

On the next day, full length BCR, sample tag and targeted mRNA libraries were prepared by nested PCR.

For sample tag library, 67 ul of the sample tag product was mixed with 133 ul sample tag PCR1 reaction mix, 50 ul per aliquot was prepared in 0.2 ml PCR tubes and run the PCR program on thermal cycler.

Table 20. Sample Tag PCR1 reaction mix.

Component	Volume (ul) with 20% overage
PCR MasterMix	120
Universal Oligo	12
Sample Tag PCR1 primer	1.2
Nuclease-free water	26.4

Table 21. PCR1 program for Sample Tag.

Step		Temperature °C	Time	Note
1	Hot start	95.0	3 min	
2	Denaturation	95.0	30 s	
3	Annealing	60.0	30 s	Repeat steps 2 – 4
4	Extension	72.0	1 min	11 cycles
5	Final extension	72.0	5 min	
6	Hold	4.0	--	

After the PCR, 4 aliquots were combined together into a new 1.5 ml LoBind tube, labelled Sample Tag PCR1.

In parallel, PCR1 reaction for the BCR panel was performed on the beads. The supernatant from exonuclease I - treated beads was removed on a magnet first, then the beads were resuspended in 200 ul BCR panel PCR1 reaction mix and 50 ul aliquots were prepared in 0.2 ml PCR tubes. Next, the tubes were placed in a thermal cycler and the PCR1 program for BCR panel was run.

Table 22. BCR panel PCR1 reaction mix.

Component	Volume (ul) with 20% overage
PCR MasterMix	120
BCR Universal Oligo N1	12
Bead RT/PCR Enhancer	14.4
Mouse BCR N1 primer	2.88
Nuclease-free water	90.72

Table 23. PCR1 program for BCR panel.

Step		Temperature °C	Time	Note
1	Hot start	95.0	3 min	
2	Denaturation	95.0	30s	

3	Annealing	60.0	1 min	Repeat steps 2 – 4
4	Extension	72.0	1 min	11 cycles
5	Final extension	72.0	5 min	
6	Hold	4.0	--	

After the PCR, 4 aliquots were placed on a strip tube magnet for 30 s. Supernatants were combined in a new 1.5 ml tube, labelled as BCR PCR1

The beads were washed with 50 ul Elution Buffer, incubated at 95 °C for 1 minute, then the supernatant was discarded and the beads were prepared for Targeted mRNA panel. 50 ul of Targeted mRNA panel PCR1 reaction mix was added into each tube (4 aliquots in 0.2 ml PCR tubes), then placed in a thermal cycler and the PCR1 program for Targeted mRNA panel was run.

Table 24. Targeted mRNA panel PCR1 reaction mix.

Component	Volume (ul) with 20% overage
PCR MasterMix	120
Universal Oligo	12
Bead RT/PCR Enhancer	14.4
PCR1 targeted mRNA primer panel	48
Nuclease-free water	45.6

Table 25. PCR1 program for Targeted mRNA panel.

Step		Temperature °C	Time	Note
1	Hot start	95.0	3 min	
2	Denaturation	95.0	30 s	
3	Annealing	60.0	3 min	Repeat steps 2 – 4
4	Extension	72.0	1 min	11 cycles
5	Final extension	72.0	5 min	
6	Hold	4.0	--	

After the PCR, 4 aliquots were combined together and placed onto a magnet, the supernatants were collected into a new 1.5 ml LoBind tube, labelled Targeted mRNA PCR1.

All PCR1 products were purified using AMPure XP beads and subsequently performed PCR2 reactions separately.

The different PCR2 reaction mixes were prepared as follows:

Table 26. BCR panel PCR2 reaction mix.

Component	Volume (ul) with 20% overage
PCR MasterMix	30
BCR Universal Oligo N2	2.4
Mouse BCR N2 primer	7.2
Nuclease-free water	14.4

Table 27. Targeted mRNA panel PCR2 reaction mix.

Component	Volume (ul) with 20% overage
PCR MasterMix	30
Universal Oligo	2.4
PCR2 targeted mRNA primer panel	12
Nuclease-free water	9.6

Table 28. Sample Tag PCR2 reaction mix.

Component	Volume (ul) with 20% overage
PCR MasterMix	30
Universal Oligo	2.4
Sample Tag PCR2 Primer	3.6
Nuclease-free water	18

4 ul of purified PCR1 products (from BCR, Targeted mRNA and Sample tag products) were mixed with 45 ul of the corresponding PCR2 reaction mix in 0.2 ml PCR tubes. Then the tubes were placed in a thermal cycler and the respective PCR2 program was run as follows.

Table 29. PCR2 program for BCR panel.

Step	Cycles	Temperature °C	Time	Note
1	1	95.0	3 min	
2	Repeat steps 2 – 4 15 cycles	95.0	30 s	
3		70.0 – 55.0	1 min	Each cycle decreases by 1 °C
4		72.0	1 min	
5	Repeat steps 5 – 7 8 cycles	95.0	30 s	
6		55.0	1 min	
7		72.0	1 min	
8	1	72.0	5 min	
9	1	4.0	--	

Table 30. PCR2 program for Targeted mRNA panel.

Step		Temperature °C	Time	Note
1	Hot start	95.0	3 min	
2	Denaturation	95.0	30 s	
3	Annealing	60.0	3 min	Repeat steps 2 – 4
4	Extension	72.0	1 min	10 cycles
5	Final extension	72.0	5 min	
6	Hold	4.0	--	

Table 31. PCR2 program for Sample Tag.

Step		Temperature °C	Time	Note
1	Hot start	95.0	3 min	
2	Denaturation	95.0	30 s	
3	Annealing	66.0	30 s	Repeat steps 2 – 4
4	Extension	72.0	1 min	10 cycles
5	Final extension	72.0	5 min	
6	Hold	4.0	--	

All PCR2 products were purified by AMPure XP beads, the eluates were stored in new 1.5 ml LoBind tube separately, labelled BCR, Sample tag, and Targeted mRNA PCR2 products. Concentration of PCR2 products were measured by a Qubit Fluorometer using the Qubit dsDNA HS Assay Kit.

BCR panel PCR2 product was diluted to 1.0 ng/ul. Then 5 ng were mixed with 41.5 ul Random primer mix and placed on the thermocycler, then the BCR random priming program was run.

Table 32. Random primer mix.

Component	Volume (ul) with 20% overage
BCR Extension Buffer	6
BCR Extension Primers	3
Nuclease-free water	40.8

Table 33. BCR random priming program.

Step		Temperature °C	Time	Note
1	Denaturation	95.0	3 min	
2	Random priming	37.0	30 s	1 cycle
3		25.0	30 s	

After BCR random priming, 3.5 ul primer extension enzyme mix was added into the random priming reaction tube (total volume 50 ul). Then the random priming extension program was run on a thermocycler.

Table 34. Primer extension enzyme mix.

Component	Volume (ul) with 20% overage
dNTP	2.4
BCR Extension Enzyme	1.8

Table 35. Random priming extension program.

Step	Temperature °C	Time	Note
1	25.0	10 min	
2	37.0	15 min	
3	45.0	10 min	1 cycle
6	55.0	10 min	

The BCR random priming extension (RPE) product was purified by AMPure XP beads, then stored in a new tube and labelled as BCR RPE product.

Next, full-length Illumina sequencing adapters and indices were added to the BCR RPE product, Sample tag and Targeted mRNA PCR2 products through a index PCR. For the BCR library, 21 ul of undiluted RPE product was added to 29 ul index PCR reaction mix.

Table 36. Index PCR reaction mix for BCR RPE product.

Component	Volume (ul) with 20% overage
PCR MasterMix	30
Library Forward Primer	2.4
Library Reverse Primer 1	2.4

For the Targeted mRNA library, the PCR2 product was diluted to 0.5 ng/ul, 3 ul were added to 47 ul index PCR reaction mix.

For the Sample tag library, 3 ul of 0.1 – 1.1 ng/ul PCR2 product was added to 47 ul index PCR reaction mix.

Table 37. Index PCR reaction mix for Sample tag and Targeted mRNA PCR2 products.

Component	Volume (ul) with 20% overage
PCR MasterMix	30
Library Forward Primer	2.4
Library Reverse Primer 1	2.4
Nuclease-free water	21.6

The reaction tubes for the BCR and Targeted mRNA libraries were placed together in a thermal cycler and the same index PCR program was run. The Sample tag library was prepared in a different program.

Table 38. Index PCR program for BCR and Targeted mRNA libraries.

Step		Temperature °C	Time	Note
1	Hot start	95.0	3 min	
2	Denaturation	95.0	30 s	
3	Annealing	60.0	30 s	Repeat steps 2 – 4
4	Extension	72.0	30 s	10 cycles
5	Final extension	72.0	1 min	
6	Hold	4.0	--	

Table 39. Index PCR program for Sample Tag libraries.

Step		Temperature °C	Time	Note
1	Hot start	95.0	3 min	
2	Denaturation	95.0	30 s	
3	Annealing	60.0	30 s	Repeat steps 2 – 4
4	Extension	72.0	30 s	6 cycles
5	Final extension	72.0	1 min	
6	Hold	4.0	--	

The products of the index PCR were purified by AMPure XP beads, then stored in new tubes and labelled as final sequencing libraries. Concentration of each library was measured by a Qubit Fluorometer and Agilent 2100 Bioanalyzer. The libraries were then sent for sequencing.

Primers used in this protocol:

Table 40. Mouse B cell PCR1 primers.

Primer name	Sequence 5´ → 3´
Ms_IGHA_N1	AACTGGCTGCTCATGGTGTA
Ms_IGHD_N1	AAGTGTGGTTGAGGTTCAGTTCTG
Ms_IGHE_N1	GAAGTTCACAGTGCTCATGTTC
Ms_IGHG1_N1	CAGAGTGTAGAGGTCAGACT
Ms_IGHG2A-IGHG2C_N1	TCGAGGTTACAGTCACTGAG
Ms_IGHG2B_N1	GATCCAGAGTTCCAAGTCACAG
Ms_IGHG3_N1	TACGTTGCAGATGACAGTCT
Ms_IGHM_N1	TGGATGACTTCAGTGTTGTTCTG
Ms_IGKC_N1	TGTAGGTGCTGTCTTTGCTG
Ms_IGLC1_N1	CTGTAACTGCTATGCCTTTCCC
Ms_IGLC2-IGLC3_N1	TTGGTGGGATTTGAAGTGTCC

Table 41. Mouse B cell PCR2 primers.

Primer name	Sequence 5´ → 3´
Ms_IGHA_N2	TGTCAGTGGGTAGATGGTGG
Ms_IGHD_N2	CTGACTTCCAATTACTAAACAGCC
Ms_IGHE_N2	TAGAGCTGAGGGTTCCTGATAG
Ms_IGHG1_N2	CAGTGGATAGACAGATGGGGGT
Ms_IGHG2A-IGHG2C_N2	ATGGGGCTGTTGTTTTGG
Ms_IGHG2B_N2	GTGGATAGACTGATGGGGGTGTT
Ms_IGHG3_N2	AGGGAAGTAGCCTTTGACAAG
Ms_IGHM_N2	GACATTTGGGAAGGACTGACTC
Ms_IGKC_N2	AGATGTTAACTGCTCACTGGATG
Ms_IGLC1_N2	GTTAGTCTCGAGCTCTTCAGA
Ms_IGLC2-IGLC3_N2	CAGTGTGGCTTTGTTTTCCT

5.6.16 EV isolation

Bone marrow cells were collected according to the protocol described in “5.6.8.2 Isolation of bone marrow cells”. The collected cells were centrifuged at 1500 rpm, 8

minutes at 4 °C. Then the cell pellet was resuspended in BMDC differentiation medium to a concentration of 1 x 10^6 cells/ml. Cells were cultured in T175 flasks for 6 days at 37 °C, 5 % CO_2. On day 3, old culture medium was discarded and fresh medium added. On day 6, BMDCs were collected and transferred to BMDC stimulation medium (3 x 10^5 cells/ml) and cultured for 72 hours.

After BMDC stimulation, supernatant was collected by centrifugation at 2000 x g, 20 minutes at 4 °C, then cell debris were removed by filtering through 0.2 um filter. The supernatant was further centrifuged at 100,000 x g, 120 minutes at 4 °C to precipitate EVs. The EV pellet was resuspended in 200 ul PBS with 1x protease inhibitor. (Concentrated to a total approximate 200ul if multiple tubes were used, by using Sartorius, Turbo 15 RC 100,000 MWCO, centrifuged at 2000 x g, 15 minutes). 200 ul EVs were added to 800 ul Diluent C and 4 ul PKH26 dye and incubated at room temperature for 5 minutes with periodic mixing, followed by incubation with 2 ml 1 % BSA for 1 minute to stop the staining reaction. The PKH26 stained EVs were washed with 4 ml PBS + protease inhibitor (3500 x g, 10 minutes, 4 °C), then purified by centrifugation at 160,000 x g, 18h at 4 °C in OptiPrep™ Density Gradient Medium.

The OptiPrep gradient contained:

- Layer 1: 650 ul OptiPrep medium + 475 ul EVs suspension.
- Layer 2: 1562 ul OptiPrep medium + 1562 ul PBS.
- Layer 3: 750 ul PBS.

Eight 500 ul fraction were collected from the top. Fraction 3 - 8 were confirmed to contain purified EVs (from previous study). These fractions were mixed and washed 5 times with 4 ml PBS with 1x protease inhibitor (centrifuged at 2000 x g, 10 minutes at 4 °C). The concentration of EVs were measured using a ZetaView® Particle Metrix nanoparticle tracker. EVs were then used to inject mice.

5.6.17 Immunofluorescence microscopy

Spleens from mice were removed and embedded in OCT cryo medium one day in advance. Cryosections were cut by a cryotome (-17°C, 7um thickness), the sections were left at room temperature for 1h to dry. Next, the sections were fixed in ice cold acetone (-20°C) for 10 minutes, followed by 30 minutes drying RT. The spleen

cryosections were encircled by a hydrophobic pen and then the sections were rehydrated and blocked with PBS + 0.5% BSA + 1% goat serum for 30 minutes in a humid chamber. Then 300ul antibody mix was added to the sections and incubated at RT for 1h. The slides were washed with PBS for 5 minutes, followed by staining with 1:1000 diluted DAPI for 5 minutes. Then the sections were washed with PBS twice. Finally, 200ul FLuoromount G mounting medium was added without air bubbles and the section covered with a coverslip. The slides were dried overnight at 4°C and analyzed on a fluorescence microscope.

5.7 Statistics and analysis software

Flow cytometry data were analysed using FlowJo, version 10.9.0. For the imaging flow cytometry data, IDEAS Application Version 6.2.189.0 was used for analysis. ImageJ 1.53a was used to process histology images.

Statistical analyses were performed on Prism 7 for Mac OS X, version 7.0e. Selection of unpaired t test with Welch's correction or one-way ANOVA with Holm-Sidak's multiple comparisons test was used depending on the number of groups. Parametric or non-parametric analyses were used depending on the equality of variance. Significance levels were labelled as: $p< 0.05$ (*), $p < 0.01$ (**), $p < 0.001$ (***) and $p < 0.0001$ (****). Bar graphs were shown as mean ± standard error (SE).

BCR and Targeted mRNA sequencing data were first aligned and annotated on the Seven Bridges Genomics platform, using the BD Rhapsody™ Sequence Analysis Pipeline. Statistical analyses were performed in R studio, version 4.3.0, platform: x86_64-apple-darwin20 (64-bit), run under macOS Big Sur 11.6.

R packages used in the analysis:

Table 42. R packages.

Name	Version
Alakazam	1.3.0
BiocManager	1.30.22
Biostrings	2.68.1
Clustree	0.5.1
Dowser	2.0.0
Dplyr	1.1.4
Drc	3.0.1
Ggplot2	3.4.4

Ggpubr	0.6.0
Ggtree	3.8.2
Immunarch	0.9.0
Irlba	2.3.5.1
Matrix	1.6.1.1
Purrr	1.0.2
Readr	2.1.4
Readxl	1.4.3
Scoper	1.3.0
Seurat	4.4.0
Shazam	1.2.0
Tidyverse	2.0.0

References were edited in EndNote 20.4. Analytical figures were processed in Affinity Designer 1.10.8 and 2.3.1. Schematic and illustrative figures were created from BioRender.

6. Results

6.1 Targeting EGFP to EVs promotes humoral immune response.

6.1.1 Mfge8-EGFP accumulates in the marginal zone.

Blood-borne EVs are rapidly eliminated from the circulation, as B cell–derived exosomes either injected intravenously (I.V.) or subcutaneously (S.C.) were rapidly captured and eliminated by $CD169^+$ SCS macrophages in the lymph node and marginal metallophilic macrophages in the MZ of the spleen (Saunderson et al., 2014). As it has been shown that EVs accumulate in lymphoid follicles, therefore, we tested the possibility of utilizing EVs in the circulation to bring antigens into the lymphoid follicles. For this, we utilized the endogenous PS binding protein Mfge8 and fused it to the model antigen EGFP (EV-targeting antigen, Figure 7 A). We hypothesized that the fusion protein Mfge8-EGFP will bind to PS on circulating EVs and then will be captured in the lymphoid follicle (Figure 7 B). To test this, Mfge8-EGFP was intravenously or intraperitoneally injected into the recipient mice. 1-1.5h later, spleens were taken to check the existence of EGFP signal. As expected, Mfge8-EGFP had accumulated in the MZ of lymphoid follicles, delimited by $CD169^+$ marginal metallophilic macrophages and SIGN-$R1^+$ MZ macrophages. Administration routes didn't affect the targeting capability of Mfge8-EGFP, as both I.V. and I.P. injections gave similar results. In contrast, conventional EGFP was not detected in the lymphoid follicle (Figure 7 C).

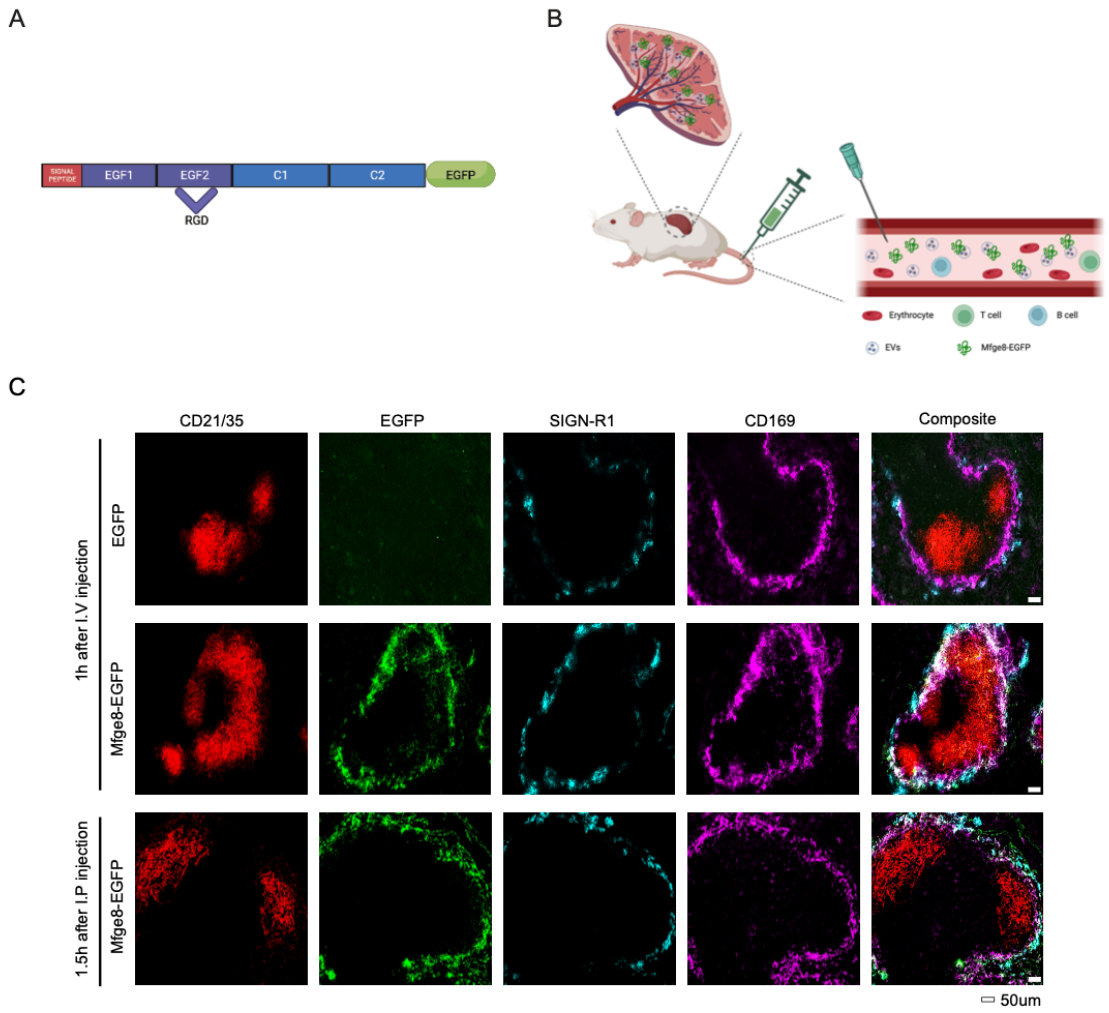

Figure 7 Mfge8-EGFP accumulates in the marginal zone.
(A) Schematic illustration of Mfge8-EGFP.
(B) Flow chart depicting the experimental setup of Mfge8-EGFP injection and hypothesized transport of EV-bound antigen to the spleen.
(C) Spleen sections from WT mice, 1h - 1.5h after intravenous or intraperitoneal injection of 1.8nmol Mfge8-EGFP or conventional EGFP. Scale bar 50 um. Staining antibodies: anti CD21/35 – PE, anti GFP – FITC, anti CD169 – APC, anti SIGN-R1 – BV421. N = 3.

We further tested Mfge8-EGFP binding on different cell types in the spleen 1h after I.V. injection by flow cytometry. Consistent with the immunohistochemical staining, marginal metallophilic macrophages ($CD11b^{+}CD169^{+}$), MZ macrophages ($CD11b^{+}$SIGN-$R1^{+}$) and the MZ B cells ($CD19^{+}CD21/35^{hi}CD23^{lo}$) were the major cell types that bound Mfge8-EGFP, followed by follicular B cells ($CD19^{+}CD21/35^{mid}CD23^{hi}$). T cells hardly bound any Mfge8-EGFP (Figure 8). These binding differences are probably attributed to the anatomic positions of these cells, cells located near marginal zone preferentially encounter blood borne EVs and proteins.

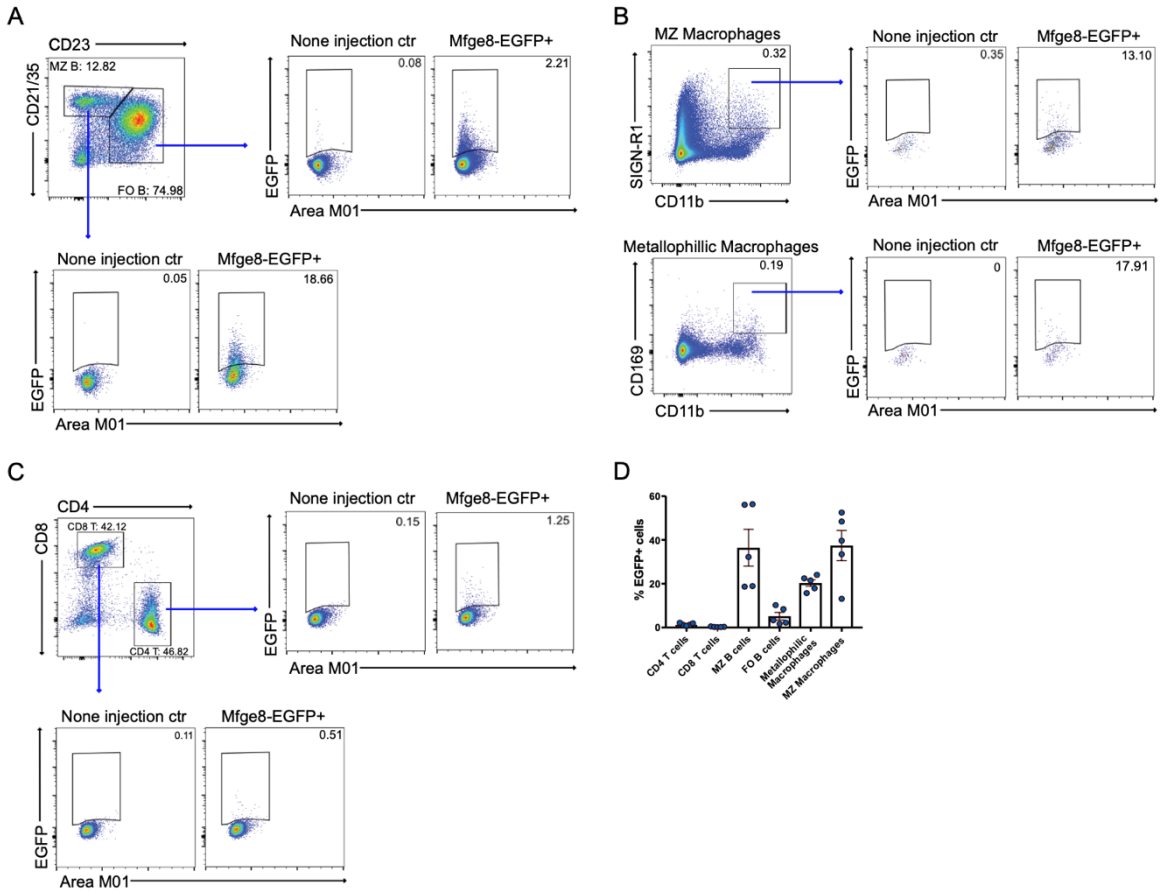

Figure 8. Mfge8-EGFP binding on different cell types.
Mice were injected 150ug Mfge8-EGFP intravenously, splenocytes were isolated after 1h and analyzed by flow cytometry.
(A-C) Representative gating strategy for Mfge8-EGFP bound cells. **(A)** MZ B cells ($CD19^+CD21/35^{hi}CD23^{lo}$) and follicular B cells ($CD19^+CD21/35^{mid}CD23^{hi}$). **(B)** Marginal metallophilic macrophages ($CD11b^+CD169^+$) and MZ macrophages ($CD11b^+SIGN\text{-}R1^+$). **(C)** $CD4^+$ and $CD8^+$ T cells. Plots shown are pre-gated on single live cells.
(D) Frequency of splenocytes bound Mfge8-EGFP after i.v. injection of 1.8 nmol Mfge8-EGFP for 1h. Mean ± SEM are shown, n = 5.

To test if Mfge8-EGFP bound to cells through EVs attached on cells, we used image-stream flow cytometry and a deep learning algorithm based on a convolutional autoencoder to classify Mfge8-$EGFP^+$ live cell images into apoptotic cells and PS^+ live cells carrying EVs on their surface (Kranich et al., 2020). From the EV^+ population, we measured expression and colocalization of the two exosome markers CD63 and CD81 (Yates et al., 2022a). The analysis showed that more than 60% of PS+ live cells co-expressed at least one of the exosome markers. Gating on Mfge8-$EGFP^+$ MZ B cells, we found that the frequency of cells co-expressing at least one of the exosome makers increased to over 95% (Figure 9 A, B). Image-stream flow cytometry images and bright detail similarity (BDS) co-localization analysis indicated Mfge8-EGFP signal showed strong co-localizion with either CD63 or CD81 signal (similarity score >1) (Figure 9 C,

D). Thus, the majority of Mfge8-EGFP bound to cells via EVs. Direct binding to PS spontaneously externalized on macrophages or captured by macrophages may also be supplementary mechanisms.

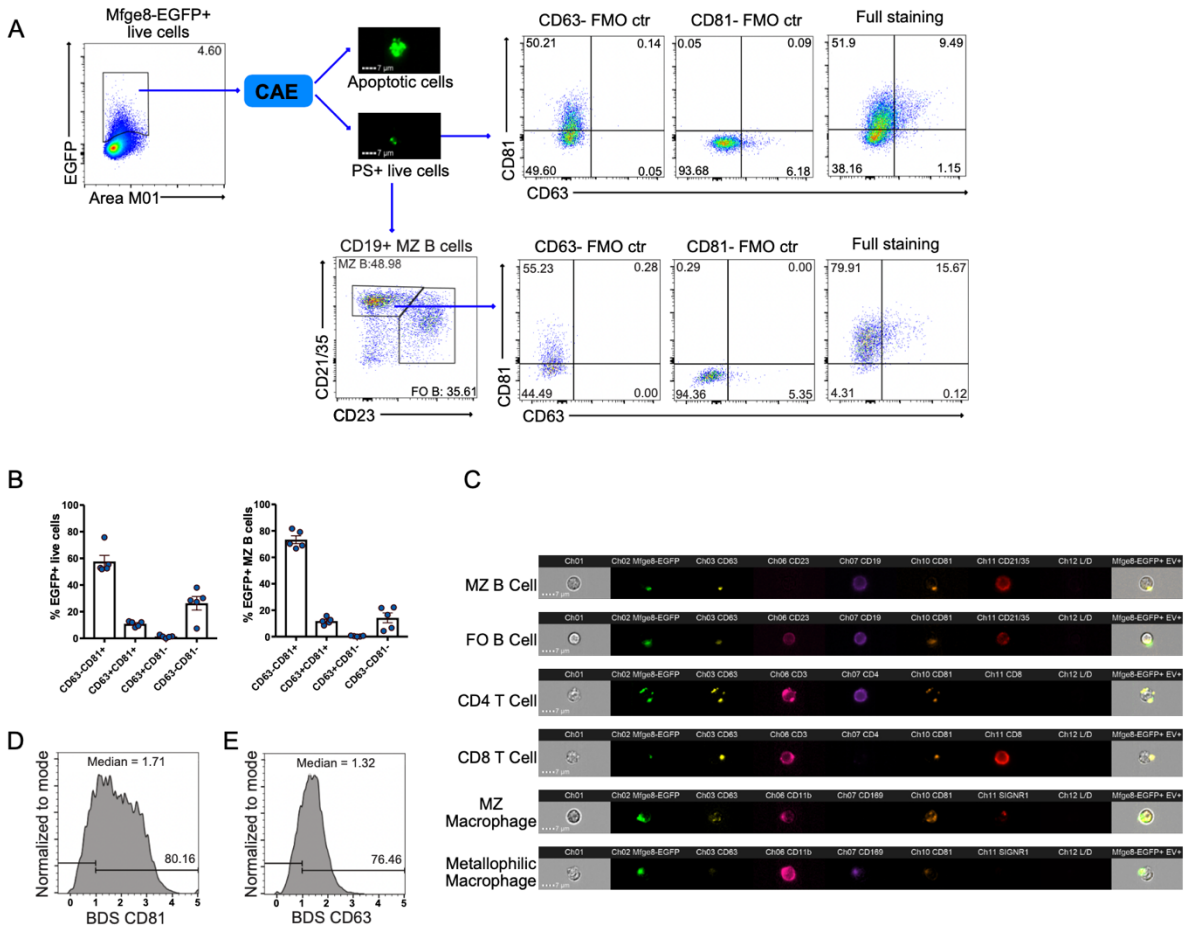

Figure 9. Mfge8-EGFP co-localizes with EVs.
Mice were injected 150ug Mfge8-EGFP intravenously, splenocytes were isolated after 1h and analyzed by image-stream flow cytometry.
(A) Representative gating strategy of Mfge8-EGFP labeled total live cells (up) and MZ B cells (down). Image-stream flow cytometry was used to acquire images of Mfge8-EGFP+ live cells, Mfge8-EGFP+ apoptotic cells were excluded by an image based convolutional autoencoder (CAE) deep learning algorithm. The remained PS+ live cells and MZ B cells were used to measure the co-expression of exosome markers CD81 and CD63.
(B) Statistic record of the frequency of CD81 and CD63 expression on Mfge8-EGFFP^{+} live cells. Data are combined from 2 independent experiments. Mean ± SEM are shown
(C) Representative images from image-stream flow cytometry show Mfge8-EGFP co-localizes with exosome markers CD63 and CD81 on different cell types. Scale bar 7 um.
(D) Mfge8-EGFP^{+} CD81^{+} cells were further measured the colocalization of the two signals by the bright detail similarity (BDS) co-localization analysis. Mask: M01. Median similarity score (SS) is shown in the middle of the figure, SS > 1 represents good colocalization.
(E) Mfge8-EGFP^{+} CD63^{+} cells were further measured the colocalization of the two signals by the bright detail similarity (BDS) co-localization analysis. Mask: M01. Median similarity score (SS) is shown in the middle of the figure, SS > 1 represents good colocalization. N = 5.

6.1.2 PS-targeting antigen strongly accumulates on FDCs.

It has been reported previously that the significant extracellular protease activity in the lymphoid follicle rapidly degrades protein antigens especially in the extrafollicular and SCS regions. In contrast, antigens in the B cell follicles and on FDCs remain intact (Aung et al., 2023). We wondered how long Mfge8-EGFP accumulating in the MZ is retained there. To assess this, we injected a group of mice intravenously with either Mfge8-EGFP or EGFP, spleens were taken after 1h, 6h and 16h. EGFP signal was observed by fluorescent immunohistochemistry (fIHC). We found that the Mfge8-EGFP signal could be detected even 16h post injection, moreover, we observed a relocation of Mfge8-EGFP from MZ to the inner B cell follicle and FDC network: 1h post injection, most Mfge8-EGFP accumulated in the MZ. 6h post injection, Mfge8-EGFP could still be detected in the MZ, but also appeared on CD21/35^{hi} FDCs, 16h post injection, only Mfge8-EGFP located in the CD21/35^{hi} area was detected (Figure 10). This phenomenon could imply a transportation mechanism, but also could be due to Mfge8-EGFP in the MZ is degraded faster than the protein accumulating on FDCs. In contrast, conventional EGFP could not be detected by fIHC, neither in the MZ nor on FDCs.

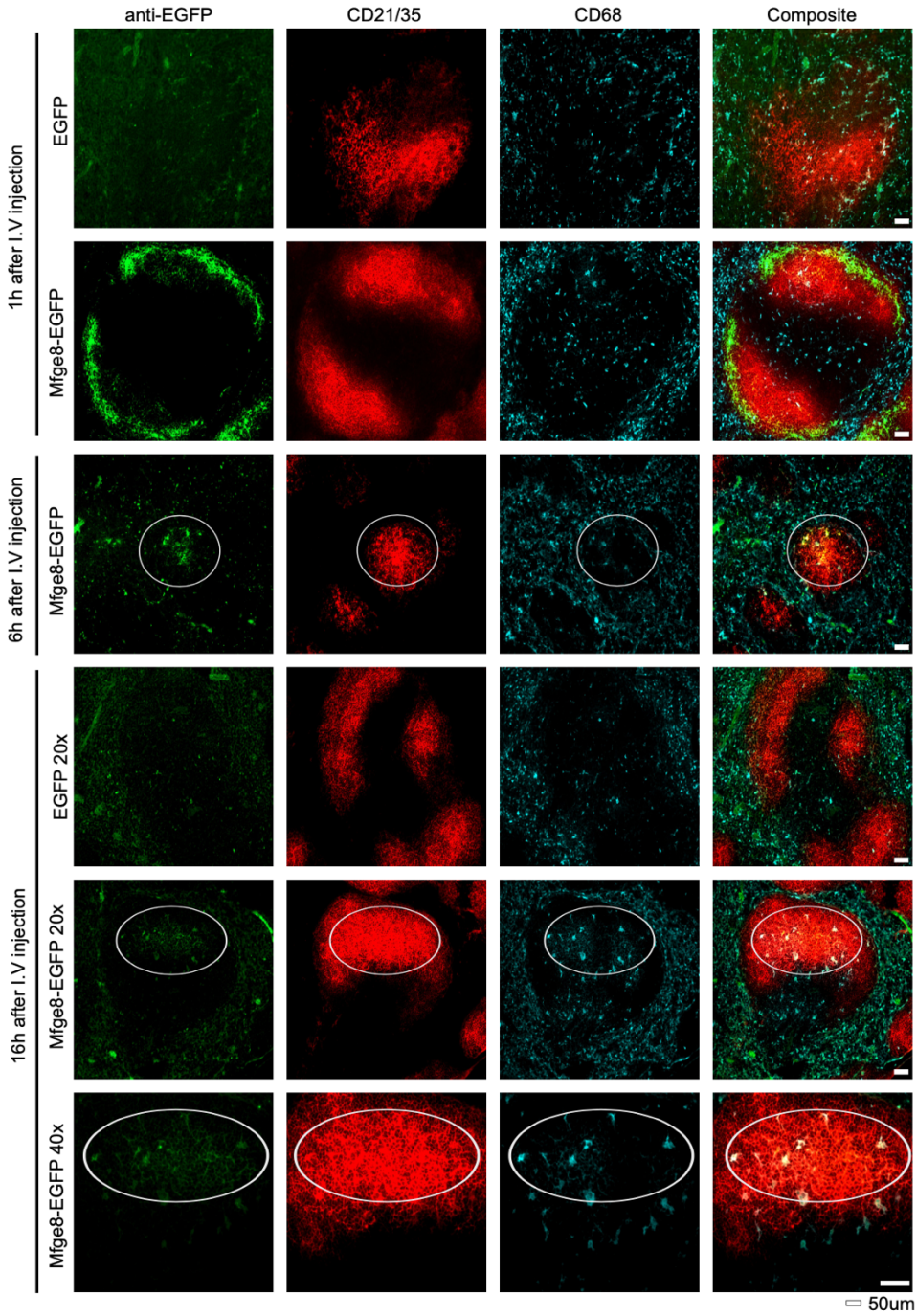

Figure 10. Mfge8-EGFP accumulates on FDCs.
Spleen cryosection (7um) from WT mice, 1h -16h after intravenous injection of 1.8 nmol Mfge8-EGFP or conventional EGFP. Scale bar 50 um. Staining antibodies: anti CD21/35 – PE, anti GFP – FITC, anti CD68– APC.

6.1.3 Mfge8-EGFP promotes anti-EGFP antibody responses.

To see if the increased antigen-deposition on FDCs after immunization with EV-targeted antigen influences antibody responses, we next sought to compare the serum anti-EGFP antibody titers induced by a single dose of EV-targeting Mfge8-EGFP or conventional EGFP. Both immunizations induced detectable EGFP specific IgM on

day 8 (Figure 11 C), but Mfge8-EGFP immunization induced 7x more IgM, indicating improved early B cell activation and extrafollicular response. We also quantified anti-EGFP IgG titers at different time points after immunization. We found substantial amounts of class-switched anti-EGFP IgG (OD450 > 0.1) as early as day 4 after Mfge8-EGFP immunization, however, it was not detected in EGFP immunized mice until day 8 (Figure 11 A). Mfge8-EGFP immunization induced considerable EGFP specific IgG titers on day 8, which was 427x higher than in mice immunized with EGFP. 14 days after immunization, EGFP specific IgG titers in Mfge8-EGFP immunized mice further increased 8x compared to day 8, and was 27x higher than EGFP immunization (Figure 11 B). Antigen specific IgG1 accounted for most of the IgG responses in the mice immunized with EGFP, however, both EGFP specific IgG1 and IgG2b were strongly increased after Mfge8-EGFP immunization (Figure 11 D). These observations imply that antibody CSR was generally accelerated when antigen was targeted to PS.

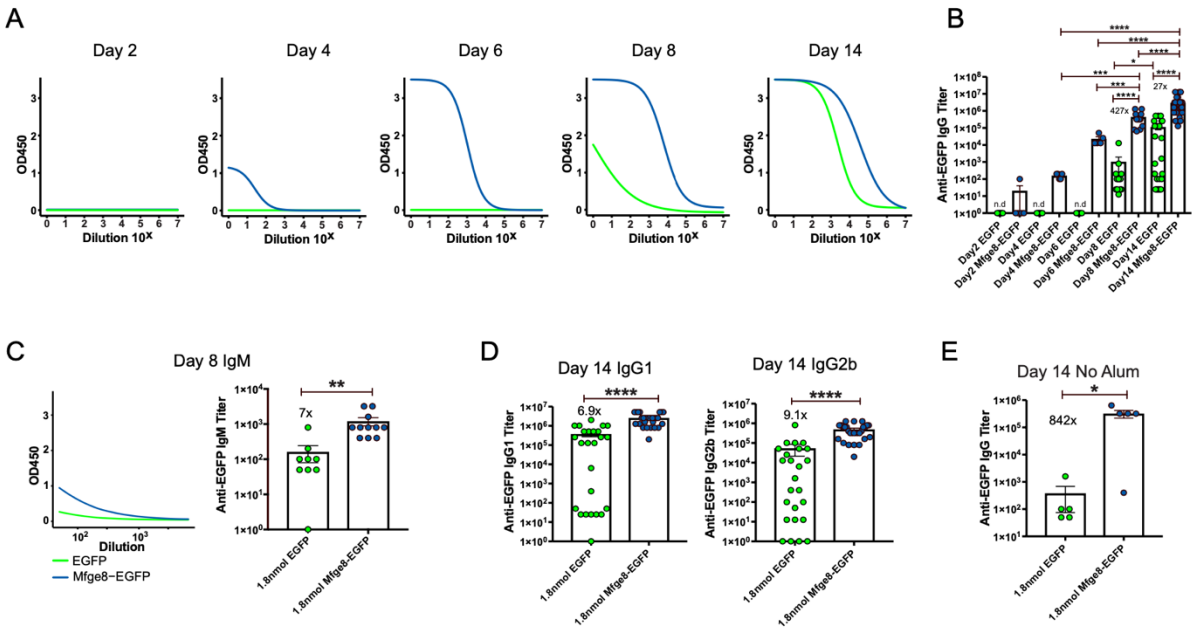

Figure 11. Mfge8-EGFP immunization promotes anti-EGFP antibody responses.
(A-D) WT mice were intraperitoneally immunized with 1.8 nmol EGFP or 1.8 nmol Mfge8-EGFP in alum. Serum antibody titers were measured on the indicated dates. Four parameter logistic titration curves **(A)** and statistic analyses of endpoint titers (OD>0.1) of serum anti-EGFP IgG are shown **(B)** for anti-EGFP IgG on different time points**.** N = 42.
(C) Serum IgM titers were measured on day 8, four parameter logistic titration curves are shown on the left, statistic analysis of endpoint titers (OD>0.1) is shown on the right. N = 20.
(D) Day 14 titers of IgG1 and IgG2b were measured respectively. N = 18.
(E) WT mice were intraperitoneally immunized with 1.8 nmol EGFP or 1.8 nmol Mfge8-EGFP without alum. Serum samples were collected 14 days after immunization. Endpoint titers (OD>0.1) of serum anti-EGFP IgG are shown. N = 10.
Data are combined from 2-3 independent experiments. Mean ± SEM are shown, and each data point represents an individual mouse. T tests were conducted. *p ≤ 0.05, **p ≤ 0.01, ***p ≤ 0.001, ****p ≤ 0.0001.

To test whether Mfge8-EGFP can promote and increase antibody production without the need of adjuvant, mice were immunized with pure Mfge8-EGFP or EGFP and we measured IgG titers after 14 days. Surprisingly, we found Mfge8-EGFP immunization without alum could still induce high titers of IgG. Lack of alum only slightly decreased the antibody titer (9.6x lower than immunization with alum). However, absence of alum sharply decreased the antibody response of EGFP immunization (301.5x lower than with alum), as a result, the difference in IgG titers between the 2 groups increased to 842x (Figure 11 E). This data shows that Mfge8-EGFP alone induces adequate activation of innate immune responses to support the subsequent adaptive antibody response, which makes PS-targeting a promising vaccination method.

Instead of systemic immunization by intraperitoneal injection, we also tested local immunization by subcutaneous injection. We found mice subcutaneously immunized with Mfge8-EGFP also showed significantly more IgG on both day 8 and day 14 (Figure 12 A). Besides, we also measured the anti-Mfge8 antibody response in the same mice, only one out of ten mice showed low levels of anti-Mfge8 IgG after immunization, but the magnitude is negligible compared with the induced anti-EGFP IgG (Figure 12 B). These antibodies might not target Mfge8 directly, but could be directed against a linker sequence or the FLAG tag which were also present in the recombinant Mfge8 version that was used for capturing for the ELISA. The mouse did not show any abnormalities in the appearances nor activities, no pathological changes were observed during the dissection. In conclusion, we hypothesize that by utilizing the PS binding capability of Mfge8, fused EGFP was transported and accumulated in the MZ of lymphoid follicles by circulating EVs, and this led to the promoted B cell activation and antibody production as well as antibody isotype switching.

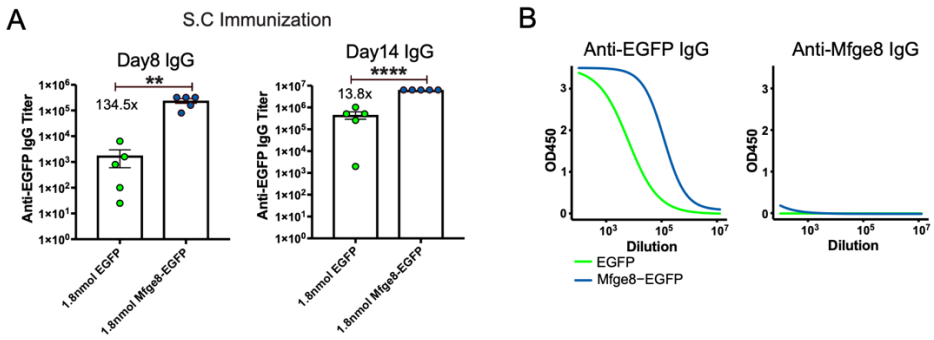

Figure 12. Subcutaneous immunization.
(A) WT mice were subcutaneously immunized with 1.8 nmol EGFP or 1.8 nmol Mfge8-EGFP with alum. Serum samples were collected 8 and 14 days after immunization. Endpoint titers (OD>0.1) of serum anti-EGFP IgG are shown as mean ± SEM, and each data point represents an individual mouse. N = 10. T tests were performed. *p ≤ 0.05, **p ≤ 0.01, ***p ≤ 0.001, ****p ≤ 0.0001.
(B) Four parameter logistic titration curves are shown for serum anti-EGFP IgG (left) and anti-Mfge8 IgG.

6.2 PS-targeting antigen is transported to FDCs independently of C3.

Antigen deposition on FDCs was previously known to be dependent on the formation of immune complexes (ICs), consisting of antigen, specific antibody and complement component 3 (C3) cleavage products (C3d and C3b), and were transferred through the cooperation between complement receptor 1 and 2 (CR1/CR2) expressed on FDCs and B cells (Kranich and Krautler, 2016, Ferguson et al., 2004, Cinamon et al., 2008). As we show in Figure 13, EGFP immunized mice showed EGFP accumulation on FDCs only after EGFP-specific antibodies had been generated by previous immunization 2 weeks earlier.

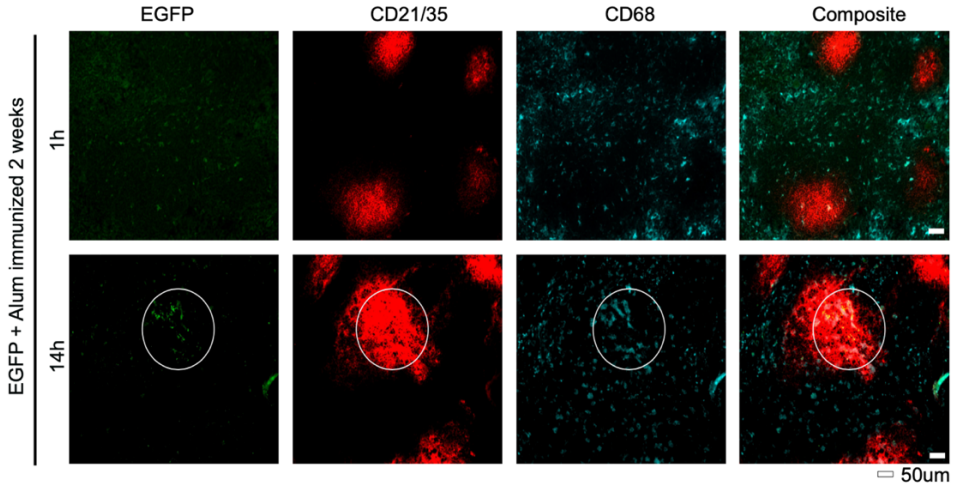

Figure 13. EGFP is transported to FDCs in pre-immunized mice.
WT mice were immunized with EGFP + alum 2 weeks earlier to generate preexisting EGFP-specific immunity. Each immunized mouse was intravenously injected with 1.8 nmol EGFP. Spleen cryosections were prepared after 1h and 14h. N = 6. Scale bar 50 um. Staining antibodies: anti CD21/35–PE, anti GFP–FITC, anti CD68–APC.

We assumed the possibiltiy that the deposition of Mfge8-EGFP on FDCs in unimmunized naïve mice could occur because the fusion protein activated the complement system or cross reacted with natural antibodies. To test that, we used B6.129S4-C3^{tm1Crr}/J mouse, in which the C3 gene was deleted. The genotype of every mouse was confirmed to ensure only C3$^{-/-}$ homozygous mouse was used for the study (Figure 14 A). C3 knock-out (C3 KO) negatively affects B cell response, when we immunized C3 KO and B6x129 WT mice with equal number of sheep red blood cells (SRBC), C3 KO mice generated significantly smaller GL7^{+} germinal centers (Figure 14 B, C).

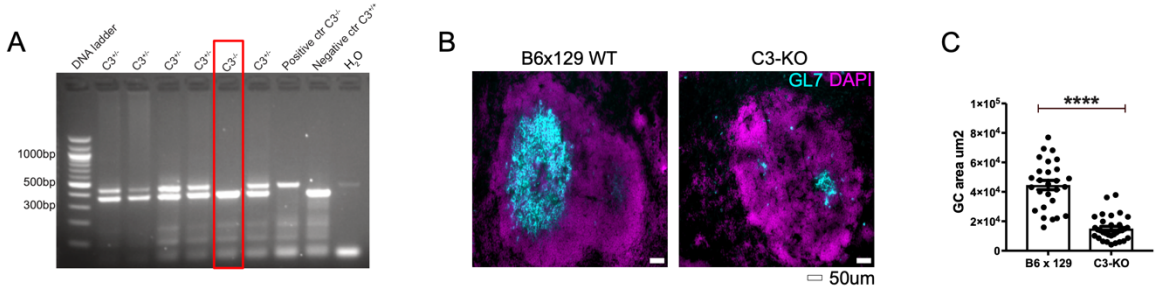

Figure 14. C3 KO negatively affects GC formation.
(A) Genotyping of B6.129S4-C3^{tm1Crr}/J mouse, standard PCR products were separated by 1.5% agarose gel electrophoresis. Image shows wild type = 350bp. mutant genotype = ~500 bp, heterozygte genotype = ~500 bp and 350 bp.
(B-C) WT B6x129 mice and C3 KO mice were immunized with 1x10^{8} SRBC for 7 days, spleen sections were stained for GL7^{+} GCs **(B)**, size of GL7^{+} GCs were measured and compared in ImageJ **(C)**. Scale bar 50 um, n = 6, Staining antibodies: anti GL7 – APC, DAPI.

We subsequently tested if the immune-boosting effects of Mfge8-EGFP still occur in C3 KO mice. C3 KO and B6x129 WT mice were immunized with a single dose of either EGFP or Mfge8-EGFP, serum anti-EGFP IgG titers were tested on day 7 and day 14. We found C3 KO mice produced significantly less antigen specific IgG on day 7, compared to WT mice receiving the same immunization. However, this negative effect disappeared at the later time points. C3 KO and WT mice that were immunized with the same antigen produced similar levels of EGFP specific IgG on day 14 (Figure 15 A, B). Nevertheless, the advantage of Mfge8-EGFP over EGFP in antibody production was also observed in C3 KO mice, C3 KO mice immunized with Mfge8-EGFP produced significantly more IgG on both early and late time points, compared to mice immunized with equal amounts of EGFP (Figure 15 A, B). Based on the above data, we assumed that C3-deficiency did not alter the targeting capability of Mfge8-EGFP. To test this directly, we intravenously injected Mfge8-EGFP into C3 KO mouse and assessed the accumulation of EGFP on FDCs. We found that Mfge8-EGFP first

accumulated in the MZ and later on FDCs (Figure 15 C, D), like we had seen in WT mice (Figure 10). In conclusion, C3KO has a negative effect in germinal center formation and early antibody production. However, Mfge8-EGFP deposition on FDCs in unimmunized naïve mice, and its advantage in inducing antibody production were independent of C3.

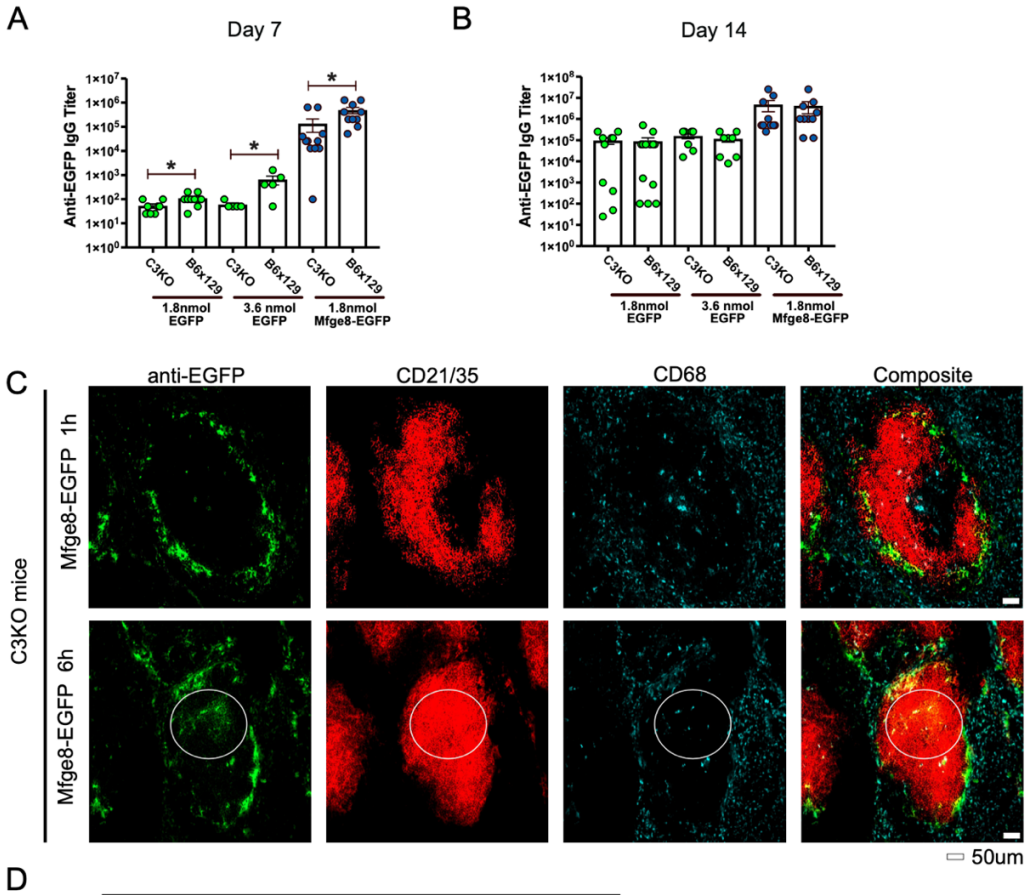

D

	LFs	EGFP+ on FDCs	%
B6x129 WT	10	4	40%
C3-KO	38	18	47.4%

Figure 15. Mfge8-EGFP deposition on FDCs is independent of C3.
(A-B) WT B6x129 and C3 KO mice were immunized with alum + 1.8nmol EGFP or Mfge8-EGFP i.p. EGFP specific IgG were measured by ELISA from serum collected on day 7 **(A)** and day 14 **(B)**. Data are pooled from 2 independent experiments. Mean ± SEM are shown, and each data point represents an individual mouse. One-way-ANOVA with Bonferroni correction was performed. *p ≤ 0.05, **p ≤ 0.01, ***p ≤ 0.001, ****p ≤ 0.0001. N = 47.
(C-D) C3 KO mice were intravenously injected with 1.8 nmol Mfge8-EGFP, spleen sections were stained 1h and 6h after injection **(C)**. Images from lymphoid follicles randomly chosen from spleen sections from mice sacrifized 6h after injection. Percentage of lymphoid follicle that contained Mfge8-EGFP on FDCs was calculated **(D)**.N = 8. Scale bar 50 um. Staining antibodies: anti CD21/35 – PE, anti GFP – FITC, anti CD68– APC.

6.3 CD169^{+} microvesicles can be found on FDCs.

6.3.1 Mfge8-EGFP colocalized with CD169^{+} microvesicles in the FDC area.

As we have shown previously, PS-targeted Mfge8-EGFP was transferred onto the FDCs in a process that is independent of C3, suggesting that this FDCs deposition in unimmunized naïve mice was key to boost antibody production. We assumed this process involved eventually a local transport mechanism in the MZ or SCS. It has been demonstrated that CD169^{+} metallophilic macrophages derived microvesicles and membrane material were associated with nearby T cells and FDCs (Chen et al., 2022, Gray et al., 2012). Based on these observations, we assumed that at least some Mfge8-EGFP might be transferred to FDCs by CD169^{+} microvesicles soon after it was captured by the metallophilic macrophages.

To test this, we injected Mfge8-EGFP intravenously into WT mice. Then we analyzed spleen sections with cell type markers using fluorescent microscopy. Within the CD21/35^{hi} FDC area where Mfge8-EGFP was deposited, we observed small dot-shaped CD169 signals, in contrast to the larger bright CD169 signal from metallophilic macrophages in the MZ (Figure 16 A). To further distinguish these CD169 signals in a higher resolution (around 50nm), we applied stimulated emission depletion (STED) microscopy. Here, we found they were powder-like CD169 particles diffused in the extracellular space of CD21/35^{hi} FDCs network (Figure 16 B). Diameters of these CD169^{+} particles were measured and showed the average diameter around 300nm (Figure 16 C), indicating these CD169^{+} particles could be microvesicles rather than cells. Then we assessed if these CD169^{+} microvesicles were also Mfge8-EGFP^{+}, we observed a partial colocalization, suggesting some antigen-containing EVs might shuttle from MZ metallophilic macrophages to FDCs. However, observing EVs in tissue sections is challenging and artefacts cannot be ruled out (Figure 16 D). To find further evidence for antigen-delivery to FDCs by EVs, we next analyzed cell-bound EVs using imaging flow cytometry as we have previously published (Kranich et al., 2020, Rausch et al., 2023, Rausch et al., 2021).

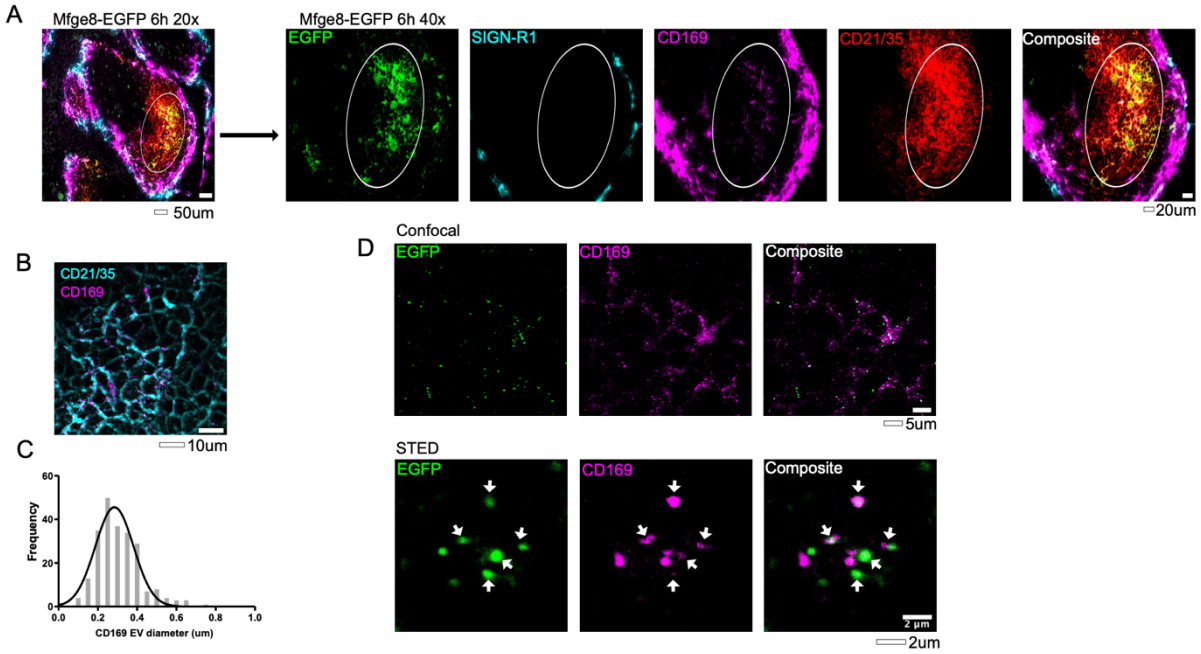

Figure 16. Mfge8-EGFP colocalizes with CD169$^+$ microvesicles in the FDC area.
(A) Spleen sections from WT B6 mice, 6h after intravenous injection of 1.8nmol Mfge8-EGFP. Magnification: 20x, scale bar 50 um, Magnification: 40x scale bar 20 um. Staining antibodies: anti CD21/35 – PE, anti GFP – FITC, anti CD169 – APC, anti SIGN-R1 – BV421
(B) Spleen section images taken from stimulated emission depletion (STED) microscope, CD21/35^{hi} FDCs area is shown. Scale bar 10um.
(C) Histogram shows the diameter of CD169$^+$ signals, measured from image **(B).**
(D) Images from confocal microscopy (scale bar 5um) and STED microscopy (scale bar 2um). Arrows indicate the colocalization of CD169$^+$ and Mfge8-EGFP$^+$ signals. Spleen sections were taken from WT B6 mice that was intravenously injected 1.8nmol Mfge8-EGFP for 6h.

6.3.2 Approx. 15% of Mfge8-EGFP are transported by CD169+ microvesicles.

To quantify to which extent CD169$^+$ microvesicles contribute to the Mfge8-EGFP transportation, we measured the Mfge8-EGFP signal in the MZ and inner B cell follicle 1h and 6h after injection by imaging flow cytometry. We could see a clear trend of shift of Mfge8-EGFP from MZ area (indicated by the CD19$^+$CD21/35^{hi}CD23^{lo} MZ B cells) to the inner B cell follicle (indicated by the CD19$^+$CD21/35^{mid}CD23^{hi} follicular B cell) over time (Figure 17 A, B). From these Mfge8-EGFP$^+$ cells we measured the co-expression of CD169 and found a constant frequency of around 15% of Mfge8-EGFP$^+$ cells co-expressed CD169 (Figure 17 C, D). Bright detail similarity (BDS) co-localization analysis (Figure 17 E) and Image-stream flow cytometry images (Figure 17 F) indicated that the Mfge8-EGFP signal strongly colocalized with CD169 (similarity score >1). In conclusion, CD169$^+$ EVs probably constitute only a minor source of antigen accumulating on FDCs, as only about 15% of all Mfge8-EGFP$^+$ EVs on B cells where positive for CD169.

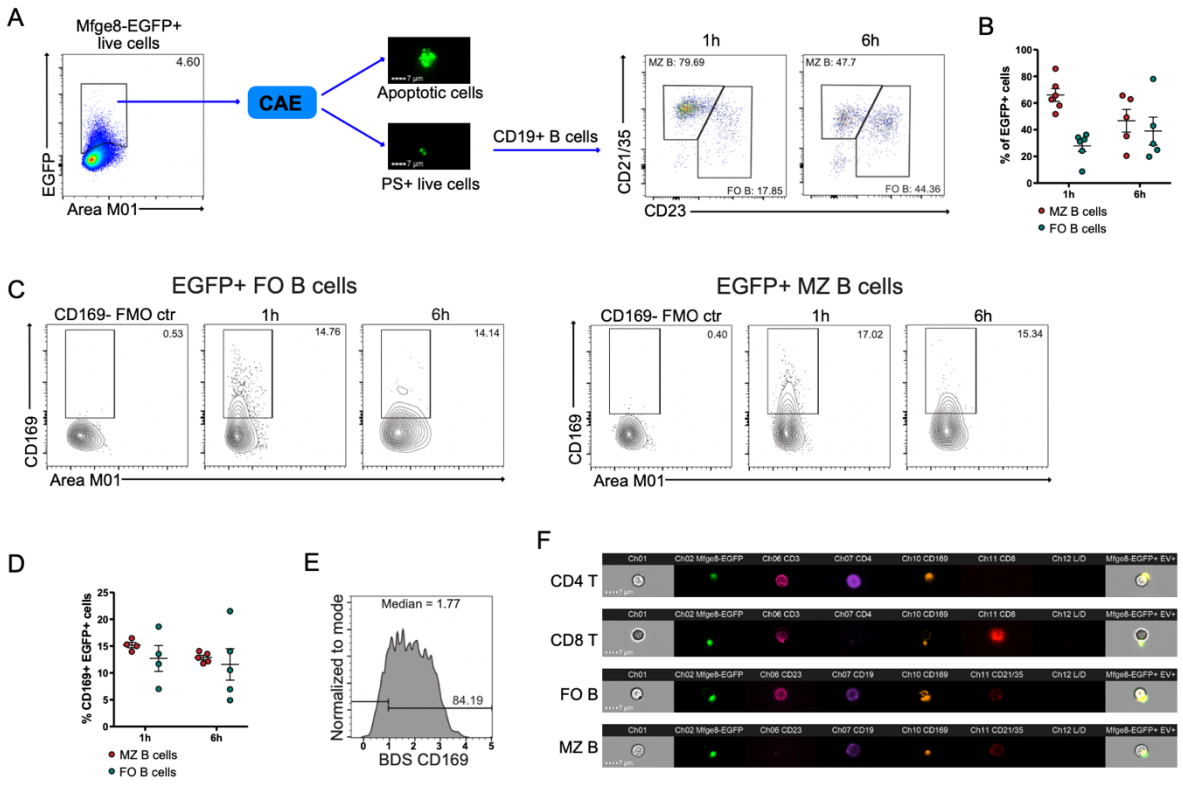

Figure 17. Quantification of CD169 co-localization on Mfge8-EGFP⁺ cells.
(A-B) Groups of WT B6 mice were injected with injected 1.8nmol Mfge8-EGFP. Spleen were analyzed after 1h or 6h by imaging stream flow cytometry. Mfge8-EGFP⁺ apoptotic cells were excluded by an image based convolutional autoencoder (CAE) deep learning algorithm (Kranich et al., 2020, Rausch et al., 2023, Rausch et al., 2021), and Mfge8-EGFP⁺ follicular B cells and MZ B cells were further analyzed **(A-B)**.
(C-D) Representative gating strategy **(C)** and analysis **(D)** of CD169 expression on Mfge8-EGFP⁺ FO B cells and MZ B cells.
(E) Mfge8-EGFP⁺ CD169⁺ B cells were further measured the colocalization of the two signals by the bright detail similarity (BDS) co-localization analysis. Median similarity score (SS) is shown in the center of the figure, SS > 1 represents good colocalization. Mask: M01.
(F) Representative images from image-stream flow cytometry show Mfge8-EGFP co-localizes with CD169 on different cell types. Scale bar 7 um.
Data are shown as mean ± SEM. Each data point represents an individual mouse. Data are collected from 2 independent experiments. N =20. One-way-ANOVA with Bonferroni correction was performed. *p ≤ 0.05, **p ≤ 0.01, ***p ≤ 0.001, ****p ≤ 0.0001.

6.4 PS-targeting antigen enhances germinal center reactions.

Antigens deposited on FDCs are essential for regulating germinal center reactions and production of high-affinity antibodies (Heesters et al., 2014). A previous study has shown that the amounts of antigens captured by light zone B cells from FDCs determine their division capacity in the dark zone (Finkin et al., 2019). Therefore, based on these previous findings, we assumed that Mfge8-EGFP deposition on FDCs in unimmunized naïve mice could probably enhance the germinal center reaction, and could be the reason why Mgfe8-EGFP induced significantly more class switched

antibodies. Therefore, we immunized mice with equimolar amounts of Mfge8-EGFP or EGFP. 14 days after the immunization, we took the spleens and stained PNA$^+$ GCs. Compared to the EGFP immunization, mice immunized with Mfge8-EGFP generated significantly larger GCs with higher PNA signal intensity (Figure 18).

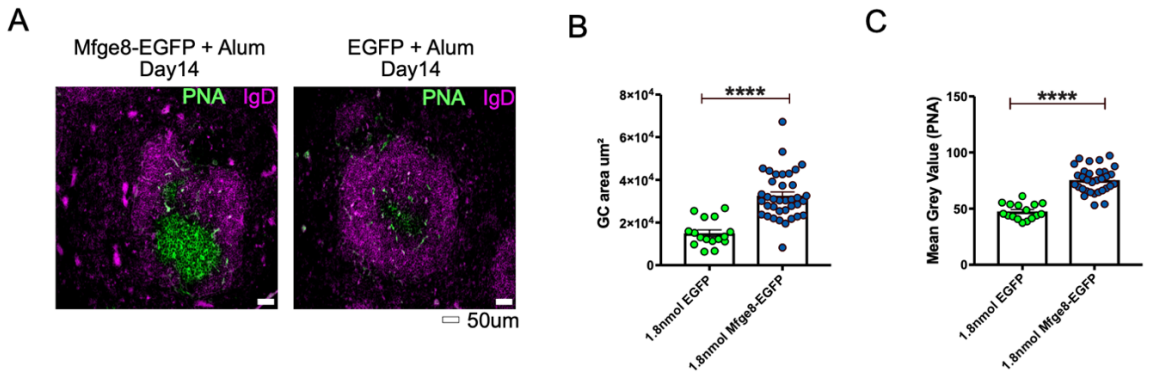

Figure 18. Mice immunized with Mfge8-EGFP generate larger GCs.
(A-C) WT B6 mice were immunized with either alum + 1.8 nmol EGFP or Mfge8-EGFP, spleens were taken 14 days after immunization and stained for PNA$^+$ GCs and IgD$^+$ follicular B cells **(A)**. Scale bar 50 um, Staining antibodies: PNA – FITC, anti IgD – eF450. Size of PNA$^+$ GCs **(B)** and mean PNA signal intensity **(C)** were measured in ImageJ. Mean ± SEM are shown, n = 4.

We further tested the antigen specific GC B cells (EGFP$^+$CD19$^+$IgD^{lo}CD95$^+$GL7$^+$) by flow cytometry. 8 days post the immunization, only few EGFP$^+$ GC B cells were detected from EGFP immunized mice, however, mice immunized with Mfge8-EGFP generated 8.25x more EGFP$^+$ GC B cells. On day 14, when the GC reaction reached its peak (determined in the previous experiment), the numbers of EGFP$^+$ GC B cells further expanded 1.65x and 2.6x in mice immunized with Mfge8-EGFP or EGFP, respectively. Although the GC B cell divisions in EGFP immunized mice seemed to be accelerated after day 8, Mfge8-EGFP immunization still induced 5.2x more EGFP$^+$ GC B cells at the peak time point (Figure 19).

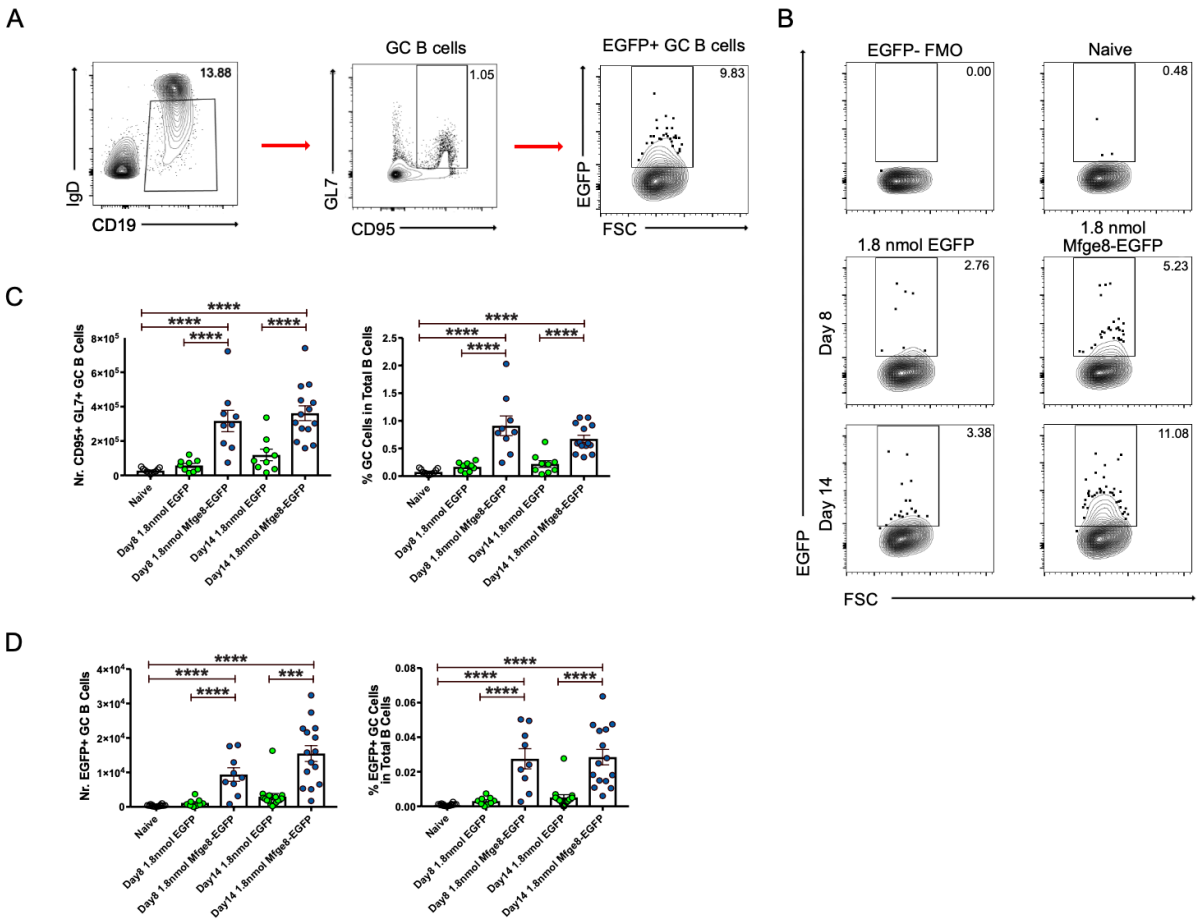

Figure 19. Mfge8-EGFP immunization promotes GC reactions.
WT B6 mice were immunized with either alum + 1.8 nmol EGFP or Mfge8-EGFP, spleens were taken 8 or 14 days after immunization.
(A-B) Representative gating strategy for EGFP specific germinal center B cells ($EGFP^+CD19^+IgD^{lo}CD95^+GL7^+$), plots shown are pre- gated on single live cells.
(C) Absolute number (left) and percentage of general $CD19^+IgD^{lo}CD95^+GL7^+$ GC B cells in $CD19^+$ B cells (right) were measured 8 days and 14 days after immunization.
(D) Absolute number (left) and percentage of EGFP binding GC B cells in total B cells (right) were measured 8 days and 14 days after immunization. Data are combined from 2-3 independent experiments. N = 65. Mean ± SEM are shown, and each data point represents an individual mouse. One-way-ANOVA with Bonferroni correction was performed. *p ≤ 0.05, **p ≤ 0.01, ***p ≤ 0.001, ****p ≤ 0.0001.

6.5 Immunization with increasing EGFP doses promotes antibody production but not GC reactions.

In contrast to a natural infection and inflammation, during which antigens are continuously supplied to the immune system, subunit vaccine components are more rapidly cleared after immunization, before high affinity IgG antibodies are produced (Tam et al., 2016, Pape et al., 2007, Moon et al., 2012). Therefore, antigen deposition on FDCs after single dose primary vaccination are associated with weak IgM antibodies, resulting in the suboptimal antigen concentration on FDCs to assist GC

reaction (Carroll, 1998, Boes, 2000). To test if escalated antigen doses in the primary immunization could promote GC reactions and humoral immune responses, four groups of mice were given increasing doses of EGFP (from 1.8nmol to 14.4 nmol), 14 days after immunization, EGFP specific GC B cells were stained. Despite an 8x increase of the EGFP dose, antigen specific GC B cells did not increase accordingly. Similarly, mice immunized with twice as much Mfge8-EGFP (3.6 nmol) did not show more EGFP^{+}GC B cells compared to mice receiving 1.8nmol Mfge8-EGFP (Figure 20 A). However, serum antibody titers measured from EGFP immunized mice showed a positive correlation with the antigen dose, but mice immunized with 14.4 nmol EGFP were still less efficient in antibody production than 1.8 nmol Mfge8-EGFP immunization. Mice immunized with 3.6 nmol Mfge8-EGFP did not show higher antibody titer, this may imply the physiological maximum of antibody production capability was reached (Figure 20 B).

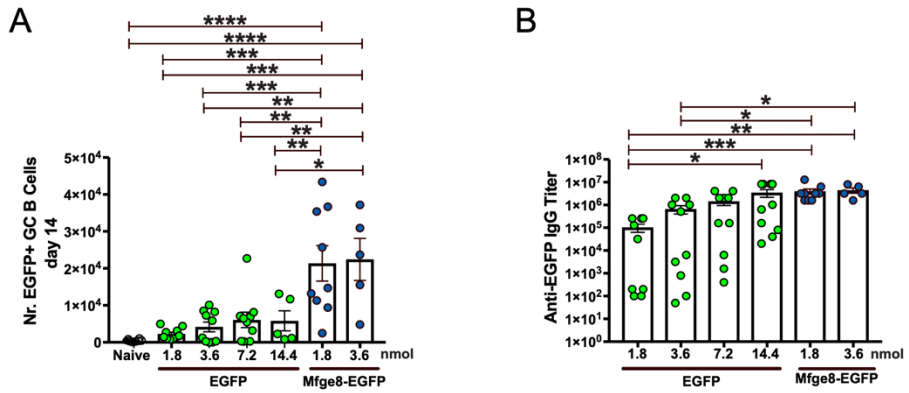

Figure 20. Mfge8-EGFP immunization out-competes 8x molar excess of EGFP.
(A-B) WT mice were immunized with increasing doses of EGFP (1.8, 3.6, 7.2, 14.4 nmol) or Mfge8-EGFP (1.8, 3.6 nmol) separately, EGFP specific GC B cells were measured 14 days after immunization **(A)**. Serum anti-EGFP IgG titers were measured from the same mice, shown as endpoint titer (OD>0.1) **(B)**. Data are shown as mean ± SEM, each data point represents an individual mouse. Data are combined from 2 independent experiments. N = 54. One-way-ANOVA with Bonferroni correction was performed. *p ≤ 0.05, **p ≤ 0.01, ***p ≤ 0.001, ****p ≤ 0.0001.

6.6 PS-targeting antigens do not prolong GC reactions.

The exact mechanism of how GC reactions terminate is still unclear, but the depletion of antigens on FDCs could be an essential reason (Victora and Nussenzweig, 2022, Arulraj et al., 2021). Considering Mfge8-EGFP was rapidly transferred onto the FDCs and therefore likely protected from extracellular proteases (Aung et al., 2023), we assumed that there was more available antigen on FDCs to sustain the GC reaction in mice immunized with Mfge8-EGFP than those who received conventional EGFP.

To test this, we immunized groups of mice with equimolar amounts of EGFP or Mfge8-EGFP and measured EGFP$^+$ GC B cells every 7 days. Mge8-EGFP immunization increased the number of GC B cells (Figure 21 A), but did not result in a prolonged GC reaction. For both immunizations, the GC B cell number reached the peak 2 weeks after immunization, then started to decline and completely disappeared within 4 weeks (Figure 21 A). We also measured the antigen binding capabilities of GC B cells over time, we found there was no difference in the median fluorescence intensity (MFI) of EGFP on early day 8. Along with the GC progress, the antigen binding GC B cells in Mfge8-EGFP immunized mice showed a significantly higher MFI of EGFP on day 14 and day 21, which indicates that these cells express BCRs with higher affinity (Figure 21 B). When the GC reaction entered the contraction phase, MFI of EGFP showed a slight decrease in both groups. This could be because high affinity GC B cells exited the GCs and differentiated into PCs, while low affinity GC B cells and newly recruited naïve B cells were left in the follicles.

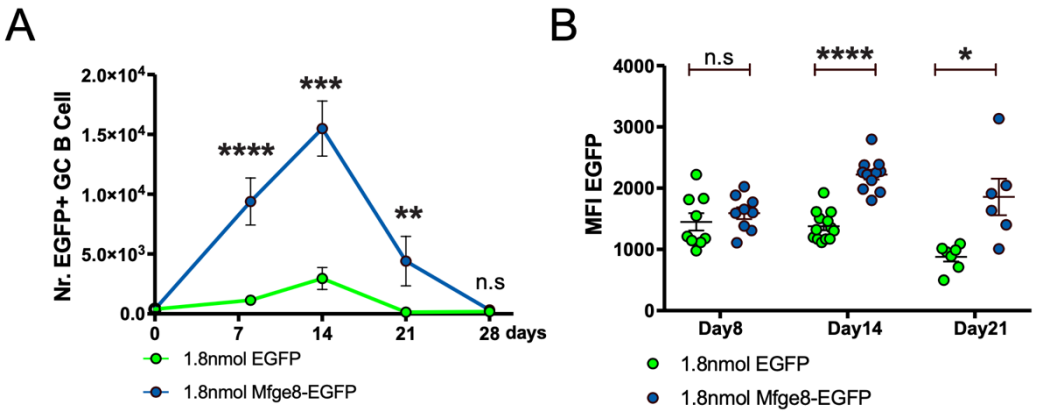

Figure 21. Mfge8-EGFP immunization boosts, but does not prolong the GC reaction.
(A-B) Groups of WT B6 mice were immunized with either alum + 1.8nmol EGFP or Mfge8-EGFP, EGFP specific GC B cells were measured on the indicated timepoints **(A)**. MFI of EGFP on EGFP-binding GC B cells are shown on different time points **(B)**. Data are shown as mean ± SEM, each data point represents an individual mouse. N = 113. Data are combined from 2 independent experiments. T test was performed. *p ≤ 0.05, **p ≤ 0.01, ***p ≤ 0.001, ****p ≤ 0.0001.

6.7 Immunization with PS-targeting antigen promotes GC B cell class switching.

To better understand and compare GC reactions induced by PS-targeting antigens and conventional antigens, we immunized mice with either Mfge8-EGFP or EGFP. On day 14 after the immunization, EGFP$^+$ PNA$^+$ GC B cells were isolated, then single cell BCR and targeted mRNA sequencing was performed. The targeted mRNA panel

contains 397 genes that are critical for immune cell phenotyping, including immunoglobulin isotypes. Among the 30 most variable genes, genes related to the immunoglobulin isotypes were differentially expressed between the two groups (Figure 22 A). UMAP plots showed GC B cells from Mfge8-EGFP immunized mice were enriched in Ighg1 and Ighg2b clusters, while GC B cells from EGFP immunized mice were enriched in Ighm and Ighd clusters (Figure 22 B, C). These data indicated differential CSR between the two immunization groups. When we analyzed the isotype of all sequenced BCR transcripts, we found over 73 % of GC B cells expressed class-switched BCRs in mice immunized with Mfge8-EGFP, however, only 42% of GC B cells from EGFP immunized mice expressed switched BCRs (Figure 22 D). This is in line with the serum antibody data obtained by ELISA (Figure. 11). Taken together, we demonstrated that CSR was significantly accelerated by PS-targeting Mfge8-EGFP.

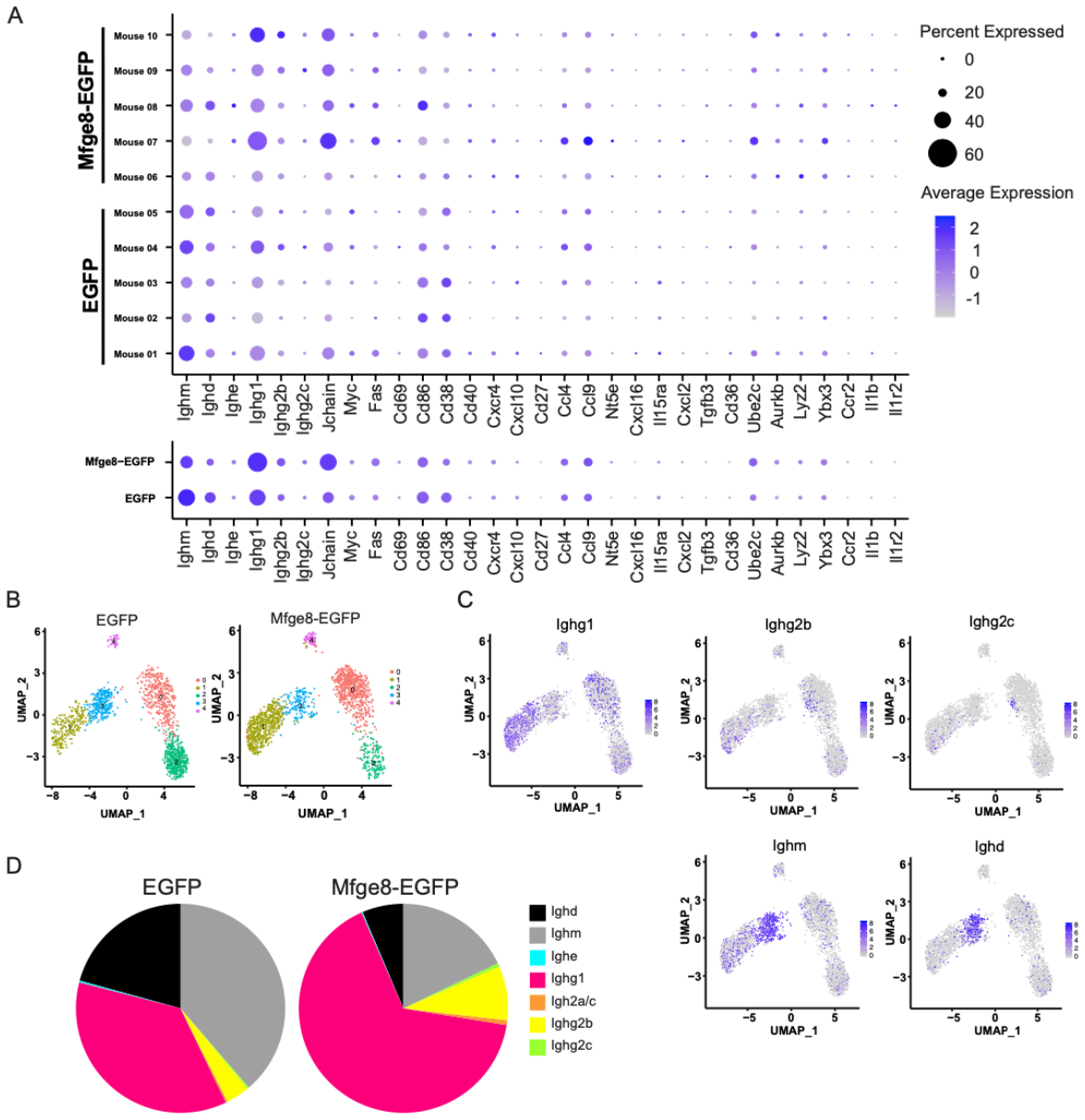

Figure 22. Mfge8-EGFP immunization promotes class switch recombination.
(A) WT B6 mice were immunized with either alum + 1.8nmol EGFP or Mfge8-EGFP. EGFP specific GC B cells were sorted 14 days post immunization. N = 10. Dot plots show the gene expression profiles (Mouse Immune Response Targeted Panel from BD) of each mouse (up), and average expression level of each immunization group.
(B-C) Uniform Manifold Approximation and Projection (UMAP) plots of scRNA-seq analysis of sorted EGFP specific GC B cells **(B),** and the expression distribution of immunoglobulin heavy constant (Igh) genes **(C).**
(D) Pie charts show the proportion of each Ig isotype within the GC B cell repertoires.

6.8 Immunization with PS-targeting antigen promotes GC B cell somatic hypermutation.

Somatic hypermutation is another important process that contributes to the generation of high affinity antibodies (affinity maturation). We calculated nucleotide mutations of each BCR variable region (VDJ genes) sequence compared to its corresponding

germline sequence. We found significantly more accumulated mutations in both heavy and light chains in the Mfge8-EGFP induced GC B cell repertoire compared to the EGFP induced repertoire (Figure 23 A). Then we calcuted the mutation frequency in each framework (FWR) and complementarity-determining region (CDR). We found SHM occured more frquently in CDRs, especially the CDR2. Furthermore, the mutation frequency was increased in every region in Mfge8-EGFP induced repertoire as compared to the EGFP induced repertoire (Figure 23 B). Next, we translated these nucleotide sequences into amino acid sequences, and found there were significantly more non-silent amino acid substitutions in the Mfge8-EGFP induced repertoire (Figure 23 C). In conclusion, by measuring mutations on both nucleotide and amino acid sequences, we demonstrated the somatic hypermutation was significantly promoted by PS-targeting Mfge8-EGFP.

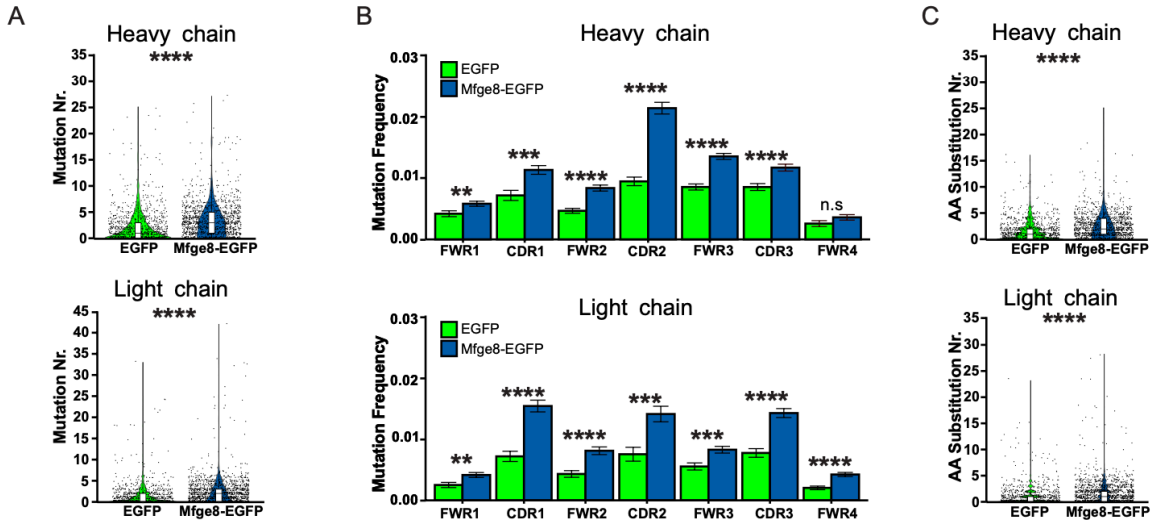

Figure 23. Mfge8-EGFP immunization promotes GC B cell somatic hypermutation.
(A) Violin plots and box plots show observed nucleotide mutations in BCR heavy chain VDJ genes (up) and light chain VJ genes (down).
(B) Bar graphs show observed nucleotide mutation frequency at each CDRs and FWRs in the BCR heavy chain variable region (up) and light chain variable region (down).
(C) Violin plots and box plots show observed non-silent amino acid substitutions in BCR heavy chain (up) and light chain (down). *p ≤ 0.05, **p ≤ 0.01, ***p ≤ 0.001, ****p ≤ 0.0001.

6.9 Immunization with PS-targeting antigen increases the selection strength.

Affinity maturation is determined by both somatic hypermutation and the competition of available antigens on FDCs and help from Tfh cells. To measure the selection strength, we did a Bayesian estimation of antigen-driven selection (BASELINe) analysis. BASELINe analysis calculates the log-odds ratio between the expected and

observed frequencies of non-synonymous mutations, and then estimates a full probability density for the selection strength using a Bayesian statistical framework. FWRs are essential to keep the integrity of BCR structure, therefore mutations in FWRs are negatively selected, while CDRs show increased mutation frequency as a result of antigen-driven positive selection (Yaari et al., 2012, Yaari and Kleinstein, 2015). The analysis of our dataset showed that the negative selection strength is similar between the two repertoires, however, the antigen-driven positive selection strength in Mfge8-EGFP immunized group was significantly higher (Figure 24). The increased selection strength could lead to the generation of antibodies with increased affinity. However, the current analysis was only based on an indirect statistical method. A strategy to compare antibody affinity of two repertoires directly could be done as Viant and his colleagues described in (Viant et al., 2020a). In this study they expressed the Fab region of each antibody clone and measured the dissociation constant.

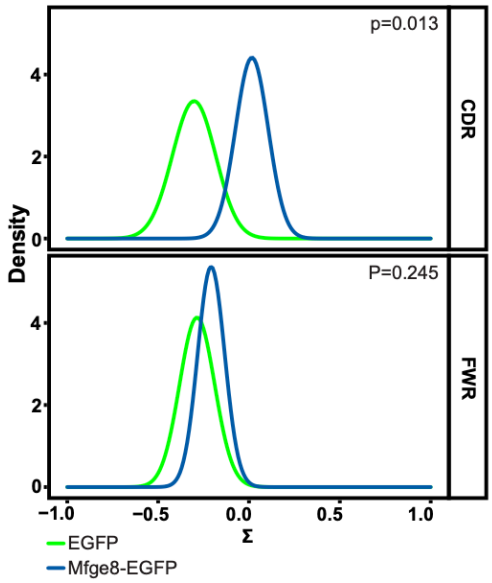

Figure 24. Mfge8-EGFP immunization increases the selection strength on day 14.

The activation-induced deaminase (AID) preferentially initiates SHM in hotspot motif targets, such as in the context of WRC / GYW (W = A / T, R = A / G, Y = C / T) and especially at WGCW hotspot (Tang et al., 2020a). BASELINe analysis identifies observed frequency of non-synonymous mutations, and calculates the expected frequency of non-synonymous mutations from the corresponding germline sequences based on an underlying targeting model to account for SHM hot / cold spots and nucleotide substitution bias. Then, a posterior probability distribution function (PDF) is calculated for replacement frequency using a binomial likelihood function and a β prior. Next, a log-odds ratio between observed and expected replacement frequency is calculated and is referred as selection strength (Σ). Results from multiple sequences are aggregated to provide a single estimate of the selection strength PDF for a group of sequences. Two selection strength PDFs are compared by using numerical integration to obtain a one-sided p value. Selection strength in the FWR represents negative selection, selection strength in the CDR represents antigen-driven positive selection (Yaari et al., 2012).

6.10 Immunization with PS-targeting antigen induces a more diverse GC B cell repertoire.

Next, we analyzed clonal diversities of the two repertoires. For this, BCR sequences were clustered into clones by the maximum likelihood method. All expanding clones

(n > 2) were used to establish phylogenetic trees. Phylogenetic trees showed how somatic mutation gradually accumulated and differentiated from the germline sequence (green root point). When the difference reached the Hamming distance threshold (the minimum number of substitutions required to change one sequence into another), it was classified as a new clone and diverged. The tip of each branch represents the isotypes of the terminal clones. We found Mfge8-EGFP immunization created a more diverse GC B cell repertoire and all the terminal clones were class-switched. Conventional EGFP immunization induced a much smaller GC B cell repertoire and some of the terminal clones were still unswitched IgM- producing clones (Figure 25 A). Statistical analysis of expanding clones are shown in Figure 25 B (Number in the middle is the total expanding clones of each repertoire.) Four clones were found in both repertoires (shared clones), representing 13.8% and 5.5% of the total EGFP induced repertoire and Mfge8-EGFP induced repertoire, respectively (Figure 25 C). In conclusion, targeting antigens to PS significantly promoted SHM and CSR, which led to the generation of more diverse GC B cells repertoire.

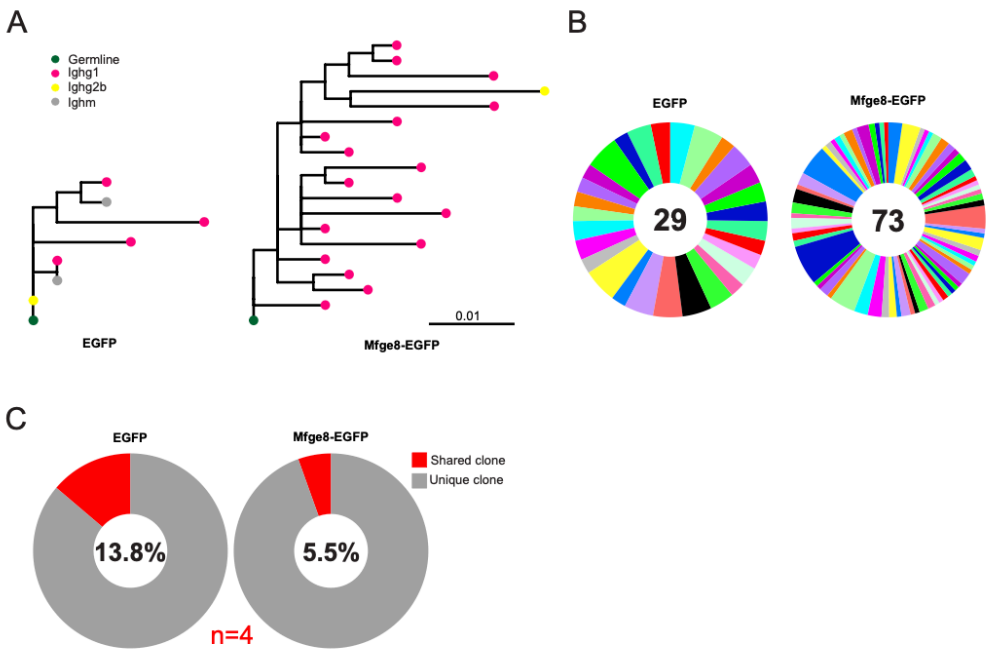

Figure 25. Mfge8-EGFP immunization induces more diverse GC B cell repertoire.
(A) Phylogenetic trees were plotted to compare the diversity of two repertoires induced by immunization.
(B) Pie charts show expanded clones (n > 2) of the two repertoires, each colored slice represents one expanded clone. Total expanded clone number for each repertoire is shown in the center.
(C) Pie charts show shared (public) clones and unique (private) clones between the 2 repertoires, percentage of shared clones is shown in the center.

6.11 Immunization with EGFP and Mfge8-EGFP show similar long-term antibody titers.

Next, we tested if Mfge8-EGFP could induce long-term antibody protection. Serum anti-EGFP IgG titers were measured for an extended period. We found that Mfge8-EGFP immunization induced very fast IgG production. Titers peaked around two weeks after immunization, then IgG titers remained at a constant level for at least 3 months. EGFP immunization induced much slower IgG production, reached the peak 4 weeks after immunization, and remained constant as well. While Mfge8-EGFP immunization induced significantly more IgG production in the first month after immunization, long-term IgG titers measured after two and three months showed no significant difference (Figure 26 D). We also measured $CD19^{low}$ $CD138^{hi}$ $CD98^{+}$ short-lived PCs in the spleen 14 days after immunization, and $CD19^{low}$ $CD138^{hi}$ $EpCAM^{+}$ $CXCR3^{+}$ LLPCs in the bone marrow 87 days after immunization. Consistent with the serum IgG data, Mfge8-EGFP immunization induced significantly more short-lived PCs, however, the percentage of short-lived PCs in total splenocytes were similar between the two groups, this may indicate that the rate of GC B cells finally differentiated to PCs were constant between the two groups, so that the PCs were proportional to the GC expansion (Figure 26 A, B). Intracellular staining of EGFP specific PCs showed that Mfge8-EGFP immunization induced more EGFP-binding PCs, although $p = 0.06$ (Figure 26 C). LLPCs measured 87 days after immunization showed no significant difference neither in the general LLPCs nor $EGFP^{+}$ LLPCs (Figure 26 E-G). In conclusion, Mfge8-EGFP immunization showed significant advantage over EGFP in the first month after immunization, induced significantly more short-lived PCs and IgG, but it did not induce more long-term antibodies nor more LLPCs.

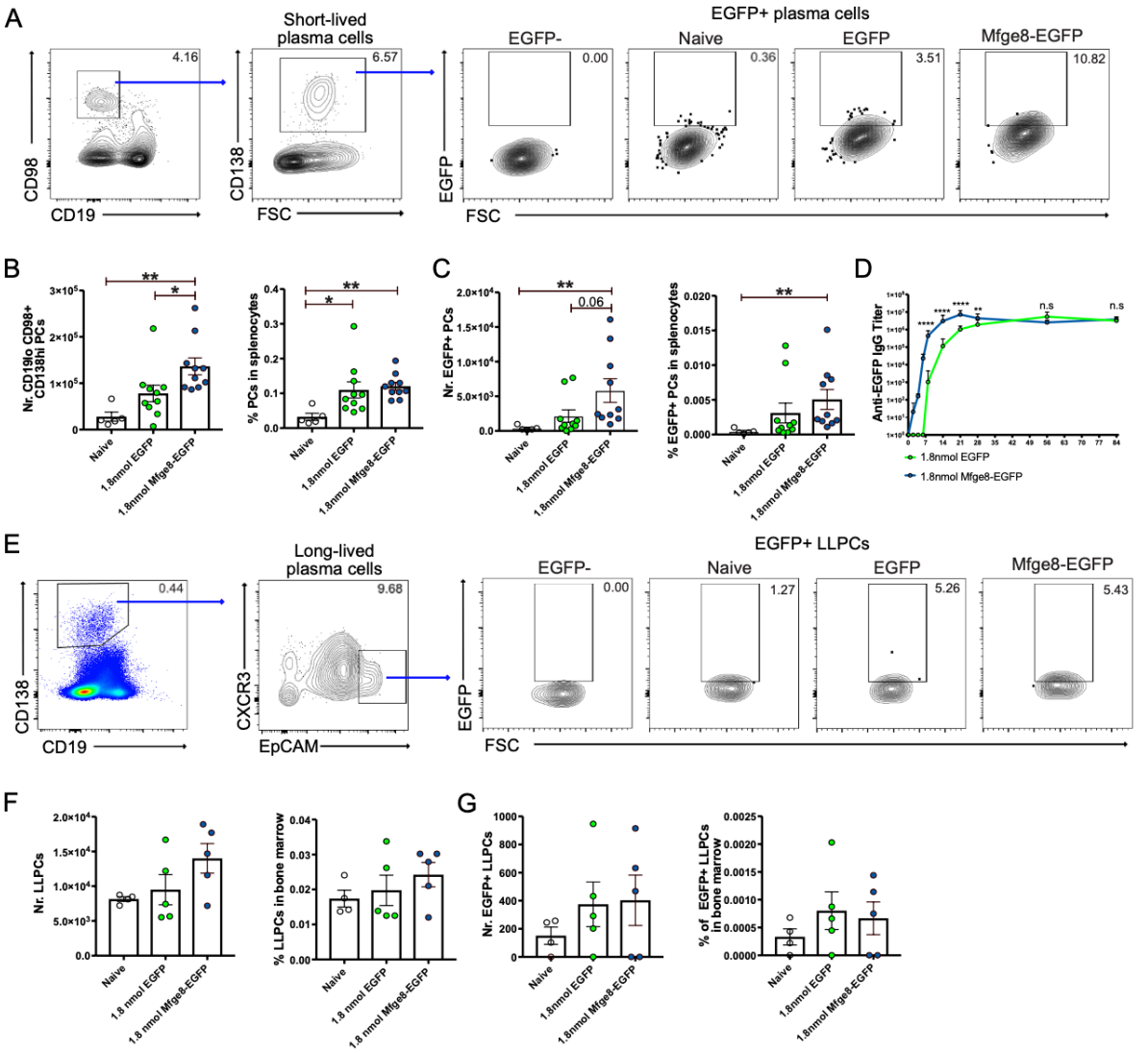

Figure 26. Immunization with EGFP and Mfge8-EGFP shows similar long-term antibody titers.
(A) WT B6 mice were immunized with either alum + 1.8nmol EGFP or Mfge8-EGFP. FACS analysis of short-lived plasma cells (PCs). Representative gating strategy for EGFP specific $CD19^{low}$ $CD138^{hi}$ $CD98^{+}$ short-lived PCs in the spleen 14 days after immunization, plots shown are pre- gated on single live cells.
(B) Absolute number (left) and percentage of short-lived PCs in total splenocytes (right) are shown. One-way-ANOVA with Bonferroni correction was performed.
(C) Absolute number (left) and percentage of EGFP specific short-lived PCs in total splenocytes (right) are shown. One-way-ANOVA with Bonferroni correction was performed, n = 15.
(D) WT B6 mice were immunized with either alum + 1.8nmol EGFP or Mfge8-EGFP, trends of serum anti-EGFP IgG titers over time were measured by ELISA. Mean ± SEM of endpoint titers (OD>0.1) are shown. T test was performed on each time point.
(E) FACS analysis of LLPCs. Representative gating strategy for EGFP specific $CD19^{low}$ $CD138^{hi}$ $EpCAM^{+}$ $CXCR3^{+}$ LLPCs in the bone marrow 87 days after immunization, plots shown are pre- gated on single live cells.
(F) Absolute number (left) and percentage of LLPCs in total bone marrow cells (right) are shown. One-way-ANOVA with Bonferroni correction was performed.
(G) Absolute number (left) and percentage of EGFP specific LLPCs in total bone marrow cells (right) are shown, n = 15. One-way-ANOVA with Bonferroni correction was performed. Data are shown as mean ± SEM, each data point represents an individual mouse. *p ≤ 0.05, **p ≤ 0.01, ***p ≤ 0.001, ****p ≤ 0.0001.

6.12 Secondary immunization with PS-targeting antigen induces faster antibody memory recall responses.

Although a single dose immunization with PS-targeting Mfge8-EGFP did not show more IgG titers after 1 month, it was possible that Mfge8-EGFP induced more MBCs that could provide superior antibody protection upon rechallenge with the same antigen. To test this, two groups of mice were immunized with either 1.8nmol Mfge8-EGFP + alum or EGFP + alum. 29 days later, both groups were rechallenged with 1.8nmol EGFP + alum, serum samples were collected (Figure 27 A red triangle). We found both groups showed similar anti–EGFP IgG titers after boost with EGFP (Figure 27 B: green line and black line), which indicated that primary immunization with PS-targeting Mfge8-EGFP may not generate more MBCs, although direct measurement by FACS may be required. However, we included a third group of mice that were primarily immunized with Mfge8-EGFP and were boosted with Mfge8-EGFP again. This group (blue line) showed significantly more (3x) IgG titers than other two groups on day 36 (7 days after boost) and around 2-fold more on day 43 (14 days after boost), although the difference was not significant (Figure 27 B). The lines of IgG titers showed a clear trend to converge on the later time point, and the advantage of Mfge8-EGFP decreased over time, just as what we have seen in the primary immunization (Figure 26 D). These data indicated that Mfge8-EGFP may not induce more MBCs, but facilitated the activation of MBCs, which reside in a specialized niche in the SCS region, and they are closely associated with memory Tfh cells, as well as $CD169^{+}$ macrophages (Inoue and Kurosaki, 2024).

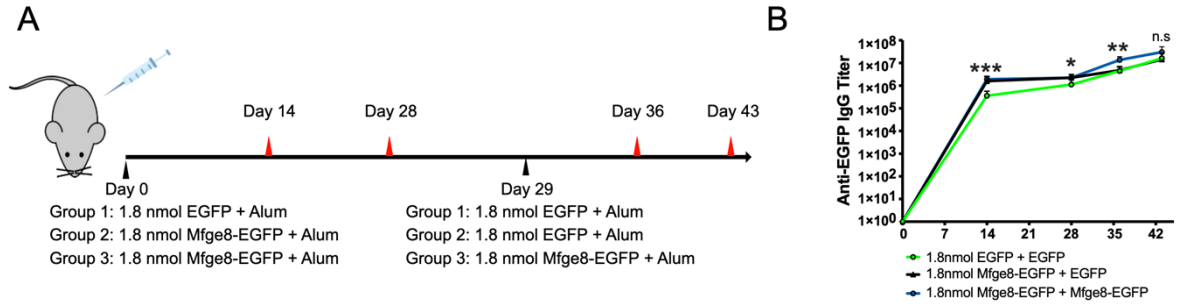

Figure 27. Secondary immunization with Mfge8-EGFP induces faster antibody memory recall responses.
(A) Schematic representation of B cell memory experiment setup**.** Red triangles represent the dates when the serum samples were collected from mice. Black triangles represent the date of immunization. **(B)** Serum IgG titers were measured on the indicated timepoints. Data are shown as mean ± SEM. N = 15. One-way-ANOVA with Bonferroni correction was performed on each time point. *p ≤ 0.05, **p ≤ 0.01, ***p ≤ 0.001, ****p ≤ 0.0001.

6.13 PS-targeting antigen enhances T cell responses.

6.13.1 PS-targeting antigen induces more T follicular helper cells.

Tfh cells play critical roles in regulating GC reactions, by providing CD40L signalling and various of cytokines such as IL-4 and IL-21 to support GC B cell survival, proliferation and antibody affinity maturation (Weinstein et al., 2016, Crotty, 2019). GC B cells with diverse BCR affinity compete for antigens presented on FDCs, then receive uneven Tfh cells' help depending on the amount of peptide-MHC II complexes presented on the GC B cell. The strength of Tfh cells' help determines the fate of GC B cells: They either re-enter DZ for more rounds of proliferation and SHM, or they differentiate into PCs and MBCs (Gitlin et al., 2014, De Silva and Klein, 2015, Inoue et al., 2018). Since Tfh cells are important regulators of humoral immunity and long-term B cell memory, successful induction of substantial Tfh cells is an important criterion for evaluating vaccine efficiency and prediction of the magnitude of GCs and neutralizing antibodies (Havenar-Daughton et al., 2016, Pauthner et al., 2017).

To compare Tfh cells number induced by PS-targeting Mfge8-EGFP and EGFP immunization, $CD4^+CD44^+CD62L^-CXCR5^+PD\text{-}1^+$ Tfh cells were analyzed by flow cytometry 8 days post immunization. In comparison to unimmunized naïve mice, conventional EGFP immunization was not efficient in inducing Tfh cells, the difference was not statistically significant. In contrast, mice immunized with Mfge8-EGFP contained a significant quantity of Tfh cells, which was 3x higher than in EGFP immunized mice. 14 days post immunization, we did not observe a further expansion of Tfh cells (Figure 28 A, B, C). This is consistent with previous studies that found Tfh cells' responses normally reach their peak between day 7 and day 9 (Baumjohann et al., 2011, Botta et al., 2017, Lederer et al., 2020). Moreover, we found very strong positive correlations between Tfh cells and either total GC B cells or $EGFP^+$ GC B cell numbers (Figure 28 D). Histology staining of spleen sections from immunized mice showed that Mfge8-EGFP immunization induced much larger Tfh cells population ($CD4^+$ $PD\text{-}1^+$), and the staining of Tfh cells completely overlapped with the entire PNA^+ GC area (Figure 28 E).

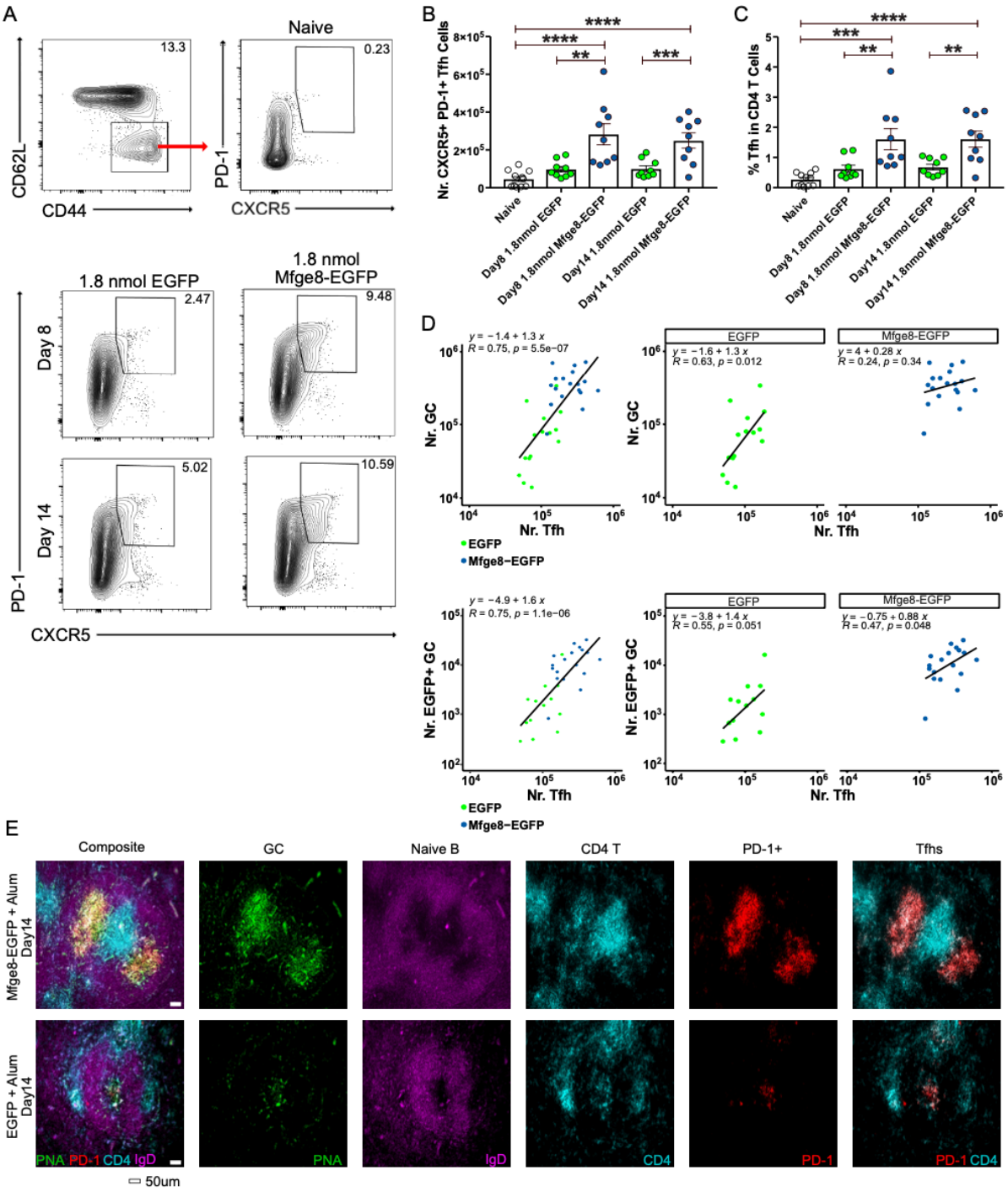

Figure 28. Mfge8-EGFP induces more T follicular helper cells.
(A) WT B6 mice were immunized with either alum + 1.8nmol EGFP or Mfge8-EGFP, Tfh cells in spleen were analyzed by flow cytometry 8 and 14 days after immunization. Representative gating strategy for $CD4^+CD44^+CD62L^-CXCR5^+PD\text{-}1^+$ Tfh cells. Plots shown are pre-gated on single live CD4 cells.
(B-C) Absolute number **(B)** and percentage of Tfh cells in CD4 T cells **(C)**. Data are shown as mean ± SEM, each data point represents an individual mouse. Data are combined from 2 independent experiments. N = 47. One-way-ANOVA with Bonferroni correction was performed. *p ≤ 0.05, **p ≤ 0.01, ***p ≤ 0.001, ****p ≤ 0.0001.
(D) Spearman correlations of Tfh cells and total GC B cells (upper figure), or EGFP binding GC B cells (lower figure) are shown.
(E) WT B6 mice were immunized with either alum + 1.8nmol EGFP or Mfge8-EGFP, spleens were taken 14 days after immunization and stained for $CD4^+PD\text{-}1^+$ Tfh cells and PNA^+ GCs. Scale bar 50 um.

6.13.2 PS-targeted antigen induces more effector CD4 and CD8 T cells.

Next, we tested the activation of effector T cells. Splenocytes from EGFP or Mfge8-EGFP immunized mice were isolated 7 days after immunization, then re-stimulated in vitro for 4h with the $EGFP_{81-95}$ (QHDFFKSAMPEGYVQ) peptide, which is a MHC II restricted epitope in C57BL/6 mice as shown previously (Mould et al., 2021, Skelton et al., 2001). Specific CD4 effector T cell activation was measured by IL-2 and IFN- γ production. We found mice immunized with Mfge8-EGFP generated significantly more EGFP specific CD4 effector T cells than those immunized with equimolar amounts of EGFP. Immunization with four times more (7.2nmol) EGFP slightly improved CD4 T cell responsiveness, but was still less efficient than 1.8nmol Mfge8-EGFP (Figure 29).

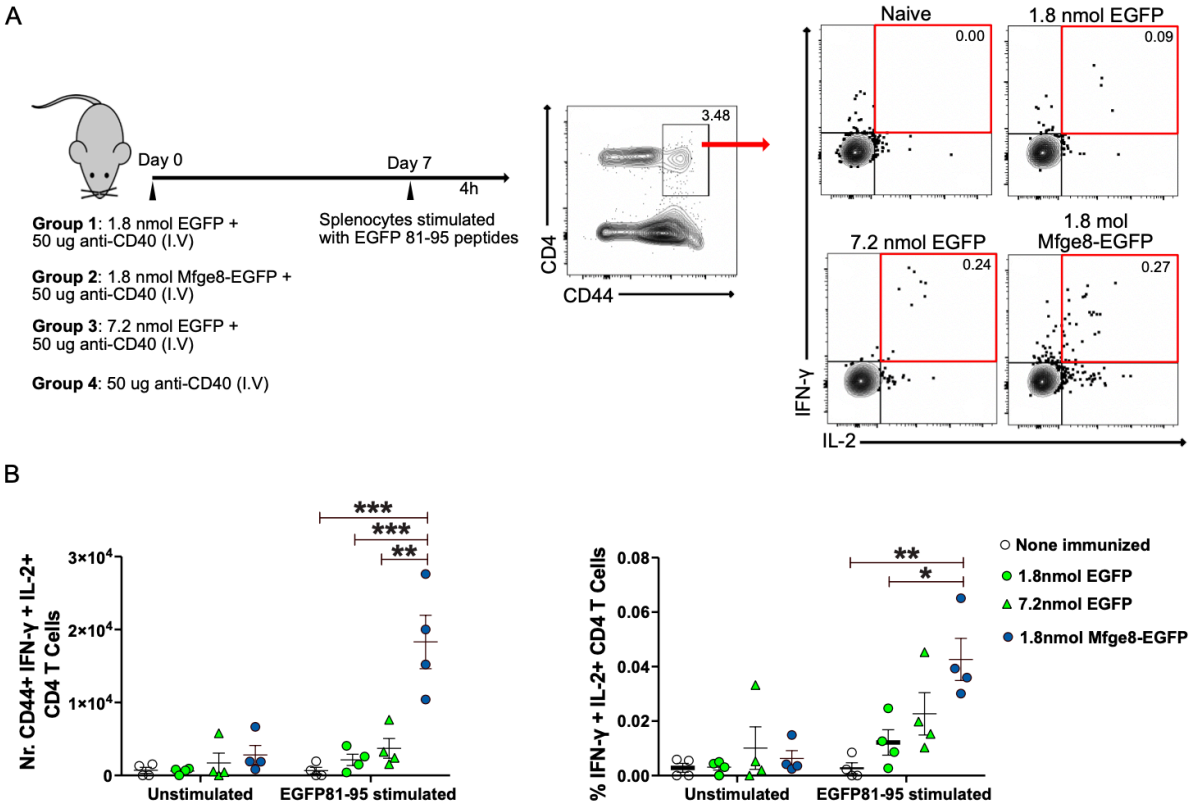

Figure 29. Mfge8-EGFP induces more effector CD4 T cells.
(A) Experimental setup is depicted in the flow chart. Representative gating strategy for activated EGFP specific CD4 T cells ($CD4^+CD44^+$ IL-2^+ IFN- γ^+) after restimulation by $EGFP_{81-95}$ peptides are shown on the right. Plots shown are pre-gated on single live cells.
(B) Absolute number (left) and percentage of activated EGFP specific CD4 T cells of total CD4 T cells (right). N = 16. Data are shown as mean ± SEM, each data point represents an individual mouse. One-way-ANOVA with Bonferroni correction was performed. *p ≤ 0.05, **p ≤ 0.01, ***p ≤ 0.001, ****p ≤ 0.0001.

CD8 T cell responses were measured by IFN-γ and CD107a expression after $EGFP_{120-128}$ (DTLVNRIEL) peptide re-stimulation. Here, we did not observe any differences

between peptide-stimulated and unstimulated cells (Figure 30 A, B). Unspecific stimulation with ionomycin (a calcium ionophore) + PMA (a protein kinase C activator) showed that Mfge8-EGFP immunized mice generated significantly more IFN-γ producing and degranulating (CD107a$^+$) CD8 T cells than mice immunized with EGFP (Figure 30 C), this could be interpreted as a reference of activated CD8 T cell response.

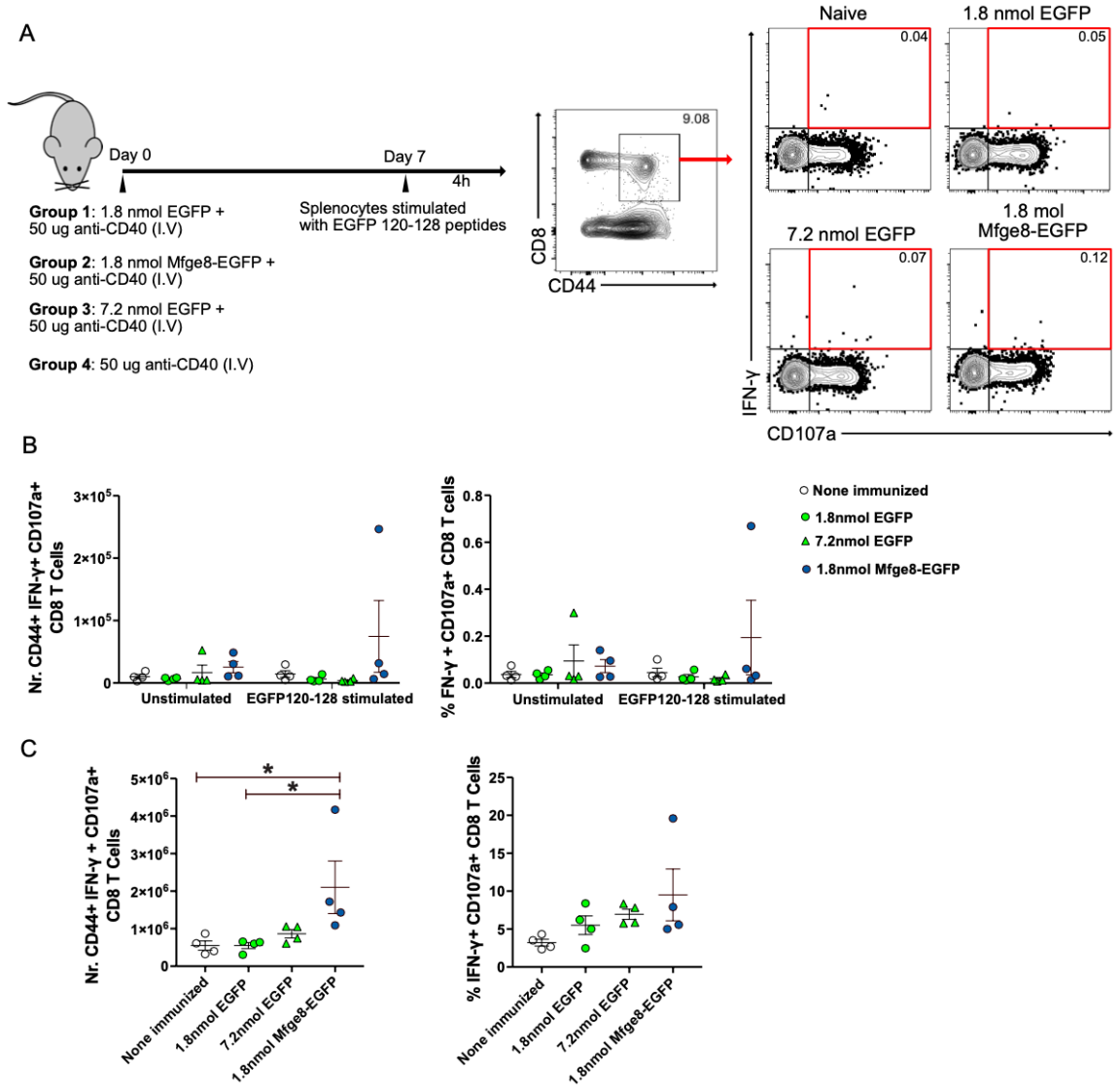

Figure 30. Mfge8-EGFP induces more effector CD8 T cells.
(A) Experimental setup is depicted in the flow chart. Representative gating strategy for activated EGFP specific CD8 T cells (CD8$^+$CD44$^+$ CD107a$^+$ IFN-γ$^+$) after restimulation by $EGFP_{120-128}$ peptides. Plots shown are pre-gated on single live cells.
(B) Absolute number (left) and percentage of activated EGFP specific CD8 T cells in total CD8 T cell population (right).
(C) Absolute number (left) and percentage of activated CD8 T cells in total CD8 T cell population (right) after PMA/ionomycin stimulation. Data are shown as mean ± SEM, each data point represents an individual mouse. N = 16. One-way-ANOVA with Bonferroni correction was performed. *p ≤ 0.05, **p ≤ 0.01, ***p ≤ 0.001, ****p ≤ 0.0001.

6.14 RGD motif is not required for the immune-boosting effect of Mfge8-EGFP.

Mfge8 is a dual binding protein that bridges PS^+ apoptotic cells and αvβ3 and αvβ5 integrins on macrophages through its C1-C2 domains and RGD motif respectively (Kamińska et al., 2018, Lemke, 2019). We have shown before that Mfge8-EGFP accumulated in the lymphoid follicles, and we hypothesized that it was because of the PS-binding capacity of Mfge8. To find out if the RGD motif plays a role in lymphoid follicle targeting and its immune boosting effects, we created a truncated C1C2-EGFP protein, in which EGF domains and the RGD motif were deleted (Figure 31 A). When C1C2-EGFP was injected into the mice intravenously, it accumulated in the MZ of lymphoid follicle and then transferred to the FDC network, similiarly to full length Mfge8-EGFP (Figure 31 B).

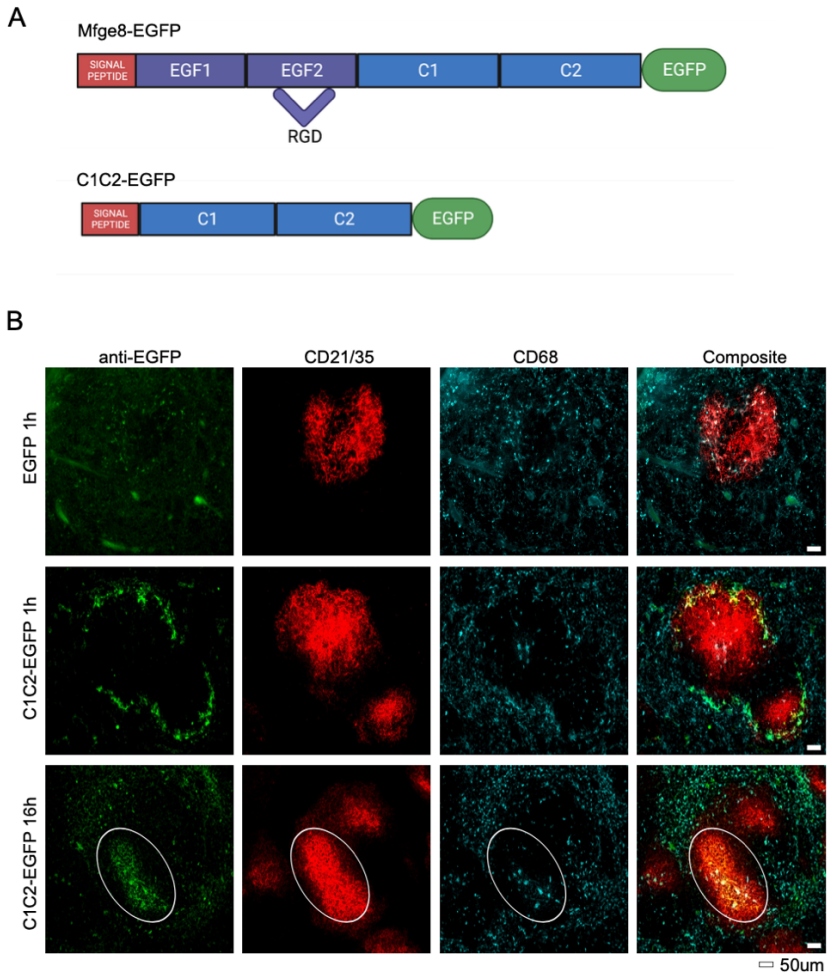

Figure 31. C1C2-EGFP is transported to FDCs.
(A) Schematic illustration and comparison of C1C2-EGFP and Mfge8-EGFP fusion protein (images were created and licensed by Biorender).
(B) Spleen sections from WT B6 mice, stained 1h and 16h after intravenous injection of 1.8nmol C1C2-EGFP or conventional EGFP. Scale bar 50 um. Staining antibodies: anti CD21/35-PE, anti GFP- FITC, anti CD68-APC.

Subsequently, we tested immune responses induced by C1C2-EGFP immunization. We found serum antigen specific antibody titers (Figure 32 A, B), day 14 EGFP specific GC B cells (Figure 32 C, D) and Tfh cells (Figure 32 E, F) were all significantly increased, compared to mice immunized with equimolar amounts of EGFP. However, when compared to mice immunized with equimolar amounts of full length Mfge8-EGFP, it showed no significant difference (number of GC B cells: $p = 0.18$; percentage of GC B cells: $p = 0.43$; number of Tfh cells: $p = 0.27$; percentage of Tfh cells: $p = 0.99$). Therefore, targeting antigens to PS^+ structures alone, could bring antigens to the lymphoid follicles and promote B cell and T cell immune responses. Lack of the RGD motif did not negatively affect this process.

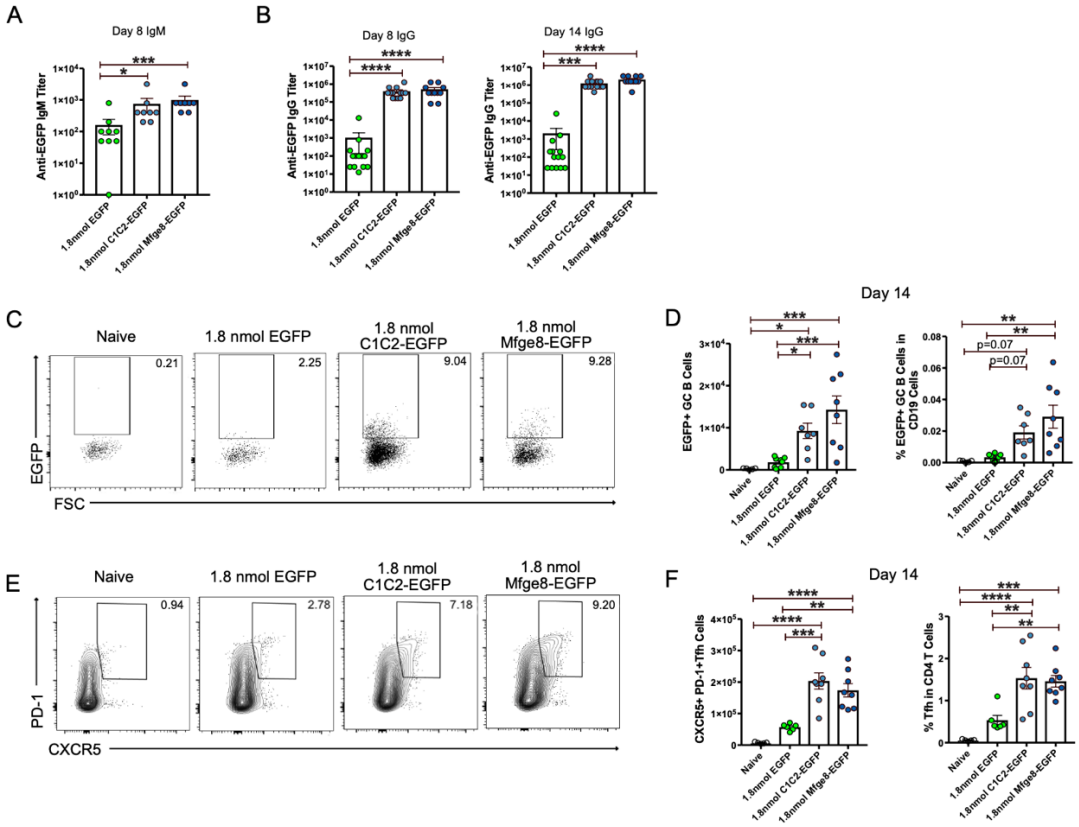

Figure 32. RGD motif is not required for the immune-boosting effect of Mfge8-EGFP.
(A-B) WT B6 mice were immunized with equal 1.8nmol of EGFP, C1C2-EGFP or Mfge8-EGFP with alum I.P. Bar graphs show serum anti-EGFP IgM titers measured on day 8 **(A)** and IgG titers measured on both day 8 and day 14 **(B).**
(C) Representative gating strategy for EGFP specific GC B cells. Plots shown are pre-gated on single live $CD19^+$ IgD^{lo} $CD95^+$ $GL7^+$ GC B cells.
(D) Statistical analysis of absolute number of EGFP specific GC B cells is shown on the left, percentages of $EGFP^+$ GC B cells in total $CD19^+$ B cells is shown on the right.
(E) Representative gating strategy for Tfh cells. Plots shown are pre-gated on single live $CD4^+$ $CD44^+$ $CD62L^-$ T cells.
(F) Statistical analysis of absolute number of Tfh cells is shown on the left, percentage of Tfh cells in total CD4 T cells is shown on the right. Data are collected from 2 independent experiments. Mean ± SEM are shown, and each data point represents an individual mouse. One-way-ANOVA with Bonferroni correction was performed. *$p \leq 0.05$, **$p \leq 0.01$, ***$p \leq 0.001$, ****$p \leq 0.0001$.

6.15 Antigens conjugated to multimerized mC1 domains promote B cell responses.

Based on the above data showing that PS binding via C domains is sufficient to target antigens to the lymphoid follicles, we generated a fast antigen-coupling platform that would allow rapid attachment of a PS-binding domain to any protein antigen. For this we used C1-tetramers. C1-tetramers consist of the PS binding mouse C1 domain (mC1) produced in E. coli. Purified mC1 was biotinylated and then tetramerized with streptavidin (SA) that was conjugated to OVA (OVA-SA) (Figure 33 A). When the OVA-SA-mC1 tetramers were injected into the mice, we observed OVA accumulated in the MZ of lymphoid follicles first, then later was deposited on FDCs, whereas conventional OVA-protein was not detected in lymphoid follicles from mice injected with OVA-SA, lacking the PS-targeting properties (Figure 33 B).

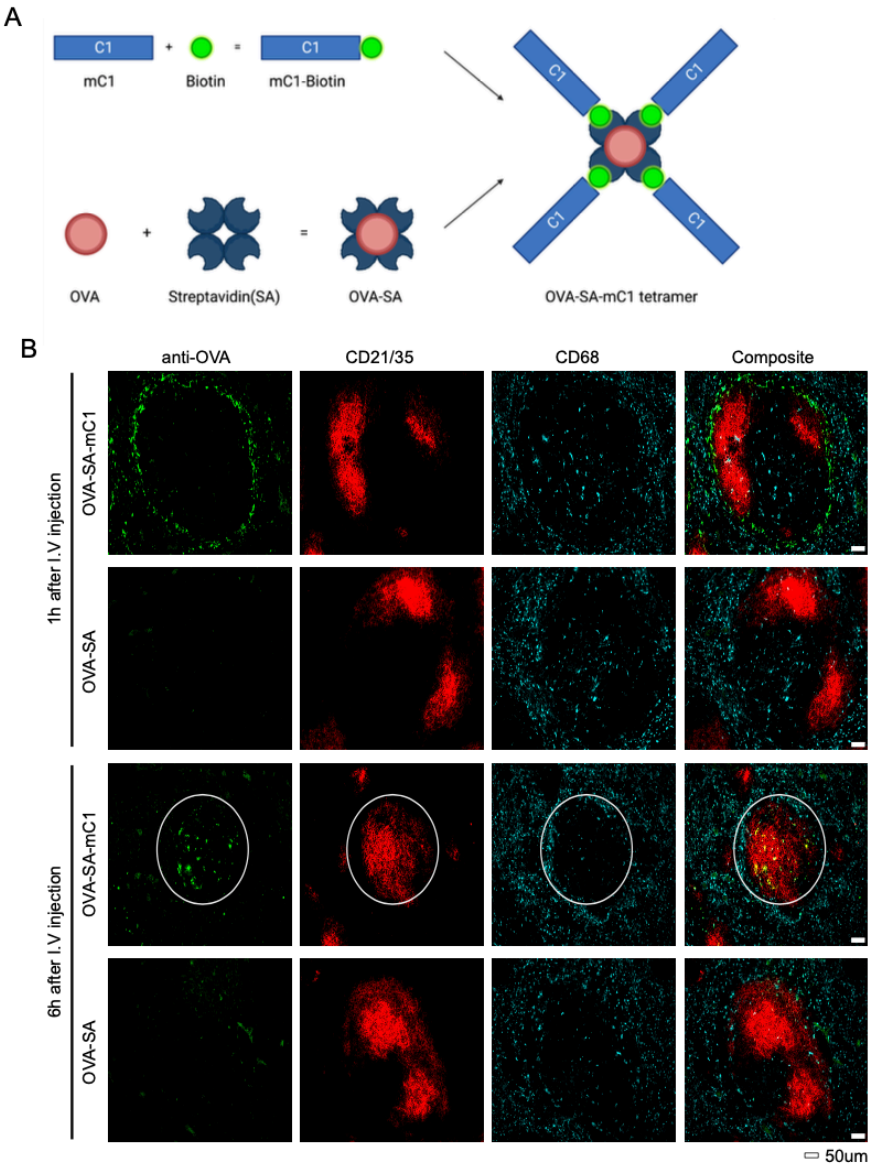

Figure 33. OVA-SA-mC1 tetramers are transported to FDCs.
(A) Schematic representation of the construction of OVA-SA-mC1 tetramer (images were created and licensed by Biorender).
(B) Spleen sections from WT B6 mice, stained 1h and 6h after intravenous injection of 1.1nmol OVA-SA-mC1 tetramer or OVA-SA. Scale bar 50 um. Staining antibodies: anti CD21/35-PE, anti OVA-FITC, anti CD68-APC.

Next, serum OVA specific IgG titers were compared among mice immunized with single doses of equimolar amounts of OVA, OVA-SA, SA-mC1 tetramer + free OVA or OVA-SA-mC1 tetramer. 7 days after immunization, OVA-SA-mC1 tetramer immunized mice produced at least 48x more OVA specific IgG than mice immunized with OVA, OVA-SA, SA-mC1 tetramer + free OVA. 14 days after immunization, serum IgG titers increased 6.7x in mice immunized with OVA-SA-mC1 tetramer, but mice immunized with OVA, OVA-SA, SA-mC1 tetramer + free OVA increased 80x in the second week post immunization, however, IgG titers in mice immunized with OVA-SA-

mC1 tetramer were still at least 4x higher than the rest of groups (Figure 34 A, B). We also observed that SA conjugation alone did not promote antibody responses to OVA, neither did SA-mC1 tetramer. OVA has to be conjugated to the PS targeting SA-mC1 tetramer to boost antibody response against OVA.

Considering the existence of SA as another strong antigen in the OVA-SA construct, we wanted to know whether the antibody response to one antigen could affect the response to the other, as a result of competition of conjugated antigen. We tested the serum anti-SA IgG in these mice and found mice immunized with SA-mC1 tetramer + free OVA and mice immunized OVA-SA-mC1 tetramer produced same level of anti-SA IgG, indicating that addition of a PS-binding domain to OVA enhanced also anti-SA responses, and the conjugated two antigens induced antibody responses independently (Figure 34 C).

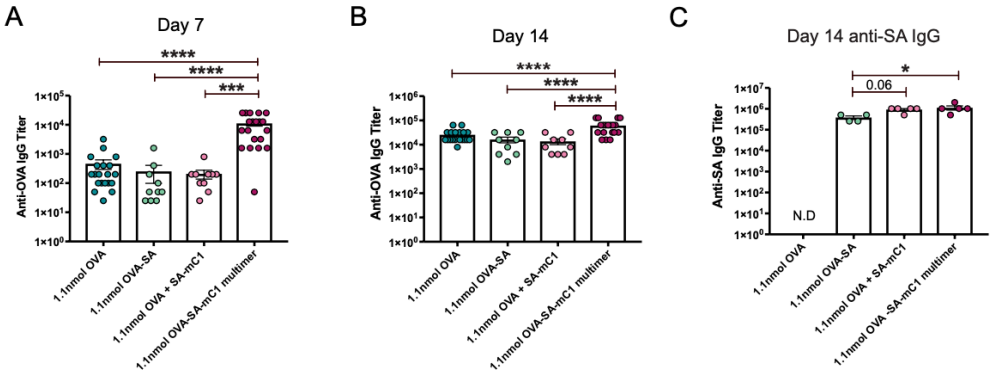

Figure 34. OVA-SA-mC1 tetramer immunization promotes antibodies production.
(A-B) WT B6 mice were immunized i.p. with alum mixed with either 1.1nmol OVA, SA-OVA, SA-mC1 tetramer + free OVA or OVA-SA-mC1 tetramer separately. Serum anti-OVA antibody titers were measured on day 7 **(A)** and day 14 **(B).**
(C) Bar graphs show serum anti-SA antibody titers measured on day 14. Data are shown as mean ± SEM, each data point represents an individual mouse. N = 60. One-way-ANOVA with Bonferroni correction was performed. *p ≤ 0.05, **p ≤ 0.01, ***p ≤ 0.001, ****p ≤ 0.0001.

GC reactions in these mice were also compared on day 14. We found immunization with OVA-SA-mC1 tetramer induced significantly more GC B cell than mice immunized with OVA or OVA-SA (Figure 35 B). Mice immunized with SA-mC1 tetramer + free OVA produced slightly fewer GC B cells than mice immunized with OVA-SA-mC1 tetramer, but significantly more than mice immunized with OVA or OVA-SA. This might be due to the SA endowed with a PS-binding domain that caused targeting to FDCs and generation of GC B cells. However, when we measured the OVA specific GC B cells, mice immunized with SA-mC1 tetramer + free OVA did not show any difference

as compared to mice immunized with OVA or OVA-SA. In contrast, mice immunized with OVA-SA-mC1 tetramer induced 5-7x more OVA specific GC B cells than the control groups. These results provide additional evidence that OVA has to be conjugated to a PS targeting domain to promote GC reactions against OVA (Figure 35 A, C).

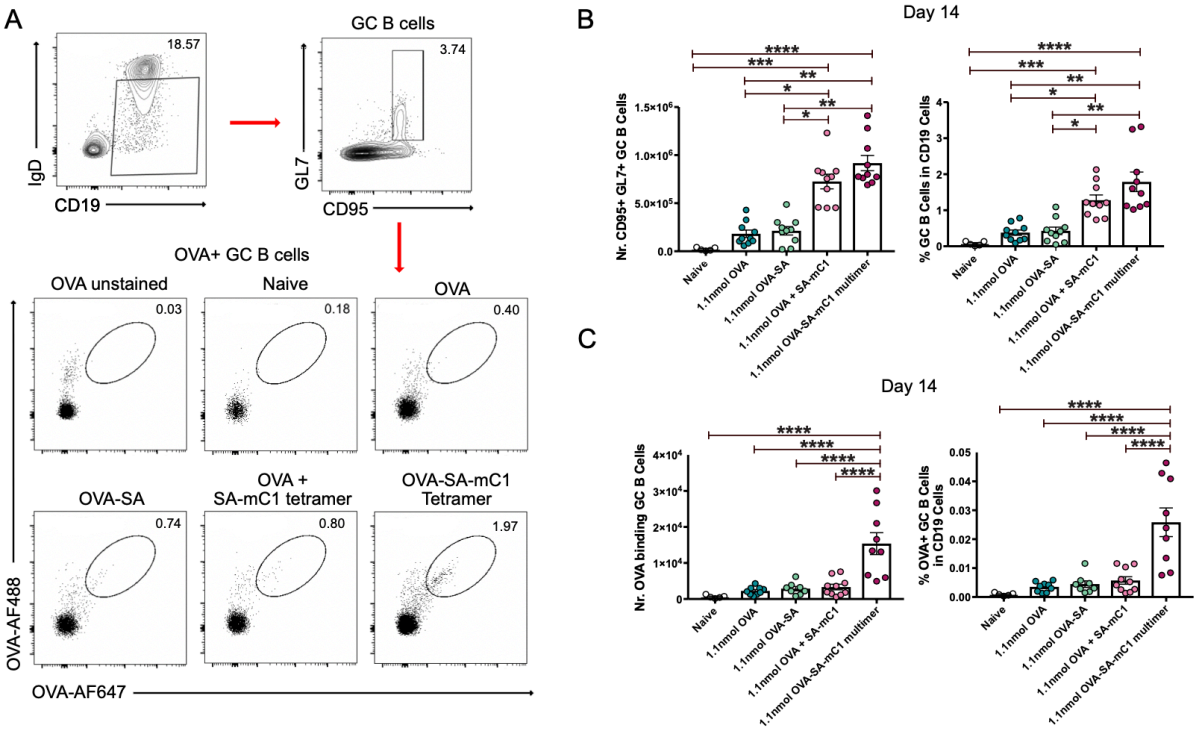

Figure 35. OVA-SA-mC1 tetramer immunization promotes GC reactions.
Groups of mice were immunized with single doses of equimolar amounts of OVA, OVA-SA, SA-mC1 tetramer + free OVA or OVA-SA-mC1 tetramer. Splenocytes were isolated 14 days after immunization and stained for OVA specific GC B cells.
(A) Representative gating strategy for OVA specific GC B cells. Plots shown are pre-gated on single live cells.
(B) Statistical analyses of total GC B cells, absolute number (left) and percentage in $CD19^+$ B cells (right).
(C) Statistical analyses of OVA specific GC B cells, absolute number (left) and percentage in $CD19^+$ B cells (right). Data are shown as mean ± SEM, each data point represents an individual mouse. Data are combined from 2 independent experiments. N = 41. One-way-ANOVA with Bonferroni correction was performed. *p ≤ 0.05, **p ≤ 0.01, ***p ≤ 0.001, ****p ≤ 0.0001.

6.16 Immunization with OVA-SA-mC1 tetramer generates robust B cell memory.

Next, we compared the memory B cell responses of mice immunized with OVA or OVA-SA-mC1 tetramer. Mice receiving either immunization were boosted with equal amounts of OVA 4 weeks after primary immunization, and serum antibody titers were measured every 7 days. We found mice immunized with OVA-SA-mC1 tetramer rapidly reached the peak IgG titers, mice immunized with OVA showed significant lower IgG titers at the early time points, but slowly caught up. On day 28, mice

immunized with either OVA or OVA-SA-mC1 tetramer showed similar levels of serum IgG. However, one week after the boost, mice initially immunized with OVA-SA-mC1 tetramer showed two-fold higher anti-OVA IgG titers. Another week later, the difference increased to 3-fold, but was not statistically significant (Figure 36 A, B). Serum anti-OVA IgM levels were similar between the two immunization groups at all measured timepoints (Figure 36 C).

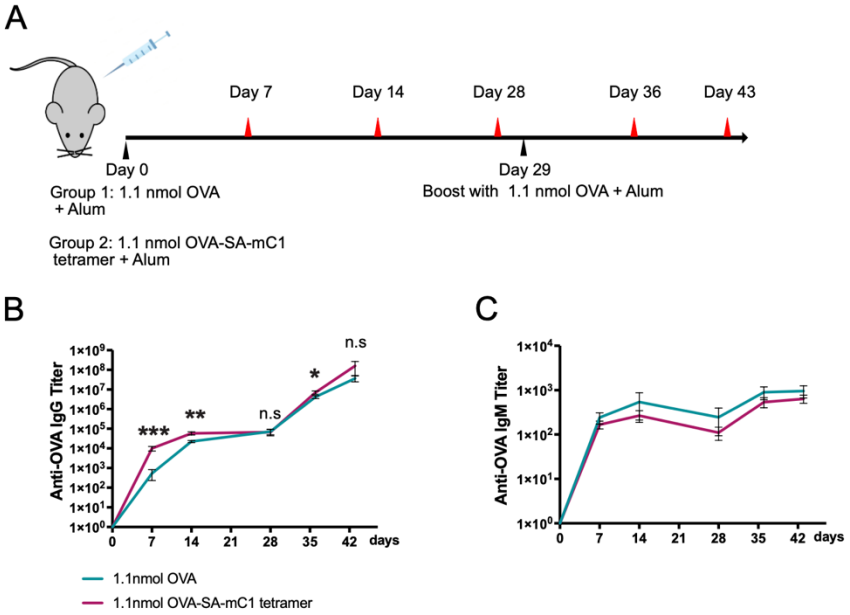

Figure 36. OVA-SA-mC1 tetramer immunization generates robust B cell memory.
(A) Schematic representation of B cell memory experiment setup**.**
(B-C) Serum IgG titers **(B)** and IgM titers **(C)** were measured on the indicated timepoints. Data are shown as mean ± SEM. Data are combined from 2 independent experiments. N = 20. T test was performed on each time point. *p ≤ 0.05, **p ≤ 0.01, ***p ≤ 0.001, ****p ≤ 0.0001.

6.17 PS-targeting antigens elicit strong CTL responses.

6.17.1 OVA-SA-mC1 induces more activated CD8 T cells.

CD8 T cells play critical roles in eliminating intracellular pathogens and controlling virus infections. However, many traditional vaccines are known to be inefficient in inducing CD8 T cell response (Hirai and Yoshioka, 2022). We therefore tested if PS-targeting antigens could improve the CD8 T cell response. For this, mice were immunized with either OVA, OVA-SA or OVA-SA-mC1 tetramer. 7 days after immunization, splenocytes were isolated and stimulated in vitro with various MHC I peptides OVA_{55}, OVA_{107} and OVA_{257} separately (Karandikar et al., 2019). Epitope specific CD8 T cell activation was measured by IFN-γ production and the degranulation marker CD107a. We found mice immunized with OVA-SA-mC1

tetramer induced significantly more activated CD8 T cells that produced IFN-γ and degranulated (IFN-g$^+$CD107a$^+$) after cognate peptide restimulation. Activated CD8 T cells in OVA, OVA-SA immunized mice showed no significant difference (Figure 37).

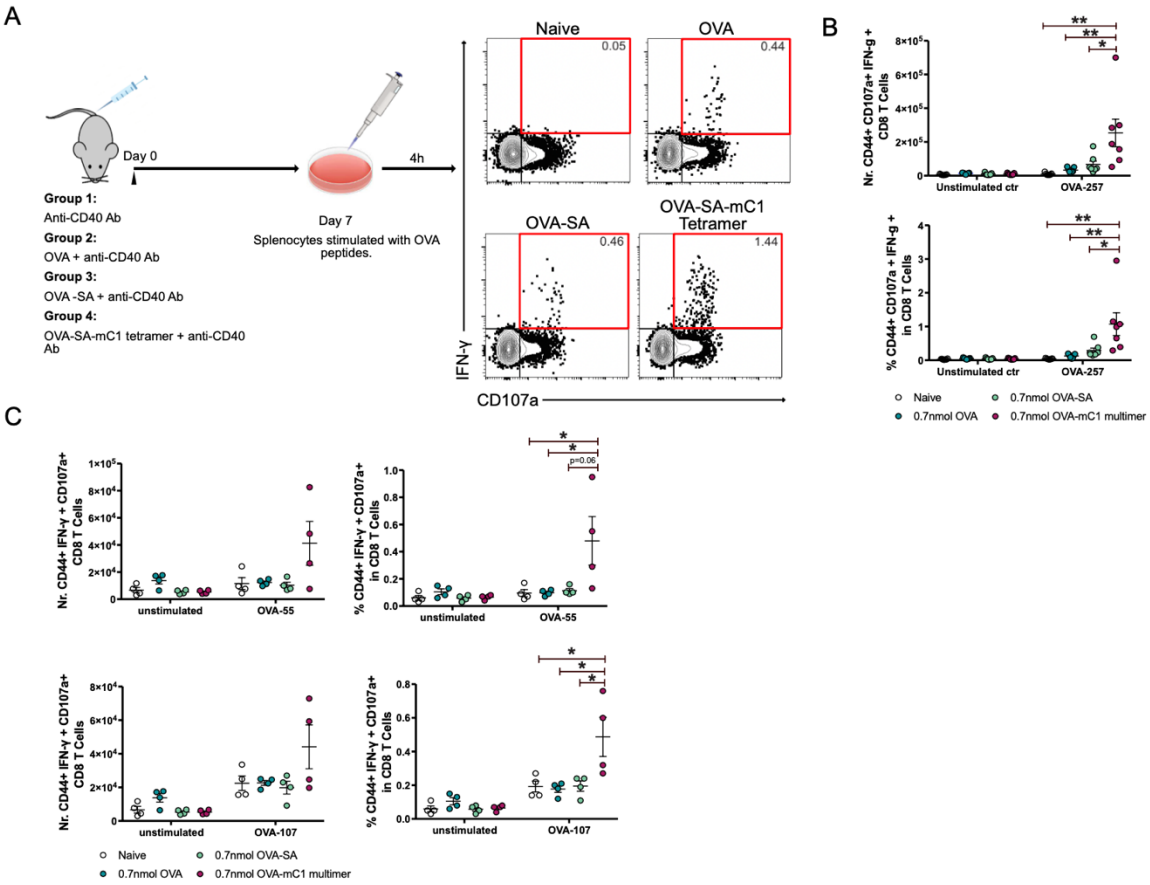

Figure 37. OVA-SA-mC1 induces more activated CD8 T cells.
(A) Schematic representation of CD8 T cell re-stimulation experimental setup and gating strategy for activated OVA specific CD8 T cells. Mice were immunized separately with 0.7nmol of OVA, OVA-SA or OVA-SA-mC1 tetramer mixed with anti-CD40 antibody. 7 days later, isolated splenocytes were stimulated with OVA_{257} peptides in vitro. Activated CD8 T cells are shown as IFN- γ^+ $CD107a^+$. Plots shown are pre-gated on single live $CD8^+$ $CD44^+$ cells.
(B) Statistical analyses of absolute number (upper panel) and percentage of activated CD8 T cell in total CD8 T cell population (lower panel) after OVA_{257} peptide re-stimulation.
(C) Statistical analyses of absolute number (left) and percentage of activated CD8 T cell in total CD8 T cell population (right) after OVA_{55} (upper panel) or OVA_{107} peptides (lower panel) re-stimulation. Data are shown as mean ± SEM. Each data point represents an individual mouse. N = 28. One-way-ANOVA with Bonferroni correction was performed. *p ≤ 0.05, **p ≤ 0.01, ***p ≤ 0.001, ****p ≤ 0.0001.

6.17.2 OVA-SA-mC1 immunization induces more efficient CTL killing of target cells.

We further tested the CTL in vivo killing capability by injecting a mix of equal numbers of $CFSE^{hi}$ OVA_{257} peptide-pulsed and $CFSE^{lo}$ peptide-free syngeneic splenocytes into recipient mice that received OVA-SA or OVA-SA-mC1 tetramer immunization 7 days earlier. CTL killing efficiency was measured by the ratio (r) of $CFSE^{hi}$ to $CFSE^{lo}$ cells

collected from blood 2h, 4h and 8h after injection, lower $CFSE^{hi}$ /$CFSE^{lo}$ ratio indicated efficient CTL elimination of target cells coated with cognate peptides. We found mice immunized with OVA-SA-mC1 tetramer were significantly more efficient in killing OVA_{257} coated cells. As early as 2h after injection, most peptide-coated cells were eliminated. In contrast, mice immunized with OVA-SA reacted to peptides presenting cells much slower (Figure 38).

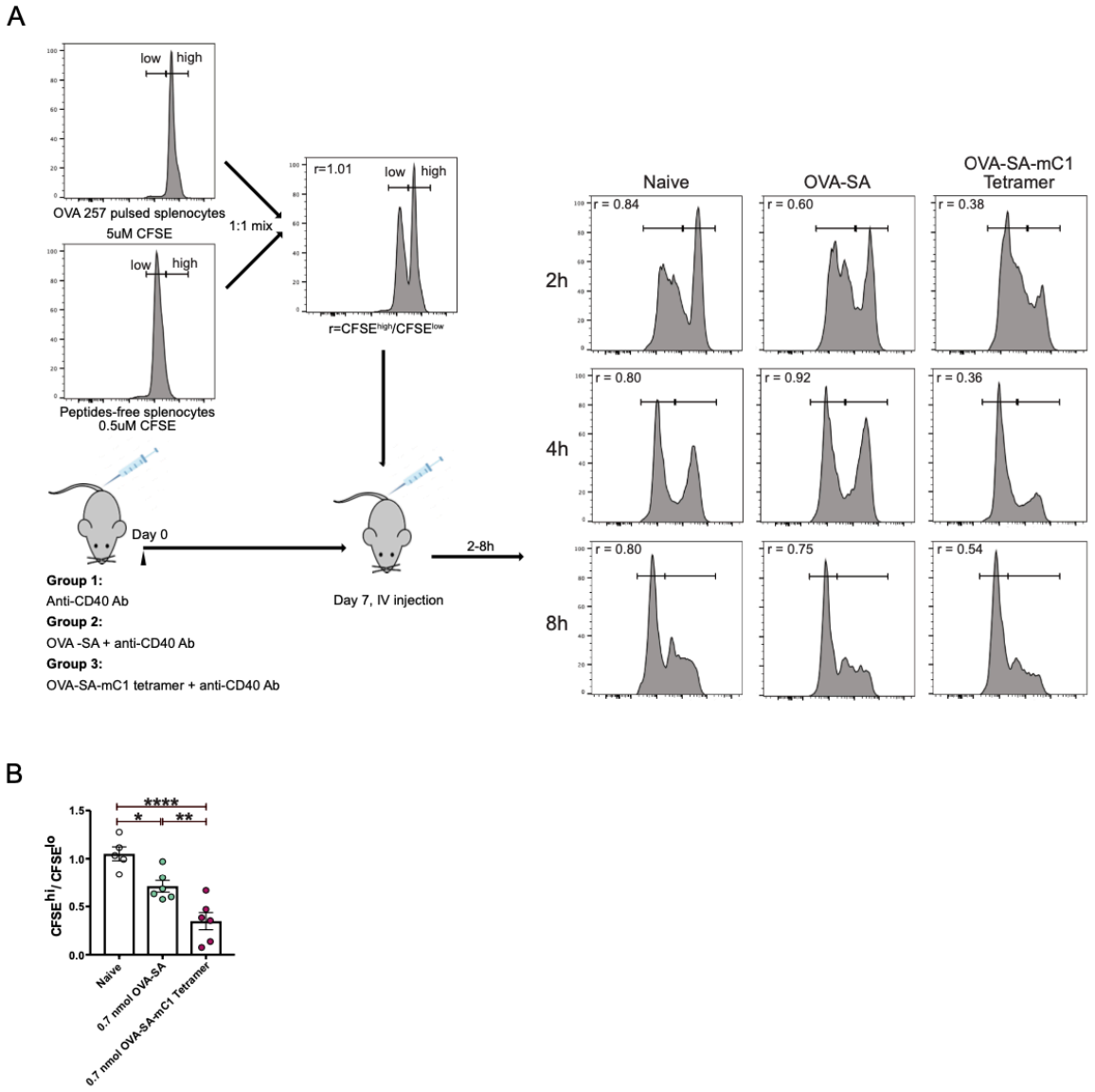

Figure 38. OVA-SA-mC1 induces more efficient CTL killing.
(A) Schematic representation of in vivo CTL killing assay setup. 1:1 mixed $CFSE^{hi}$ OVA_{257} peptide-pulsed and $CFSE^{lo}$ peptides-free allogeneic splenocytes were injected into recipient mice that received OVA-SA or OVA-SA-mC1 tetramer immunization 7 days earlier. CTL killing efficiency was measured by the ratio of $CFSE^{hi}$ to $CFSE^{lo}$ cells (r) collected from blood 2h, 4h and 8h after injection. **(B)** Statistical analysis of the ratio of $CFSE^{hi}$ to $CFSE^{lo}$ cells (r) collected from blood 2h after injection. Data are shown as mean ± SEM. Each data point represents an individual mouse. Data are collected from 2 independent experiments. N = 23. One-way-ANOVA with Bonferroni correction was performed. *p ≤ 0.05, **p ≤ 0.01, ***p ≤ 0.001, ****p ≤ 0.0001.

6.18 Immunization with OVA-SA-mC1 tetramer generates robust CD8 T cell memory.

Next, we evaluated the memory CD8 T cell response. Mice initially immunized with either OVA or OVA-SA-mC1 tetramer received a booster immunization 4 weeks later. The boost contained a mixture of 50μg OVA_{55}, OVA_{107} and OVA_{257} peptides, together with 100μg poly I:C and 50μg anti-CD40 antibody. 4 days after the boost, splenocytes were isolated and re-stimulated with various MHC I peptides separately. Memory recall responses were assessed by quantifiying IFN-γ $^{+}$CD107a^{+} CD8 T cells. We found that, when re-stimulated with OVA_{257} peptides, mice immunized with OVA-SA-mC1 tetramer as primary immunization induced significantly more IFN-g^{+}CD107a^{+} activated CD8 T cells after boost than mice initially immunized with OVA (Figure 39 A, B). However, re-stimulation with OVA_{107} and OVA_{55} peptides did not generate adequate responses compared to their respective unstimulated control. These data are contrary to the acute 7-day immunization, in which CD8 T cell immune responses were elicited by both the immunodominant epitope (OVA_{257}) and subdominant epitopes (OVA_{55} and OVA_{107}). Memory recall responses in both immunization groups were dominated by the CD8 T cells that recognized the immunodominant OVA_{257} (Figure 39 C). In conclusion, OVA-SA-mC1 tetramer could more efficiently induce acute CD8 T cell response and develop robust CD8 memory after a single dose of immunization, but it did not expand the memory CD8 T cell repertoire.

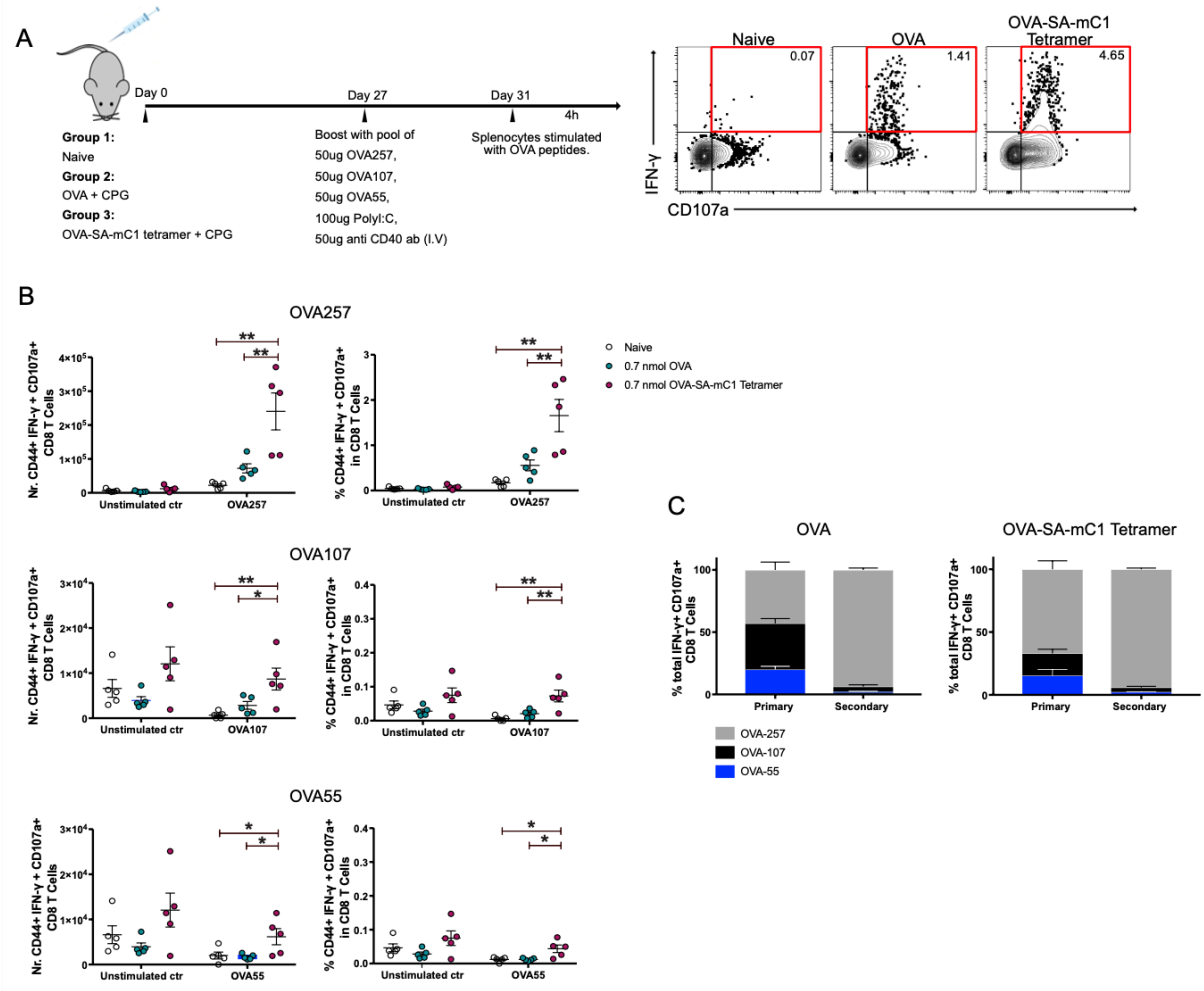

Figure 39. OVA-SA-mC1 immunization generates robust CD8 T cell memory.
(A) Schematic representation of CD8 T cell memory recall assay setup and gating strategy for activated OVA specific CD8 T cells. Mice were immunized separately with 0.7nmol of OVA or OVA-SA- mC1 tetramer mixed with CPG. 27 days later, all mice received the same boost with a mixture of OVA_{55}, OVA_{107} and OVA_{257} peptides, together with poly I:C and anti-CD40 antibody as adjuvant. 4 days later, isolated splenocytes were stimulated with OVA_{257} peptides in vitro, activated CD8 T cells were shown as IFN-$g^{+}CD107a^{+}$. Plots shown are pre-gated on single live $CD8^{+}$ $CD44^{+}$ cells.
(B) Statistical analyses of absolute number (left) and percentage of activated CD8 T cell in total CD8 T cell population (right) after OVA_{257}, OVA_{107} and OVA_{55} peptide re-stimulation. Data are shown as mean ± SEM. Each data point represents an individual mouse. N = 15. One-way-ANOVA with Bonferroni correction was performed. *p ≤ 0.05, **p ≤ 0.01, ***p ≤ 0.001, ****p ≤ 0.0001.
(C) Comparison of CD8 T cell responses to different OVA epitopes between acute immune response and memory recall response.

6.19 OVA-SA-mC1 tetramer immunization induces more Tfh cells.

The number of Tfh cells was measured 14 days after immunizing mice with either OVA, OVA-SA, SA-mC1 tetramer + free OVA or OVA-SA-mC1 tetramer. Mice immunized with OVA-SA-mC1 tetramer had more Tfh cells than mice immunized with OVA, OVA-SA or SA-mC1 tetramer + free OVA, although the difference was not significant. Due to the inability to analyze antigen-specific Tfh cells , immunization with

SA-mC1 tetramer + free OVA also showed more Tfh cells than mice immunized with OVA or OVA-SA, probably because of the presence of PS-targeting SA, which could also induce considerable amount of the SA-specific Tfh cells (Figure 40).

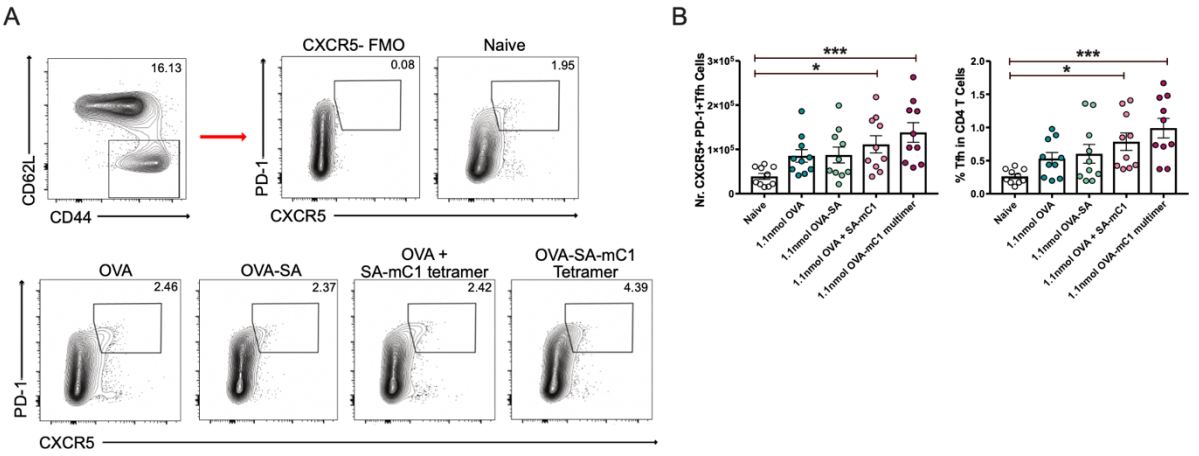

Figure 40. OVA-SA-mC1 tetramer immunization induces more Tfh cells.
(A) Representative gating strategy for Tfh cells. WT mice were immunized i.p. with either 1.1nmol OVA, SA-OVA, SA-mC1 tetramer + free OVA or OVA-SA-mC1 tetramer. Tfh cells were measured 14 days after immunization. Plots shown are pre-gated on single live CD4 cells.
(B) Absolute number (left) and percentage of Tfh cells in CD4 T cells (right). Mean ± SEM are shown, and each data point represents an individual mouse. N = 50. One-way-ANOVA with Bonferroni correction was performed. *p ≤ 0.05, **p ≤ 0.01, ***p ≤ 0.001, ****p ≤ 0.0001.

7. Discussion

7.1 PS-targeting antigens are transferred to FDCs in unimmunized naïve mice.

7.1.1 PS-targeting antigens are transferred to FDCs independent of C3.

PS is a type of phospholipid in plasma membranes that is asymmetrically confined to the inner membrane leaflet in healthy live cells, and is exposed to the outer surface in apoptotic cells (Suzuki et al., 2013, Suzuki et al., 2014). EVs are cell-derived membrane-bound particles that are abundant in the blood stream and lymphatic fluid, they also expose PS on their surface (Groß et al., 2024, Rausch et al., 2023). From our unpublished data, over 95% of $CFSE^+$ membrane particles in the serum are PS positive, they are assumed to be EVs because over 90% of these PS^+ particles express exosome markers CD81 or CD9 (data from Lavinia Flaskamp). In addition to their abundance in the serum, due to their small size, EVs show high curvature, which leads to preferential binding of EVs by Mfge8 (Shi et al., 2004). Therefore, targeting antigens to PS by Mfge8 will preferentially target antigens to EVs. We hypothesized that these PS-targeting antigens would be brought to the organs and tissues where EVs accumulate. Previous studies have shown that EVs in the circulation are rapidly captured by $CD169^+$ macrophages and accumulate in the SCS of lymph nodes and MZ of the spleen (Saunderson et al., 2014). Here in our study, we targeted antigens to PS via Mfge8 or only the C1 domain. We found these PS-targeting antigens accumulated in the MZ of the lymphoid follicles after injection, either intravenously or intraperitoneally.

PS-targeting by mC1 tetramer or C1C2-EGFP, in which RGD motif is absent, could still accumulate in the marginal zone. These data indicated that direct capture by macrophages via RGD-integrin interaction may not be the dominant mechanism contributing to their accumulation in the MZ. On the other hand, the majority (60-95%) of PS-targeting antigens colocalized with exosome markers CD81 or CD63, indicating those antigens were brought to the MZ mainly through EVs accumulation.

PS-targeting antigens that accumulated in the MZ were found to be deposited on FDCs at the later time points. Surprisingly, this happened in unimmunized naïve mice that did not have pre-existing antigen-specific antibodies. Antigen deposition on FDCs is known to depend on the formation of immune complexes, which requires specific

antibodies and participation of complement system (Kranich and Krautler, 2016). As a control, we injected EGFP into both EGFP-naïve mice and pre-immunized mice and observed anti-EGFP staining in FDC area in pre-immunized mice only. These data ruled out the possibility of false positive results caused by the detection antibody. In addition, serum anti-EGFP antibody tested in WT naïve mice showed no pre-existing EGFP specific antibody, neither natural antibody that cross-reacted to EGFP. These data showed an immune complex independent way of transporting PS-targeting antigens to FDCs.

The acquisition of antigens by FDCs is depended on the binding of their complement receptors (CR1/CD35 or CR2/CD21) to antigens opsonized with C3d (Victora and Nussenzweig, 2022, Heesters et al., 2014). The activation and cleavage of C3 is initiated by the specific antibody binding to the pathogen (classical pathway), but can also be activated by MBL, which binds to glycoproteins and glycolipids on pathogens that contain mannose residues, then activates the classical pathway without specific antibody (Abbas, 2005, Pouw and Ricklin, 2021). After ruling out the pre-existence of EGFP specific or cross-reactive antibodies in naïve WT mouse, we next thought that the glycosylated PS-targeting antigens may activate the mannose-binding lectin pathway and they were targeted to FDCs in a complement dependent way, as similar observations were also documented with HIV nanoparticles (Tokatlian et al., 2019). However, when we injected PS-targeting antigens into unimmunized naive C3 KO mice, PS-targeting antigens were still transported to FDCs. These data demonstrated that deposition of PS-targeted antigens onto FDCs is independent of the complement system.

7.1.2 CD169+ microvesicles transport PS-targeting antigens to FDCs.

We tried to explore the potential mechanisms contributing to this antigen deposition. Considering that PS-targeting antigens accumulated in the MZ were attached to EVs, we hypothesized that EVs (or certain type of EVs) could pass-through the MZ macrophages' capture, entering the lymphoid follicle and were preferentially captured by FDCs. We injected PKH26 labeled EVs (isolated form BMDC or DC2.4 cell culture) into the naïve WT mice, but we didn't see these EVs on FDCs, on the contrary, they remained in the MZ for over 16h (data not shown). Previous research, in which CD169 macrophages were depleted, showed exosomes invaded splenic red pulp and cortex

of lymph nodes, rather than B cell follicles or FDCs (Saunderson et al., 2014). These data implied that EVs in the circulation were unlikely to penetrate MZ macrophages and directly bind to FDCs. However, we should keep in mind that both of the two studies used only DC-or B cell-derived EVs that were produced in vitro. These observations could not rule out the possibility that EVs derived from other cell types, or EVs generated under physiological condition, may express different integrin/receptor patterns that enable them to be preferentially captured by FDCs. Another difference to our study was that the PKH26 labeled EVs can be detected in the MZ even 16h after injection, which is opposite to the previous research which suggested EVs (labeled by biotin) captured in the MZ are rapidly eliminated within 2h (Saunderson et al., 2014). This controversial result may be due to the limitations in the EVs staining and tracking methods. PKH26 may not be a proper dye to study EVs metabolism, because PKH26 is known to be taken up by macrophages and remain stable for around a month (Murphy et al., 2008). The persistent signal in the MZ we saw in our study could be PKH26 residues that remained after macrophage engulfed those labeled EVs. Besides, PKH26 tends to form microaggregates that are preferentially taken up by macrophages, these fake signals could make it difficult to track EVs.

In additional to the hypothesis that the same EV carried PS-targeting antigens to the MZ and then transported to FDCs, an alternative hypothesis is that EVs in the circulation brought PS-targeting antigens to the MZ. The macrophages in the MZ captured and endocytosed these EVs, then the PS-targeting antigens were re-sorted into new EVs by ESCRT machinery and transported to FDCs. Previous studies have showed that $CD169^+$ macrophages capture Mfge8 bound PS+ viral-like particles (VLPs) via αvβ3 integrins, the transient abutment of the FDCs network and direct contact to the overlying $CD169^+$ macrophages could allow the direct transfer of VLPs to FDCs (Park and Kehrl, 2019). Besides, there are also studies which demonstrated that $CD169^+$ macrophage derived EVs are associated with nearby IL-17 committed innate-like lymphocytes and FDCs (Gray et al., 2012, Chen et al., 2022). In our study, we also found by histological analyses that $CD169^+$ particles (average diameter 300nm, assumably microvesicles) were abundant in the FDC area. The other SIGN-$R1^+$macrophages, were not shown to release microvesicles into FDC area. However, further quantification indicated only 15 % of PS-targeting antigens that have been

transported into the inner B cell follicles were carried by CD169$^+$ EVs. One of the limitations of this study was that we could not isolate FDCs leaving the associated EVs intact (enzyme digestion), therefore, we could only assume that a similar percentage of CD169$^+$ EVs were attached to FDCs. Future studies could reveal if FDCs preferentially take up EVs from CD169$^+$ macrophages.

The fact that only 15 % of PS-targeting antigens in the B cell follicles were CD169$^+$ also indicated that other transportation mechanisms might have been involved. Direct transfer by FDC – CD169$^+$ macrophage contact is very likely to be another method. Besides, we tried to test if PS-targeting antigens that have been transported onto the FDCs colocalized with CD81$^+$exosomes, however, these attempts failed, probably due to the strict requirement of staining antibody required for STED microscope. Therefore, it is still an open question that whether exosomes originate from MZ cell types contribute to the transportation of PS-targeting antigens to FDCs.

Although in our entire study, we hypothesized that PS-targeting antigens were transported from MZ to FDCs. However, we cannot rule out the possibility that rather than being passively transported, soluble PS-targeting antigens may infuse into the B cell follicles as soon as they entered the lymphoid follicles, FDC surface is covered by exosomes (Denzer et al., 2000), providing adequate PS for PS-targeting antigens to bind, although the signals were masked or overshadowed by most PS-targeting antigens accumulated in the MZ. Protein antigens degraded much slower in the B cell follicle, especially near FDCs than in other areas of lymphoid follicles. This is because of the differences in the protease expression and activity in these regions (Aung et al., 2023). As a result, PS-targeting antigens accumulated in the MZ were gradually degraded, while those entered the follicles were better preserved, causing the impression that PS-targeting antigens were transported from the MZ to FDCs. This may also explain why only 15% of Mfge8-EFP in the follicle were CD169$^+$, probably because CD169$^+$ macrophages derived EVs only account for 15% of total PS$^+$ EVs in the lymphoid follicles, B cells and FDCs are also major sources of EVs.

7.2 PS-targeting antigens induce fast serum immune responses.

7.2.1 PS-targeting antigens induce rapid IgG production.

One of the most important findings in this study is that PS-targeting antigens induced rapid IgG production. Although the peak titers and long-term titers are similar between the PS-targeting antigens and conventional antigens, the significant advantage of PS-targeting antigens in the first month, especially the fast IgG production in the first two weeks are of great value. In the situation of pandemics, the faster the immune protection is established, the more people are saved. Besides, herd immunity will be established much faster which provides another layer of protection to the population. The possibility of using PS-targeting antigens as a method of post-exposure prophylaxis is another attractive topic.

Another big advantage of using PS-targeting antigens as vaccines is that immunization with pure PS-targeting antigens without adjuvant (alum) was sufficient to induce considerable antibody responses. On the contrary, conventional antigens were largely depending on adjuvant to induce serum immune response. This self-adjuvanting effect of PS-targeting antigens could be because PS-targeting antigens attached on EVs mimicked the size dimension and spatial structure of pathogens. The immune system has evolved to recognize particulate antigens that are microscale or nanoscale, which are the size dimensions of viruses and bacteria. Therefore, PS-targeting antigens attached on EVs may facilitate antigens uptake by APCs (Zhao et al., 2023, Smith et al., 2013). Precipitation of antigens on aluminum hydroxide particles enhance antigen internalization by DCs, which is one of the mechanisms that alum promotes immune responses (Morefield et al., 2005). In our study, mice immunized with EGFP + alum were divided into low and high IgG groups, those mice in the low IgG group were similar to mice immunized with pure EGFP without alum, and produced around 10^4 folds lower IgG than Mfge8-EGFP immunization, these data indicated that alum could only inefficiently improve the immune responses to EGFP in some mice, but the self-adjuvanting effect of PS-targeting antigens was more homogenous and stable.

IgG titers after a single-dose immunization showed no significant difference between conventional antigens immunization and PS-targeting antigens immunization after one month. When these immunized mice were re-challenged with the same conventional

antigen after 4 weeks, both two groups generated comparable secondary antibody responses. This result may indirectly suggest that immunization with PS-targeting antigens did not generate more memory B cells after primary immunization. However, when we use PS-targeting antigens as booster, we observed significantly higher IgG titers one week after booster, although this advantage shrank over time and showed a clear trend to have similar long-term IgG titers as other groups. These data indicated that using PS-targeting antigens as booster could accelerate MBCs reactivation. The potential mechanism is that resting MBCs stay in specialized compartments in the SCS region in lymph nodes and also MZ and perifollicular areas of the spleen (Inoue and Kurosaki, 2024, Allie and Randall, 2020, Elgueta et al., 2015, Liu et al., 1988), where they reside in close proximity with memory Tfh cells and $CD169^+$ macrophages. $CD169^+$ macrophages capture particulate antigens and immune complexes from the blood circulation. As soon as MBCs recognize the specific antigen on $CD169^+$ macrophages, they present peptide-MHC II complexes and rapidly activate the nearby memory Tfh cells (Ise et al., 2014, Moran et al., 2018, Zhang et al., 2022). MBCs in turn are also activated, they either differentiate into PCs or enter the GC to form recall GC responses (Inoue and Kurosaki, 2024). In our study PS-targeting antigens are carried by PS^+ EVs, trapped in the MZ, and facilitate antigen presentation and activation between $CD169^+$ macrophages, memory Tfh cells and MBCs. This may cause accelerated initiation of memory recall responses.

7.2.2 PS-targeting antigens promote GC reactions.

Antibody responses against protein antigens and the generation of high affinity class-switched IgG is the result of GC reaction. In our study, we showed that immunization with PS-targeting antigens significantly improved GC reaction both quantitatively and qualitatively: GC B cell proliferation was increased at its peak, both immunoglobulin SHM and CSR were accelerated. However, the duration of GC reaction was not prolonged by PS-targeting antigens, both reached the peak 2 weeks after immunization, then declined and disappeared within 4 weeks. As for the mechanisms of how PS-targeting antigens improves GC reaction, we hypothesize that PS-targeting antigens could assist B cell responses not only at B cell activation stage, but also during the GC reaction: PS-targeting antigens that accumulated in the lymphoid follicles could facilitate the encounter and interaction between antigens and cognate B cells, causing rapid B cell activation (BCR cross-linking. Additionally, B cell clones

that enter the GC reaction are only a subset of all cognate naïve B cells. The number of B cells that enter the GC reaction is determined by the features of the antigen and the competition between B cells for limited T cell help at the T-B border: primed B cells migrate to the T-B border, where they present peptide-MHC complexes to Tfh - committed CD4 cells. B cells that received adequate help from Tfh cells progress toward the GC path. Studies have found that B cells express low affinity BCRs are not selected to enter the GC reaction, but they can be recruited to GCs when the availability of Tfh cells' help is increased or competition from other clones is eliminated (Victora and Nussenzweig, 2022, Shih et al., 2002, Schwickert et al., 2011, Dal Porto et al., 1998). In our study, PS-targeting antigens accumulated in the lymphoid follicles providing increased amounts of antigen for B cells to bind. Meanwhile, significantly more Tfh cells were induced. Therefore, we speculate that more B cell clones, even those with lower BCR affinity to the antigens were selected to GC path. The large number of B cells to initiate GC reaction may explain the fast expansion of GC B cell population in the first week after immunization.

During the GC reaction, newly generated GC B cells bearing mutated BCRs compete for antigens on FDCs, then present peptide-MHC complexes to Tfh cells and receive survival signals in return, only GC B cells expressing relatively high affinity BCRs got the chance to survive (positive selection). This process points out that the amount of antigens deposited on FDCs are important regulators that control the magnitude of GC reaction, and also determine when the GC reaction ends (Victora and Nussenzweig, 2022). Many studies have tried to target antigens to FDCs, and they have proved that it is a valid method to improve GC reaction. For example: Tokatlian and his colleagues created heavily glycosylated HIV envelope antigen (gp120 or gp140) nanoparticles, which were rapidly shuttled to the FDCs network in a MBL and complement dependent manner. GC reactions, Tfh cells and IgG titers were all significantly enhanced in mice immunized with FDC-targeting nanoparticles, compared to mice immunized with de-glycosylated nanoparticles that no longer localized FDCs (Tokatlian et al., 2019). Aung and his colleagues used the same glycosylated nanoparticles and showed in another study that targeting antigens to FDCs could better preserve the structural integrity of antigens, which selectively enhanced B cell responses to original antigens rather than irrelevant antigen degradation intermediates (Aung et al., 2023). Lycke and his colleagues developed a

novel adjuvant CTA1-DD, which contains a dimer of the D fragment of the protein A in *Staphylococcus aureus* and a cholera toxin derived ADP-ribosylating CTA1 subunit. CTA1-DD could activate complement and bind to CR1/CR2 on FDCs. They fused CTA1-DD with matrix protein 2 ectodomain epitope (CTA1-3M2e-DD) of human influenza A virus. Immunization with this FDC-targeting antigen increased both Tfh cells and GC B cells, as a result, it significantly promoted antigen specific antibodies, which greatly reduced the mice morbidity after a potentially lethal infection with influenza virus (Mattsson et al., 2011, Eliasson et al., 2008, Schussek et al., 2020). Other attempts, such as immunization with pre-formed immune complexes also showed antigen deposition on FDCs. Antigens on FDCs undergo low level of degradation, and the B cell responses were positively correlated to the duration of antigens displayed on FDCs (Martinez-Riano et al., 2023). To sum up, targeting antigens to FDCs significantly improves B cell responses. However, currently existing methods to target antigens to FDCs all require activation of complement system and formation of immune complexes.

In our study, we showed that PS-targeting was a complement independent method to deposit antigens on FDCs. We hypothesized that this was one of the most important reasons that PS-targeting antigens enhanced GC reactions: With more antigens available on FDCs and more Tfh cells, this allowed more GC B cells pass the positive selection and survive. Besides, the amount of antigens light zone GC B cells capture from FDCs induces proportional Myc expression, which determines the number of cell divisions in the dark zone (Finkin et al., 2019). All these mechanisms could contribute to the increased GC B cell proliferation after immunization with PS-targeting antigens.

In conclusion, we propose two potential mechanisms that PS-targeting antigens promoted GC reactions: by facilitating B cell activation and enable more B cells to seed GC, as well as increasing antigen deposition on FDCs that enable more GC B cells pass positive selection and undergo more cell divisions. Whether these two mechanisms contributed equally to promote the GC reaction, or if only one of them played the dominant role is still an open question. To further clarify mechanisms, how antibody responses are enhanced by PS-targeting antigens, we will extend the study to include more animal and antigen models that target antigens to the MZ, but not deposit on FDCs (depletion of FDCs by pharmacological inhibition of lymphotoxin

signaling)(Aguzzi et al., 2003), and target antigens to FDCs but not accumulate in the MZ (target antigen to CD21/35 in CD169 knock out mice)(Bernhard et al., 2015).

7.2.3 PS-targeting antigens induce a more diverse GC B cell repertoire.

Optimal vaccines are expected to induce antibodies against highly conserved epitopes that are critical to the pathogenicity. However, not all pathogens express conserved antigens, and the most immunogenic structures of a pathogen are often the most variable components. This is driven by the selection pressure from the immune system (antigenic drift and shift). Therefore, vaccines that can induce broad antibody repertoires are especially favorable to protect against highly variable pathogens that are prone to evade the immune responses. Besides, a diversified antibody repertoire can also indue cross-protection against new variants of the original pathogen (Pollard and Hill, 2011). Many studies have been performed to broaden antibody repertoires induced by vaccines. For example, Khurana and colleagues have shown that oil-in-water adjuvant MF59 not only promoted the antibody production against H5N1 flu, it also increased the antibody repertoire diversity. These antibodies bind to a broad variety of H5N1 antigens, they could also bind to hemagglutinin from other strains more effectively (Khurana et al., 2010). Wiley and his colleagues have demonstrated that by adding TLRs agonists (TLR 4/7/8) to the malaria vaccine formulation, diversity of IgG repertoire was significantly increased, it also broadened the range of polymorphic variants these antibodies could bind (Wiley et al., 2011). Other factors, such as time interval between immunizations, was also shown to affect antibody repertoire in a COVID-19 vaccine study. Here, long-interval vaccination induced increased size of BCR repertoire and led to higher and broader antibody responses that could neutralize various SARS-CoV-2 variants (Guo et al., 2023). Besides, repeated boost was also shown to affect memory B cell repertoire: immunization with three doses of Moderna (mRNA-1273) or Pfizer-BioNTech (BNT162b2) mRNA vaccine generated diverse memory B cell repertoires and increased antibody breadth that can neutralize diversified variants such as Omicron (Muecksch et al., 2022). In our study, we have shown that SHM was significantly promoted by PS-targeting antigens. As a result, the size of GC B cell repertoire was larger and more diverse in mice immunized with PS-targeting antigens than those immunized with conventional antigens. This could lead to the production of antibodies with broader protection. Although the long-term IgG titers and the number of LLPCs showed no significant

difference, the repertoire diversity could still be different and worth further investigation.

Diversity of antibody repertoire is not only crucial for broad protective immunity, but also affects secondary B cell responses after consecutive exposures to the same or antigenically related pathogens. Tas and his colleagues demonstrated that the quantity and affinity of antibodies induced during the primary immune responses affect the naive B cells recruitment to GCs after secondary challenge. The effects can be either enhancing or restrictive: antibody repertoires that are diverse, low-affinity, and with low-titers will enhance recruitment. In contrast, if the antibody repertoires consist of high titers of mono-epitope-specific antibodies with high affinity, it will restrict the cognate naive B cell recruitment to secondary GCs (Tas et al., 2022). According to this finding, vaccines that induce low-titers, low-affinity but diverse antibody repertoire will potentially boost secondary humoral responses when the host encounters mutated strains. In our study, PS-targeting antigens induced more diverse and higher titers of IgG. How will it affect the secondary GC reaction will be an interesting topic, and the conclusion will be important to guide the development of broad protective vaccines.

7.2.4 Immunization with PS-targeting antigens improves the quality of antibodies.

The serum antigen specific antibodies tested by ELISA and GC B cell BCR sequencing analysis showed that immunoglobulin isotype switching (BCR class-switching recombination) was significantly promoted by PS-targeting antigens. On day 4 after immunization with PS-targeting antigens, class-switched IgG was readily detectable. In contrast, antigen specific IgG was not detected until day 8 in mice immunized with conventional antigens. Furthermore, the day 14 GC B cell repertoire showed that over 70% of GC B cell expressed class-switched BCR after immunization with PS-targeting antigens, while only around 40% of GC B cells expressed class-switched BCR in mice immunization with conventional antigens. IgG is usually of higher affinity. Due to the time limit of this study, we were not able to express pure BCRs from dominant GC B cells clones and directly measure binding affinities (dissociation constant) by biolayer interferometry (Viant et al., 2020a). However, we got some indirect evidence that could imply higher affinity of antibodies induced after immunization with PS-targeting antigens: first of all, GC B cells showed significantly higher MFI for antigen binding,

which represents higher affinity in previous studies (Sundling et al., 2021, Viant et al., 2020b). Secondly, BCR sequencing results showed that there were significantly more somatic mutations on both heavy and light chains. The number of mutations was shown to be positively correlated with the number of cell divisions in the dark zone and the BCR affinity (Viant et al., 2020a). Thirdly, the BASELINe (Bayesian estimation of antigen-driven selection) analysis showed that antigen-driven positive selection strength in PS-targeting antigens immunized mice was significantly higher, the increased selection strength could lead to the generation of antibodies with higher affinity (Yaari et al., 2012). In summary, the data we showed may imply that PS-targeting antigens may induce antibodies with higher affinity.

The BASELINe analysis showed increased selection strength on day 14 after immunization with PS-targeting antigens. This result was opposite to our expectation because we thought there were more antigens deposited on FDCs, therefore we expected the selection strength to be decreased to allow more GC B cell to survive. To explain the increased positive selection strength, we hypothesized that the selection strength undergoes a dynamic change over time: in the early stage of GC reaction, there was more PS-targeted antigen available on FDCs, which allowed more cells (even low-affinity GC B cells) to pass selection and continued proliferation (low selection strength in the early stage). These GC B cells kept exponential expansion and consumed proportional more antigens on FDCs, while antigens were not supplied continuously. Therefore, in the later stage of GC reaction, there were more GC B cells competing for fewer residual antigens on FDCs. As a result, the selection strength gradually increased in the later time point of GC reaction. This could explain why the GC reaction was not prolonged and the positive selection strength was higher on day 14 after PS-targeting antigen immunization. It could also explain why the speed of GC B cell division is significantly faster in the first week, but relatively slower in the second week than mice immunized with conventional antigens. More studies are needed to prove this hypothesis, first thing to do is to measure selection strength on the early stage of GC reaction, but this can be difficult due to the low GC B cell number in the early time point. On the other hand, BASELINe analysis is only a statistical tool to estimate the selection strength, its result can be used as a reference. Data form well-designed animal experiments are required to draw a final conclusion.

7.3 PS-targeting antigens induce robust T cell responses.

T cells are key regulators of adaptive immune responses. After activation by APCs, CD4 T cells differentiated into various Th cells (mainly Th1 and Th2) and Tfh cells. As for CD8 T cells, they mainly differentiate to CTLs that directly kill target cells (de la Roche et al., 2016, Halle et al., 2016). Here in our study, by targeting antigens to PS, we found significantly more Tfh cells were induced, and that was one of the reasons GC reaction was significantly promoted. Besides, we also found that immunization with PS-targeting antigens induced significantly more activated antigen -specific CTLs, which led to very efficient elimination of target cells in vivo. Moreover, immunization with PS-targeting antigens also generated robust memory response. These data indicated that targeting antigens to PS is a promising method to induce strong and long-lasting protection against viral infections, it also points out the potential to use it as a platform for tumor vaccines.

Although we did not investigate the mechanisms by which PS-targeting antigens promoted T cell responses, some hypotheses were proposed. First of all, as we have discussed earlier, PS-targeting antigens that coated on EVs could mimic the size dimension and spatial structure of real pathogens, thus facilitate APCs' antigen presentation (Zhao et al., 2023, Smith et al., 2013).

Secondly, previous researches have implied that $CD169^+$ macrophages (including MZ metallophilic macrophages in spleen, SCS and medullary macrophages in lymph nodes) may be important mediators. Due to their special anatomic locations that are exposed to blood and lymph, blood and lymph-borne antigens that are captured by these macrophages are then presented to T cells, $CD8a^+$DCs and B cells (Crocker and Gordon, 1989, Martinez-Pomares and Gordon, 2012, Backer et al., 2010, Bernhard et al., 2015, Asano et al., 2011). As we have shown in the results, PS-targeting antigens accumulated in the MZ, and were efficiently captured by $CD169^+$ macrophages probably via EVs. This could facilitate the antigen presentation by metallophilic macrophages and enhance the activation of T cells. Besides, previous study has shown that $CD169^+$ macrophages were sufficient to cross-prime a broader CTL repertoire, including those recognizing less potent epitopes. In contrast, cross-presenting DCs only elicit CTLs with limited specificity towards strong epitopes (Bernhard et al., 2015). In our study we found that CTLs from mice immunized with

PS-targeting antigens showed significant higher responsiveness to all three epitopes with various affinities to MHC I, whereas CTLs from mice immunized with conventional antigen only responded to the most potent epitope. These data implied that $CD169^+$ macrophages may contribute to the boosted CTLs responses after immunization with PS-targeting antigen, but due to the time limit of this study, we couldn't verify this hypothesis by testing the immune responses in CD169 deficient mice, this will be an important work in the future. Memory recall responses in both immunization groups were all dominated by CTLs that recognized the immunodominant epitope. This could because T cells that recognize immunodominant epitopes or conserved epitopes are more likely to differentiate to long-term memory T cells (Kuse et al., 2022).

Thirdly, DCs are one of the major cell types that release and also bind EVs (Diaz-Garrido et al., 2022, Lindenbergh and Stoorvogel, 2018, Lindenbergh et al., 2020, Torralba et al., 2018). Therefore, PS-targeting antigen may not only target antigens to FDCs, but also target antigens to other conventional migratory and resident DCs via EVs associated on them. Targeting antigens to DCs has been achieved in a variety of studies, one of the most used methods to target antigens to DCs is to conjugate or genetic fuse the antigens to the Fc region of antibodies that recognize endocytic receptors on DCs, including DEC-205, Clec9A and Clec12A (Macri et al., 2016). For example: DEC-205 is expressed predominantly on $CD8^+$ DCs (Witmer-Pack et al., 1995). Immunization with OVA conjugated anti DEC-205 antibodies induced robust antigen specific CD8 T cells activation and promoted their differentiation. CD4 T cell activation was also improved. However, the antigen presentation was only prolonged by MHC I molecules (Dudziak et al., 2007, Bonifaz et al., 2004, Bonifaz et al., 2002). DEC-205 targeting can be used both prophylactically to prevent infections, and also therapeutically to treat mice that already possessed tumors nodules (Mahnke et al., 2005, Bonifaz et al., 2004, Volckmar et al., 2017). OVA conjugated to anti Clec9A antibodies was shown to induce the proliferation of antigen specific T cells and promoted the production of OVA specific antibodies (Sancho et al., 2008, Caminschi et al., 2008). Other studies also demonstrated that mice immunized with antigens conjugated to anti-Clec9A antibodies induced more Tfh cells to support GC reaction, antibody affinity maturation and MBCs formation (Lahoud et al., 2011, Park et al., 2013). Other DCs targeting methods, such as ligand-based DC targeted vaccines,

which conjugate antigens to pattern recognition receptor ligands (e.g CpG, which is a TLR9 ligand) were shown to induce stronger CD4, CD8 and antibody responses as compared to free antigens (Chen et al., 2016, Tighe et al., 2000a, Tighe et al., 2000b, Horner et al., 2001). Mannosylation of the antigens or mannan-decoration of antigen-loaded nanoparticles were also shown to bind mannose receptor on DCs, and it enhanced antigen specific T cell responses (Hamdy et al., 2011). With the data we currently have, we cannot conclude that the PS-targeting antigens also accumulate antigens on DCs, whether the PS-targeting antigens, or EVs coated with PS-targeting antigens can be preferentially captured and endocytosed by DCs to enhance antigen presentation. But this will be another important research topic in the future.

8. Conclusions

In this study, we used the PS binding protein Mfge8 or tetramerized PS binding C1 domains of Mfge8 as antigen carriers to target antigens to PS. After injection, PS-targeting antigens were detectable in the MZ of the lymphoid follicles probably due to the uptake of PS^+ EVs by macrophages in the MZ. Several hours later, the PS-targeting antigens were only detectable on FDCs, we assume that they were transported from the MZ to FDCs in a complement-independent way, EVs from $CD169^+$ macrophages partially contributed to this antigen transportation.

The PS-targeting antigens coated on EVs may facilitate the antigen uptake and presentation by DCs. Subsequent antigen deposition on FDCs greatly boosted every aspect of GC reaction. SHM, affinity maturation and CSR were all promoted, resulted in a larger size and more diverse GC B cell repertoire. Boosted GC reaction led to more short-lived PCs and significantly higher titers of antigen specific antibodies within the first month after immunization, although long-term antibody titers and LLPCs showed no difference.

Concomitant with boosted GC reaction, PS-targeting antigens also induced significantly more Tfh cells that positively correlated with the GC B cells number. Besides this, the number of antigen specific CTLs was also increased, resulting in more efficient elimination of target cells as compared to mice immunized with conventional antigens.

In conclusion, in this study, we proved that targeting antigens to PS by Mfge8 is a promising vaccination method and can improve both B- and T- cell responses.

9. References

ABBAS, A. K. L., ANDREW H 2005. *Cellular and Molecular Immunology,* Philadelphia, USA, Elsevier.

AGUZZI, A., HEPPNER, F. L., HEIKENWALDER, M., PRINZ, M., MERTZ, K., SEEGER, H. & GLATZEL, M. 2003. Immune system and peripheral nerves in propagation of prions to CNS. *Br Med Bull,* 66**,** 141-59.

ALLAN, R. S., WAITHMAN, J., BEDOUI, S., JONES, C. M., VILLADANGOS, J. A., ZHAN, Y., LEW, A. M., SHORTMAN, K., HEATH, W. R. & CARBONE, F. R. 2006. Migratory dendritic cells transfer antigen to a lymph node-resident dendritic cell population for efficient CTL priming. *Immunity,* 25**,** 153-62.

ALLIE, S. R. & RANDALL, T. D. 2020. Resident Memory B Cells. *Viral Immunol,* 33**,** 282-293.

ALVAREZ-ERVITI, L., SEOW, Y., YIN, H., BETTS, C., LAKHAL, S. & WOOD, M. J. 2011. Delivery of siRNA to the mouse brain by systemic injection of targeted exosomes. *Nat Biotechnol,* 29**,** 341-5.

ANSEL, K. M., MCHEYZER-WILLIAMS, L. J., NGO, V. N., MCHEYZER-WILLIAMS, M. G. & CYSTER, J. G. 1999. In vivo-activated CD4 T cells upregulate CXC chemokine receptor 5 and reprogram their response to lymphoid chemokines. *J Exp Med,* 190**,** 1123-34.

ARITA, S., BABA, E., SHIBATA, Y., NIIRO, H., SHIMODA, S., ISOBE, T., KUSABA, H., NAKANO, S. & HARADA, M. 2008. B cell activation regulates exosomal HLA production. *Eur J Immunol,* 38**,** 1423-34.

ARSTILA, T. P., CASROUGE, A., BARON, V., EVEN, J., KANELLOPOULOS, J. & KOURILSKY, P. 1999. A direct estimate of the human alphabeta T cell receptor diversity. *Science,* 286**,** 958-61.

ARULRAJ, T., BINDER, S. C., ROBERT, P. A. & MEYER-HERMANN, M. 2021. Germinal Centre Shutdown. *Front Immunol,* 12**,** 705240.

ASANO, K., NABEYAMA, A., MIYAKE, Y., QIU, C. H., KURITA, A., TOMURA, M., KANAGAWA, O., FUJII, S. & TANAKA, M. 2011. CD169-positive macrophages dominate antitumor immunity by crosspresenting dead cell-associated antigens. *Immunity,* 34**,** 85-95.

AUNG, A., CUI, A., MAIORINO, L., AMINI, A. P., GREGORY, J. R., BUKENYA, M., ZHANG, Y., LEE, H., COTTRELL, C. A., MORGAN, D. M., SILVA, M., SUH, H., KIRKPATRICK, J. D., AMLASHI, P., REMBA, T., FROEHLE, L. M., XIAO, S., ABRAHAM, W., ADAMS, J., LOVE, J. C., HUYETT, P., KWON, D. S., HACOHEN, N., SCHIEF, W. R., BHATIA, S. N. & IRVINE, D. J. 2023. Low protease activity in B cell follicles promotes retention of intact antigens after immunization. *Science,* 379**,** eabn8934.

AZIZ, M., JACOB, A., MATSUDA, A. & WANG, P. 2011. Review: milk fat globule-EGF factor 8 expression, function and plausible signal transduction in resolving inflammation. *Apoptosis,* 16**,** 1077-86.

BACKER, R., SCHWANDT, T., GREUTER, M., OOSTING, M., JÜNGERKES, F., TÜTING, T., BOON, L., O'TOOLE, T., KRAAL, G., LIMMER, A. & DEN HAAN, J. M. 2010. Effective collaboration between marginal metallophilic macrophages and CD8+ dendritic cells in the generation of cytotoxic T cells. *Proc Natl Acad Sci U S A,* 107**,** 216-21.

BAUMJOHANN, D., OKADA, T. & ANSEL, K. M. 2011. Cutting Edge: Distinct waves of BCL6 expression during T follicular helper cell development. *J Immunol,* 187**,** 2089-92.

BERNHARD, C. A., RIED, C., KOCHANEK, S. & BROCKER, T. 2015. CD169+ macrophages are sufficient for priming of CTLs with specificities left out by cross-priming dendritic cells. *Proc Natl Acad Sci U S A,* 112**,** 5461-6.

BHATNAGAR, S., SHINAGAWA, K., CASTELLINO, F. J. & SCHOREY, J. S. 2007. Exosomes released from macrophages infected with intracellular pathogens stimulate a proinflammatory response in vitro and in vivo. *Blood,* 110**,** 3234-44.

BOES, M. 2000. Role of natural and immune IgM antibodies in immune responses. *Mol Immunol,* 37**,** 1141-9.

BONIFAZ, L., BONNYAY, D., MAHNKE, K., RIVERA, M., NUSSENZWEIG, M. C. & STEINMAN, R. M. 2002. Efficient targeting of protein antigen to the dendritic cell receptor DEC-205 in the steady state leads to antigen presentation on major histocompatibility complex class I products and peripheral CD8+ T cell tolerance. *J Exp Med,* 196**,** 1627-38.

BONIFAZ, L. C., BONNYAY, D. P., CHARALAMBOUS, A., DARGUSTE, D. I., FUJII, S., SOARES, H., BRIMNES, M. K., MOLTEDO, B., MORAN, T. M. & STEINMAN, R. M. 2004. In vivo targeting of antigens to maturing dendritic cells via the DEC-205 receptor improves T cell vaccination. *J Exp Med,* 199**,** 815-24.

BONILLA, F. A. & OETTGEN, H. C. 2010. Adaptive immunity. *J Allergy Clin Immunol,* 125**,** S33-40.

BOTTA, D., FULLER, M. J., MARQUEZ-LAGO, T. T., BACHUS, H., BRADLEY, J. E., WEINMANN, A. S., ZAJAC, A. J., RANDALL, T. D., LUND, F. E., LEÓN, B. & BALLESTEROS-TATO, A. 2017. Dynamic regulation of T follicular regulatory cell responses by interleukin 2 during influenza infection. *Nature Immunology,* 18**,** 1249-1260.

BRINEY, B., INDERBITZIN, A., JOYCE, C. & BURTON, D. R. 2019. Commonality despite exceptional diversity in the baseline human antibody repertoire. *Nature,* 566**,** 393-397.

BROWN, M., JOHNSON, L. A., LEONE, D. A., MAJEK, P., VAAHTOMERI, K., SENFTER, D., BUKOSZA, N., SCHACHNER, H., ASFOUR, G., LANGER, B., HAUSCHILD, R., PARAPATICS, K., HONG, Y. K., BENNETT, K. L., KAIN, R., DETMAR, M., SIXT, M., JACKSON, D. G. & KERJASCHKI, D. 2018. Lymphatic exosomes promote dendritic cell migration along guidance cues. *J Cell Biol,* 217**,** 2205-2221.

BURGELMAN, M., VANDENDRIESSCHE, C. & VANDENBROUCKE, R. E. 2021. Extracellular Vesicles: A Double-Edged Sword in Sepsis. *Pharmaceuticals (Basel),* 14.

BUSCHOW, S. I., NOLTE-'T HOEN, E. N., VAN NIEL, G., POLS, M. S., TEN BROEKE, T., LAUWEN, M., OSSENDORP, F., MELIEF, C. J., RAPOSO, G., WUBBOLTS, R., WAUBEN, M. H. & STOORVOGEL, W. 2009. MHC II in dendritic cells is targeted to lysosomes or T cell-induced exosomes via distinct multivesicular body pathways. *Traffic,* 10**,** 1528-42.

BUZAS, E. I. 2023. The roles of extracellular vesicles in the immune system. *Nat Rev Immunol,* 23**,** 236-250.

CAMINSCHI, I., PROIETTO, A. I., AHMET, F., KITSOULIS, S., SHIN TEH, J., LO, J. C., RIZZITELLI, A., WU, L., VREMEC, D., VAN DOMMELEN, S. L., CAMPBELL, I. K., MARASKOVSKY, E., BRALEY, H., DAVEY, G. M., MOTTRAM, P., VAN DE VELDE, N., JENSEN, K., LEW, A. M., WRIGHT, M. D., HEATH, W. R., SHORTMAN, K. & LAHOUD, M. H. 2008. The dendritic cell subtype-restricted C-type lectin Clec9A is a target for vaccine enhancement. *Blood,* 112**,** 3264-73.

CARROLL, M. C. 1998. The role of complement and complement receptors in induction and regulation of immunity. *Annu Rev Immunol,* 16**,** 545-68.

CHAUDHURI, J. & ALT, F. W. 2004. Class-switch recombination: interplay of transcription, DNA deamination and DNA repair. *Nat Rev Immunol,* 4**,** 541-52.

CHEN, P., LIU, X., SUN, Y., ZHOU, P., WANG, Y. & ZHANG, Y. 2016. Dendritic cell targeted vaccines: Recent progresses and challenges. *Hum Vaccin Immunother,* 12**,** 612-22.

CHEN, S., DATTA-CHAUDHURI, A., DEME, P., DICKENS, A., DASTGHEYB, R., BHARGAVA, P., BI, H. & HAUGHEY, N. J. 2019. Lipidomic characterization of extracellular vesicles in human serum. *J Circ Biomark,* 8**,** 1849454419879848.

CHEN, X., ZHENG, Y., LIU, S., YU, W. & LIU, Z. 2022. CD169(+) subcapsular sinus macrophage-derived microvesicles are associated with light zone follicular dendritic cells. *Eur J Immunol,* 52**,** 1581-1594.

CINAMON, G., ZACHARIAH, M. A., LAM, O. M., FOSS, F. W., JR. & CYSTER, J. G. 2008. Follicular shuttling of marginal zone B cells facilitates antigen transport. *Nat Immunol,* 9**,** 54-62.

COLOMBO, M., RAPOSO, G. & THÉRY, C. 2014. Biogenesis, secretion, and intercellular interactions of exosomes and other extracellular vesicles. *Annu Rev Cell Dev Biol,* 30**,** 255-89.

COOPER, J. M., WIKLANDER, P. B., NORDIN, J. Z., AL-SHAWI, R., WOOD, M. J., VITHLANI, M., SCHAPIRA, A. H., SIMONS, J. P., EL-ANDALOUSSI, S. & ALVAREZ-ERVITI, L. 2014. Systemic exosomal siRNA delivery reduced alpha-synuclein aggregates in brains of transgenic mice. *Mov Disord,* 29**,** 1476-85.

CROCKER, P. R. & GORDON, S. 1989. Mouse macrophage hemagglutinin (sheep erythrocyte receptor) with specificity for sialylated glycoconjugates characterized by a monoclonal antibody. *J Exp Med,* 169**,** 1333-46.

CROTTY, S. 2014. T follicular helper cell differentiation, function, and roles in disease. *Immunity,* 41**,** 529-42.

CROTTY, S. 2019. T Follicular Helper Cell Biology: A Decade of Discovery and Diseases. *Immunity,* 50**,** 1132-1148.

CYSTER, J. G. & ALLEN, C. D. C. 2019. B Cell Responses: Cell Interaction Dynamics and Decisions. *Cell,* 177**,** 524-540.

DAL PORTO, J. M., HABERMAN, A. M., SHLOMCHIK, M. J. & KELSOE, G. 1998. Antigen drives very low affinity B cells to become plasmacytes and enter germinal centers. *J Immunol,* 161**,** 5373-81.

DASGUPTA, S. K. & THIAGARAJAN, P. 2014. MFG-E8 in the Blood Cell Homeostasis and Coagulation. *In:* WANG, P. (ed.) *MFG-E8 and Inflammation.* Dordrecht: Springer Netherlands.

DE GREGORIO, E., TRITTO, E. & RAPPUOLI, R. 2008. Alum adjuvanticity: unraveling a century old mystery. *Eur J Immunol,* 38**,** 2068-71.

DE JONG, O. G., KOOIJMANS, S. A. A., MURPHY, D. E., JIANG, L., EVERS, M. J. W., SLUIJTER, J. P. G., VADER, P. & SCHIFFELERS, R. M. 2019. Drug Delivery with Extracellular Vesicles: From Imagination to Innovation. *Acc Chem Res,* 52**,** 1761-1770.

DE LA ROCHE, M., ASANO, Y. & GRIFFITHS, G. M. 2016. Origins of the cytolytic synapse. *Nat Rev Immunol,* 16**,** 421-32.

DE SILVA, N. S. & KLEIN, U. 2015. Dynamics of B cells in germinal centres. *Nat Rev Immunol,* 15**,** 137-48.

DEATHERAGE, B. L. & COOKSON, B. T. 2012. Membrane vesicle release in bacteria, eukaryotes, and archaea: a conserved yet underappreciated aspect of microbial life. *Infect Immun,* 80**,** 1948-57.

DEN HAAN, J. M., LEHAR, S. M. & BEVAN, M. J. 2000. CD8(+) but not CD8(-) dendritic cells cross-prime cytotoxic T cells in vivo. *J Exp Med,* 192**,** 1685-96.

DENZER, K., VAN EIJK, M., KLEIJMEER, M. J., JAKOBSON, E., DE GROOT, C. & GEUZE, H. J. 2000. Follicular dendritic cells carry MHC class II-expressing microvesicles at their surface. *J Immunol,* 165**,** 1259-65.

DI NOIA, J. M. & NEUBERGER, M. S. 2007. Molecular mechanisms of antibody somatic hypermutation. *Annu Rev Biochem,* 76**,** 1-22.

DIAZ-GARRIDO, N., BADIA, J. & BALDOMÀ, L. 2022. Modulation of Dendritic Cells by Microbiota Extracellular Vesicles Influences the Cytokine Profile and Exosome Cargo. *Nutrients,* 14.

DUAN, L., LIU, D., CHEN, H., MINTZ, M. A., CHOU, M. Y., KOTOV, D. I., XU, Y., AN, J., LAIDLAW, B. J. & CYSTER, J. G. 2021. Follicular dendritic cells restrict interleukin-4 availability in germinal centers and foster memory B cell generation. *Immunity,* 54**,** 2256-2272.e6.

DUDZIAK, D., KAMPHORST, A. O., HEIDKAMP, G. F., BUCHHOLZ, V. R., TRUMPFHELLER, C., YAMAZAKI, S., CHEONG, C., LIU, K., LEE, H. W., PARK, C. G., STEINMAN, R. M. & NUSSENZWEIG, M. C. 2007. Differential antigen processing by dendritic cell subsets in vivo. *Science,* 315**,** 107-11.

EISENHUT, M., PARANJOTHY, S., ABUBAKAR, I., BRACEBRIDGE, S., LILLEY, M., MULLA, R., LACK, K., CHALKLEY, D. & MCEVOY, M. 2009. BCG vaccination reduces risk of infection with Mycobacterium tuberculosis as detected by gamma interferon release assay. *Vaccine,* 27**,** 6116-20.

ELGUETA, R., MARKS, E., NOWAK, E., MENEZES, S., BENSON, M., RAMAN, V. S., ORTIZ, C., O'CONNELL, S., HESS, H., LORD, G. M. & NOELLE, R. 2015. CCR6-dependent positioning of memory B cells is essential for their ability to mount a recall response to antigen. *J Immunol,* 194**,** 505-13.

ELIASSON, D. G., EL BAKKOURI, K., SCHÖN, K., RAMNE, A., FESTJENS, E., LÖWENADLER, B., FIERS, W., SAELENS, X. & LYCKE, N. 2008. CTA1-M2e-DD: a novel mucosal adjuvant targeted influenza vaccine. *Vaccine,* 26**,** 1243-52.

ELLIOTT, M. R. & RAVICHANDRAN, K. S. 2010. Clearance of apoptotic cells: implications in health and disease. *J Cell Biol,* 189**,** 1059-70.

ELSHARKASY, O. M., NORDIN, J. Z., HAGEY, D. W., DE JONG, O. G., SCHIFFELERS, R. M., ANDALOUSSI, S. E. & VADER, P. 2020. Extracellular vesicles as drug delivery systems: Why and how? *Adv Drug Deliv Rev,* 159**,** 332-343.

ENCINAR, J. A., LUDEÑA, M. D., SÁNCHEZ-YAGÜE, J. & LLANILLO, M. 1996. Enzymatic determination of phosphatidylcholine, sphingomyelin and phosphatidylglycerol in lipid dispersions, blood cell membranes and rat pulmonary surfactant. *Eur J Clin Chem Clin Biochem,* 34**,** 9-15.

ERAZO, A., KUTCHUKHIDZE, N., LEUNG, M., CHRIST, A. P., URBAN, J. F., JR., CUROTTO DE LAFAILLE, M. A. & LAFAILLE, J. J. 2007. Unique maturation program of the IgE response in vivo. *Immunity,* 26**,** 191-203.

FAGARASAN, S. & HONJO, T. 2000. T-Independent immune response: new aspects of B cell biology. *Science,* 290**,** 89-92.

FERGUSON, A. R., YOUD, M. E. & CORLEY, R. B. 2004. Marginal zone B cells transport and deposit IgM-containing immune complexes onto follicular dendritic cells. *Int Immunol,* 16**,** 1411-22.

FINKIN, S., HARTWEGER, H., OLIVEIRA, T. Y., KARA, E. E. & NUSSENZWEIG, M. C. 2019. Protein Amounts of the MYC Transcription Factor Determine Germinal Center B Cell Division Capacity. *Immunity,* 51**,** 324-336 e5.

FITZGERALD, W., FREEMAN, M. L., LEDERMAN, M. M., VASILIEVA, E., ROMERO, R. & MARGOLIS, L. 2018. A System of Cytokines Encapsulated in ExtraCellular Vesicles. *Sci Rep,* 8**,** 8973.

GAIPL, U. S., VOLL, R. E., SHERIFF, A., FRANZ, S., KALDEN, J. R. & HERRMANN, M. 2005. Impaired clearance of dying cells in systemic lupus erythematosus. *Autoimmun Rev,* 4**,** 189-94.

GITLIN, A. D., SHULMAN, Z. & NUSSENZWEIG, M. C. 2014. Clonal selection in the germinal centre by regulated proliferation and hypermutation. *Nature,* 509**,** 637-640.

GRAY, E. E., FRIEND, S., SUZUKI, K., PHAN, T. G. & CYSTER, J. G. 2012. Subcapsular sinus macrophage fragmentation and CD169+ bleb acquisition by closely associated IL-17-committed innate-like lymphocytes. *PLoS One,* 7**,** e38258.

GROS, R., RESSI, H., VON MALTITZ, P., ALBERS, D., SCHNEIDER, L., BLEY, H., HOFFMANN, M., CORTESE, M., GUPTA, D., DENIZ, M., CHOI, J. Y., JANSEN, J., PREUSSE, C., SEEHAFER, K., PÖHLMANN, S., VOELKER, D. R., GOFFINET, C., POGGE-VON STRANDMANN, E., BUNZ, U., BARTENSCHLAGER, R., EL ANDALOUSSI, S., SPARRER, K. M. J., HERKER, E., BECKER, S., KIRCHHOFF, F., MÜNCH, J. & MÜLLER, J. A. 2024. Phosphatidylserine-exposing extracellular vesicles in body fluids are an innate defence against apoptotic mimicry viral pathogens. *Nat Microbiol,* 9**,** 905-921.

GRUELL, H., VANSHYLLA, K., WEBER, T., BARNES, C. O., KREER, C. & KLEIN, F. 2022. Antibody-mediated neutralization of SARS-CoV-2. *Immunity,* 55**,** 925-944.

GUIMARAES, C. P., WITTE, M. D., THEILE, C. S., BOZKURT, G., KUNDRAT, L., BLOM, A. E. & PLOEGH, H. L. 2013. Site-specific C-terminal and internal loop labeling of proteins using sortase-mediated reactions. *Nat Protoc,* 8**,** 1787-99.

GUNN, M. D., NGO, V. N., ANSEL, K. M., EKLAND, E. H., CYSTER, J. G. & WILLIAMS, L. T. 1998. A B-cell-homing chemokine made in lymphoid follicles activates Burkitt's lymphoma receptor-1. *Nature,* 391**,** 799-803.

GUO, S., ZHENG, Y., GAO, Z., DUAN, M., LIU, S., DU, P., XU, X., XU, K., ZHAO, X., CHAI, Y., WANG, P., ZHAO, Q., GAO, G. F. & DAI, L. 2023. Dosing interval regimen shapes potency and breadth of antibody repertoire after vaccination of SARS-CoV-2 RBD protein subunit vaccine. *Cell Discov,* 9**,** 79.

HALLE, S., HALLE, O. & FÖRSTER, R. 2017. Mechanisms and Dynamics of T Cell-Mediated Cytotoxicity In Vivo. *Trends Immunol,* 38**,** 432-443.

HALLE, S., KEYSER, K. A., STAHL, F. R., BUSCHE, A., MARQUARDT, A., ZHENG, X., GALLA, M., HEISSMEYER, V., HELLER, K., BOELTER, J., WAGNER, K., BISCHOFF, Y., MARTENS, R., BRAUN, A., WERTH, K., UVAROVSKII, A., KEMPF, H., MEYER-HERMANN, M., ARENS, R., KREMER, M., SUTTER, G., MESSERLE, M. & FÖRSTER, R. 2016. In Vivo Killing Capacity of Cytotoxic T Cells Is Limited and Involves Dynamic Interactions and T Cell Cooperativity. *Immunity,* 44**,** 233-45.

HAMDY, S., HADDADI, A., SHAYEGANPOUR, A., SAMUEL, J. & LAVASANIFAR, A. 2011. Activation of antigen-specific T cell-responses by mannan-decorated PLGA nanoparticles. *Pharm Res,* 28**,** 2288-301.

HANAYAMA, R., MIYASAKA, K., NAKAYA, M. & NAGATA, S. 2006. MFG-E8-dependent clearance of apoptotic cells, and autoimmunity caused by its failure. *Curr Dir Autoimmun,* 9**,** 162-72.

HANAYAMA, R., TANAKA, M., MIWA, K., SHINOHARA, A., IWAMATSU, A. & NAGATA, S. 2002. Identification of a factor that links apoptotic cells to phagocytes. *Nature,* 417**,** 182-7.

HANAYAMA, R., TANAKA, M., MIYASAKA, K., AOZASA, K., KOIKE, M., UCHIYAMA, Y. & NAGATA, S. 2004. Autoimmune disease and impaired uptake of apoptotic cells in MFG-E8-deficient mice. *Science,* 304**,** 1147-50.

HANEY, M. J., KLYACHKO, N. L., ZHAO, Y., GUPTA, R., PLOTNIKOVA, E. G., HE, Z., PATEL, T., PIROYAN, A., SOKOLSKY, M., KABANOV, A. V. & BATRAKOVA, E. V. 2015. Exosomes as drug delivery vehicles for Parkinson's disease therapy. *J Control Release,* 207**,** 18-30.

HARDING, C., HEUSER, J. & STAHL, P. 1984. Endocytosis and intracellular processing of transferrin and colloidal gold-transferrin in rat reticulocytes: demonstration of a pathway for receptor shedding. *Eur J Cell Biol,* 35**,** 256-63.

HAVENAR-DAUGHTON, C., CARNATHAN, D. G., TORRENTS DE LA PEÑA, A., PAUTHNER, M., BRINEY, B., REISS, S. M., WOOD, J. S., KAUSHIK, K., VAN GILS, M. J., ROSALES, S. L., VAN DER WOUDE, P., LOCCI, M., LE, K. M., DE TAEYE, S. W., SOK, D., MOHAMMED, A. U. R., HUANG, J., GUMBER, S., GARCIA, A., KASTURI, S. P., PULENDRAN, B., MOORE, J. P., AHMED, R., SEUMOIS, G., BURTON, D. R., SANDERS, R. W., SILVESTRI, G. & CROTTY, S. 2016. Direct Probing of Germinal Center Responses Reveals Immunological Features and Bottlenecks for Neutralizing Antibody Responses to HIV Env Trimer. *Cell Reports,* 17**,** 2195-2209.

HE, B., QIAO, X. & CERUTTI, A. 2004. CpG DNA induces IgG class switch DNA recombination by activating human B cells through an innate pathway that requires TLR9 and cooperates with IL-10. *J Immunol,* 173**,** 4479-91.

HEESTERS, B. A., MYERS, R. C. & CARROLL, M. C. 2014. Follicular dendritic cells: dynamic antigen libraries. *Nat Rev Immunol,* 14**,** 495-504.

HELFT, J., JACQUET, A., JONCKER, N. T., GRANDJEAN, I., DOROTHÉE, G., KISSENPFENNIG, A., MALISSEN, B., MATZINGER, P. & LANTZ, O. 2008. Antigen-specific T-T interactions regulate CD4 T-cell expansion. *Blood,* 112**,** 1249-58.

HERRMANN, I. K., WOOD, M. J. A. & FUHRMANN, G. 2021. Extracellular vesicles as a next-generation drug delivery platform. *Nat Nanotechnol,* 16**,** 748-759.

HIRAI, T. & YOSHIOKA, Y. 2022. Considerations of CD8(+) T Cells for Optimized Vaccine Strategies Against Respiratory Viruses. *Front Immunol,* 13**,** 918611.

HORNER, A. A., DATTA, S. K., TAKABAYASHI, K., BELYAKOV, I. M., HAYASHI, T., CINMAN, N., NGUYEN, M. D., VAN UDEN, J. H., BERZOFSKY, J. A., RICHMAN, D. D. & RAZ, E. 2001. Immunostimulatory DNA-based vaccines elicit multifaceted immune responses against HIV at systemic and mucosal sites. *J Immunol,* 167**,** 1584-91.

HORNUNG, V., BAUERNFEIND, F., HALLE, A., SAMSTAD, E. O., KONO, H., ROCK, K. L., FITZGERALD, K. A. & LATZ, E. 2008. Silica crystals and aluminum salts activate the NALP3 inflammasome through phagosomal destabilization. *Nat Immunol,* 9**,** 847-56.

HOSHINO, A., COSTA-SILVA, B., SHEN, T. L., RODRIGUES, G., HASHIMOTO, A., TESIC MARK, M., MOLINA, H., KOHSAKA, S., DI GIANNATALE, A., CEDER, S., SINGH, S., WILLIAMS, C., SOPLOP, N., URYU, K., PHARMER, L., KING, T., BOJMAR, L., DAVIES, A. E., ARARSO, Y., ZHANG, T., ZHANG, H., HERNANDEZ, J., WEISS, J. M., DUMONT-COLE, V. D., KRAMER, K., WEXLER, L. H., NARENDRAN, A., SCHWARTZ, G. K., HEALEY, J. H., SANDSTROM, P., LABORI, K. J., KURE, E. H., GRANDGENETT, P. M., HOLLINGSWORTH, M. A., DE SOUSA, M., KAUR, S., JAIN, M., MALLYA, K., BATRA, S. K., JARNAGIN, W. R., BRADY, M. S., FODSTAD, O., MULLER, V., PANTEL, K., MINN, A. J., BISSELL, M. J., GARCIA, B. A., KANG, Y., RAJASEKHAR, V. K., GHAJAR, C. M., MATEI, I., PEINADO, H., BROMBERG, J. & LYDEN, D. 2015. Tumour exosome integrins determine organotropic metastasis. *Nature,* 527**,** 329-35.

HU, T., SHI, J., JIAO, X., ZHOU, J. & YIN, X. 2008. Measurement of annexin V uptake and lactadherin labeling for the quantification of apoptosis in adherent Tca8113 and ACC-2 cells. *Braz J Med Biol Res,* 41**,** 750-7.

INOUE, T. & KUROSAKI, T. 2024. Memory B cells. *Nat Rev Immunol,* 24**,** 5-17.

INOUE, T., MORAN, I., SHINNAKASU, R., PHAN, T. G. & KUROSAKI, T. 2018. Generation of memory B cells and their reactivation. *Immunol Rev,* 283**,** 138-149.

INOUE, T., SHINNAKASU, R., KAWAI, C., ISE, W., KAWAKAMI, E., SAX, N., OKI, T., KITAMURA, T., YAMASHITA, K., FUKUYAMA, H. & KUROSAKI, T. 2021. Exit from germinal center to become quiescent memory B cells depends on metabolic reprograming and provision of a survival signal. *J Exp Med,* 218.

ISE, W., FUJII, K., SHIROGUCHI, K., ITO, A., KOMETANI, K., TAKEDA, K., KAWAKAMI, E., YAMASHITA, K., SUZUKI, K., OKADA, T. & KUROSAKI, T. 2018. T Follicular Helper Cell-Germinal Center B Cell Interaction Strength Regulates Entry into Plasma Cell or Recycling Germinal Center Cell Fate. *Immunity,* 48**,** 702-715.e4.

ISE, W., INOUE, T., MCLACHLAN, J. B., KOMETANI, K., KUBO, M., OKADA, T. & KUROSAKI, T. 2014. Memory B cells contribute to rapid Bcl6 expression by memory follicular helper T cells. *Proc Natl Acad Sci U S A,* 111**,** 11792-7.

JACOB, J. & KELSOE, G. 1992. In situ studies of the primary immune response to (4-hydroxy-3-nitrophenyl)acetyl. II. A common clonal origin for periarteriolar lymphoid sheath-associated foci and germinal centers. *J Exp Med,* 176**,** 679-87.

JANEWAY, C., TRAVERS, P. & WALPORT, M. 2001. *Immunobiology: The Immune System in Health and Disease. 5th edition.*

, New York, Garland Science.

JANKOVIČOVÁ, J., SEČOVÁ, P., MICHALKOVÁ, K. & ANTALÍKOVÁ, J. 2020. Tetraspanins, More than Markers of Extracellular Vesicles in Reproduction. *Int J Mol Sci,* 21.

KAMIŃSKA, A., ENGUITA, F. J. & STĘPIEŃ, E. 2018. Lactadherin: An unappreciated haemostasis regulator and potential therapeutic agent. *Vascul Pharmacol,* 101**,** 21-28.

KARANDIKAR, S. H., SIDNEY, J., SETTE, A., SELBY, M. J., KORMAN, A. J. & SRIVASTAVA, P. K. 2019. New epitopes in ovalbumin provide insights for cancer neoepitopes. *JCI Insight,* 5.

KHURANA, S., CHEARWAE, W., CASTELLINO, F., MANISCHEWITZ, J., KING, L. R., HONORKIEWICZ, A., ROCK, M. T., EDWARDS, K. M., DEL GIUDICE, G., RAPPUOLI, R. & GOLDING, H. 2010. Vaccines with MF59 adjuvant expand the antibody repertoire to target protective sites of pandemic avian H5N1 influenza virus. *Sci Transl Med,* 2**,** 15ra5.

KLINKER, M. W., LIZZIO, V., REED, T. J., FOX, D. A. & LUNDY, S. K. 2014. Human B Cell-Derived Lymphoblastoid Cell Lines Constitutively Produce Fas Ligand and Secrete MHCII(+)FasL(+) Killer Exosomes. *Front Immunol,* 5**,** 144.

KOH, C. H., LEE, S., KWAK, M., KIM, B. S. & CHUNG, Y. 2023. CD8 T-cell subsets: heterogeneity, functions, and therapeutic potential. *Exp Mol Med,* 55**,** 2287-2299.

KRANICH, J., CHLIS, N. K., RAUSCH, L., LATHA, A., SCHIFFERER, M., KURZ, T., FOLTYN-ARFA KIA, A., SIMONS, M., THEIS, F. J. & BROCKER, T. 2020. In vivo identification of apoptotic and extracellular vesicle-bound live cells using image-based deep learning. *J Extracell Vesicles,* 9**,** 1792683.

KRANICH, J. & KRAUTLER, N. J. 2016. How Follicular Dendritic Cells Shape the B-Cell Antigenome. *Front Immunol,* 7**,** 225.

KRANICH, J., KRAUTLER, N. J., FALSIG, J., BALLMER, B., LI, S., HUTTER, G., SCHWARZ, P., MOOS, R., JULIUS, C., MIELE, G. & AGUZZI, A. 2010. Engulfment of cerebral apoptotic bodies controls the course of prion disease in a mouse strain-dependent manner. *J Exp Med,* 207**,** 2271-81.

KRANICH, J., KRAUTLER, N. J., HEINEN, E., POLYMENIDOU, M., BRIDEL, C., SCHILDKNECHT, A., HUBER, C., KOSCO-VILBOIS, M. H., ZINKERNAGEL, R., MIELE, G. & AGUZZI, A. 2008. Follicular dendritic cells control engulfment of apoptotic bodies by secreting Mfge8. *J Exp Med,* 205**,** 1293-302.

KUSE, N., ZHANG, Y., CHIKATA, T., NGUYEN, H. T., OKA, S., GATANAGA, H. & TAKIGUCHI, M. 2022. Long-term memory CD8(+) T cells specific for SARS-CoV-2 in individuals who received the BNT162b2 mRNA vaccine. *Nat Commun,* 13**,** 5251.

LAHOUD, M. H., AHMET, F., KITSOULIS, S., WAN, S. S., VREMEC, D., LEE, C. N., PHIPSON, B., SHI, W., SMYTH, G. K., LEW, A. M., KATO, Y., MUELLER, S. N., DAVEY, G. M., HEATH, W. R., SHORTMAN, K. & CAMINSCHI, I. 2011. Targeting antigen to mouse dendritic cells via Clec9A induces potent CD4 T cell responses biased toward a follicular helper phenotype. *J Immunol,* 187**,** 842-50.

LEDERER, K., CASTANO, D., GOMEZ ATRIA, D., OGUIN, T. H., 3RD, WANG, S., MANZONI, T. B., MURAMATSU, H., HOGAN, M. J., AMANAT, F., CHERUBIN, P., LUNDGREEN, K. A., TAM, Y. K., FAN, S. H. Y., EISENLOHR, L. C., MAILLARD, I., WEISSMAN, D., BATES, P., KRAMMER, F., SEMPOWSKI, G. D., PARDI, N. & LOCCI, M. 2020. SARS-CoV-2 mRNA Vaccines Foster Potent Antigen-Specific Germinal Center Responses Associated with Neutralizing Antibody Generation. *Immunity,* 53**,** 1281-1295 e5.

LEMKE, G. 2019. How macrophages deal with death. *Nature Reviews Immunology,* 19**,** 539-549.

LEVIN, M. J., OXMAN, M. N., ZHANG, J. H., JOHNSON, G. R., STANLEY, H., HAYWARD, A. R., CAULFIELD, M. J., IRWIN, M. R., SMITH, J. G., CLAIR, J., CHAN, I. S., WILLIAMS, H., HARBECKE, R., MARCHESE, R., STRAUS, S. E., GERSHON, A. & WEINBERG, A. 2008. Varicella-zoster virus-specific immune responses in elderly recipients of a herpes zoster vaccine. *J Infect Dis,* 197**,** 825-35.

LIMA, L. G., HAM, S., SHIN, H., CHAI, E. P. Z., LEK, E. S. H., LOBB, R. J., MÜLLER, A. F., MATHIVANAN, S., YEO, B., CHOI, Y., PARKER, B. S. & MÖLLER, A. 2021. Tumor microenvironmental cytokines bound to cancer exosomes determine uptake by cytokine receptor-expressing cells and biodistribution. *Nat Commun,* 12**,** 3543.

LINDENBERGH, M. F. S. & STOORVOGEL, W. 2018. Antigen Presentation by Extracellular Vesicles from Professional Antigen-Presenting Cells. *Annu Rev Immunol,* 36**,** 435-459.

LINDENBERGH, M. F. S., WUBBOLTS, R., BORG, E. G. F., VAN 'T VELD, E. M., BOES, M. & STOORVOGEL, W. 2020. Dendritic cells release exosomes together with phagocytosed pathogen; potential implications for the role of exosomes in antigen presentation. *J Extracell Vesicles,* 9**,** 1798606.

LIU, Y., LI, D., LIU, Z., ZHOU, Y., CHU, D., LI, X., JIANG, X., HOU, D., CHEN, X., CHEN, Y., YANG, Z., JIN, L., JIANG, W., TIAN, C., ZHOU, G., ZEN, K., ZHANG, J., ZHANG, Y., LI, J. & ZHANG, C. Y. 2015. Targeted exosome-mediated delivery of opioid receptor Mu siRNA for the treatment of morphine relapse. *Sci Rep,* 5**,** 17543.

LIU, Y. J., OLDFIELD, S. & MACLENNAN, I. C. 1988. Memory B cells in T cell-dependent antibody responses colonize the splenic marginal zones. *Eur J Immunol,* 18**,** 355-62.

LIU, Z., WANG, F. & CHEN, X. 2008. Integrin alpha(v)beta(3)-Targeted Cancer Therapy. *Drug Dev Res,* 69**,** 329-339.

LUNDY, S. K. & KLINKER, M. W. 2014. Characterization and activity of Fas ligand producing $CD5^+$ B cells. *Methods Mol Biol,* 1190**,** 81-102.

MACRI, C., DUMONT, C., JOHNSTON, A. P. & MINTERN, J. D. 2016. Targeting dendritic cells: a promising strategy to improve vaccine effectiveness. *Clin Transl Immunology,* 5**,** e66.

MAHNKE, K., QIAN, Y., FONDEL, S., BRUECK, J., BECKER, C. & ENK, A. H. 2005. Targeting of antigens to activated dendritic cells in vivo cures metastatic melanoma in mice. *Cancer Res,* 65**,** 7007-12.

MALDONADO-LÓPEZ, R., DE SMEDT, T., MICHEL, P., GODFROID, J., PAJAK, B., HEIRMAN, C., THIELEMANS, K., LEO, O., URBAIN, J. & MOSER, M. 1999. CD8alpha+ and CD8alpha- subclasses of dendritic cells direct the development of distinct T helper cells in vivo. *J Exp Med,* 189**,** 587-92.

MARTINEZ-POMARES, L. & GORDON, S. 2012. CD169+ macrophages at the crossroads of antigen presentation. *Trends Immunol,* 33**,** 66-70.

MARTINEZ-RIANO, A., WANG, S., BOEING, S., MINOUGHAN, S., CASAL, A., SPILLANE, K. M., LUDEWIG, B. & TOLAR, P. 2023. Long-term retention of antigens in germinal centers is controlled by the spatial organization of the follicular dendritic cell network. *Nat Immunol,* 24**,** 1281-1294.

MATHIEU, M., MARTIN-JAULAR, L., LAVIEU, G. & THERY, C. 2019. Specificities of secretion and uptake of exosomes and other extracellular vesicles for cell-to-cell communication. *Nat Cell Biol,* 21**,** 9-17.

MATTSSON, J., YRLID, U., STENSSON, A., SCHÖN, K., KARLSSON, M. C., RAVETCH, J. V. & LYCKE, N. Y. 2011. Complement activation and complement receptors on follicular dendritic cells are critical for the function of a targeted adjuvant. *J Immunol,* 187**,** 3641-52.

MCELHANEY, J. E., XIE, D., HAGER, W. D., BARRY, M. B., WANG, Y., KLEPPINGER, A., EWEN, C., KANE, K. P. & BLEACKLEY, R. C. 2006. T cell responses are better correlates of vaccine protection in the elderly. *J Immunol,* 176**,** 6333-9.

MENTKOWSKI, K. I. & LANG, J. K. 2019. Exosomes Engineered to Express a Cardiomyocyte Binding Peptide Demonstrate Improved Cardiac Retention in Vivo. *Sci Rep,* 9**,** 10041.

MONTECALVO, A., SHUFESKY, W. J., STOLZ, D. B., SULLIVAN, M. G., WANG, Z., DIVITO, S. J., PAPWORTH, G. D., WATKINS, S. C., ROBBINS, P. D., LARREGINA, A. T. & MORELLI, A. E. 2008. Exosomes as a short-range mechanism to spread alloantigen between dendritic cells during T cell allorecognition. *J Immunol,* 180**,** 3081-90.

MOON, J. J., SUH, H., LI, A. V., OCKENHOUSE, C. F., YADAVA, A. & IRVINE, D. J. 2012. Enhancing humoral responses to a malaria antigen with nanoparticle vaccines that expand Tfh cells and promote germinal center induction. *Proc Natl Acad Sci U S A,* 109**,** 1080-5.

MORAN, I., NGUYEN, A., KHOO, W. H., BUTT, D., BOURNE, K., YOUNG, C., HERMES, J. R., BIRO, M., GRACIE, G., MA, C. S., MUNIER, C. M. L., LUCIANI, F., ZAUNDERS, J., PARKER, A., KELLEHER, A. D., TANGYE, S. G., CROUCHER, P. I., BRINK, R., READ, M. N. & PHAN, T. G. 2018. Memory B cells are reactivated in subcapsular proliferative foci of lymph nodes. *Nat Commun,* 9**,** 3372.

MOREFIELD, G. L., SOKOLOVSKA, A., JIANG, D., HOGENESCH, H., ROBINSON, J. P. & HEM, S. L. 2005. Role of aluminum-containing adjuvants in antigen internalization by dendritic cells in vitro. *Vaccine,* 23**,** 1588-95.

MOULD, R. C., VAN VLOTEN, J. P., AUYEUNG, A. W. K., WALSH, S. R., DE JONG, J., SUSTA, L., MUTSAERS, A. J., PETRIK, J. J., WOOD, G. A., WOOTTON, S. K., KARIMI, K. & BRIDLE, B. W. 2021. Using a Prime-Boost Vaccination Strategy That Proved Effective for High Resolution Epitope Mapping to Characterize the Elusive Immunogenicity of Survivin. *Cancers (Basel),* 13.

MUECKSCH, F., WANG, Z., CHO, A., GAEBLER, C., BEN TANFOUS, T., DASILVA, J., BEDNARSKI, E., RAMOS, V., ZONG, S., JOHNSON, B., RASPE, R., SCHAEFER-BABAJEW, D., SHIMELIOVICH, I., DAGA, M., YAO, K. H., SCHMIDT, F., MILLARD, K. G., TURROJA, M.,

JANKOVIC, M., OLIVEIRA, T. Y., GAZUMYAN, A., CASKEY, M., HATZIIOANNOU, T., BIENIASZ, P. D. & NUSSENZWEIG, M. C. 2022. Increased memory B cell potency and breadth after a SARS-CoV-2 mRNA boost. *Nature,* 607**,** 128-134.

MUNTASELL, A., BERGER, A. C. & ROCHE, P. A. 2007. T cell-induced secretion of MHC class II-peptide complexes on B cell exosomes. *Embo j,* 26**,** 4263-72.

MURPHY, J., SUMMER, R., WILSON, A. A., KOTTON, D. N. & FINE, A. 2008. The prolonged life-span of alveolar macrophages. *Am J Respir Cell Mol Biol,* 38**,** 380-5.

NAGATA, S. 2018. Apoptosis and Clearance of Apoptotic Cells. *Annu Rev Immunol,* 36**,** 489-517.

NAPOLITANI, G., RINALDI, A., BERTONI, F., SALLUSTO, F. & LANZAVECCHIA, A. 2005. Selected Toll-like receptor agonist combinations synergistically trigger a T helper type 1-polarizing program in dendritic cells. *Nat Immunol,* 6**,** 769-76.

NEUTZNER, M., LOPEZ, T., FENG, X., BERGMANN-LEITNER, E. S., LEITNER, W. W. & UDEY, M. C. 2007. MFG-E8/lactadherin promotes tumor growth in an angiogenesis-dependent transgenic mouse model of multistage carcinogenesis. *Cancer Res,* 67**,** 6777-85.

NOLTE-'T HOEN, E. N., BUSCHOW, S. I., ANDERTON, S. M., STOORVOGEL, W. & WAUBEN, M. H. 2009. Activated T cells recruit exosomes secreted by dendritic cells via LFA-1. *Blood,* 113**,** 1977-81.

NUTT, S. L., HODGKIN, P. D., TARLINTON, D. M. & CORCORAN, L. M. 2015. The generation of antibody-secreting plasma cells. *Nat Rev Immunol,* 15**,** 160-71.

O'DONNELL, V. B., MURPHY, R. C. & WATSON, S. P. 2014. Platelet lipidomics: modern day perspective on lipid discovery and characterization in platelets. *Circ Res,* 114**,** 1185-203.

ODEGARD, V. H. & SCHATZ, D. G. 2006. Targeting of somatic hypermutation. *Nat Rev Immunol,* 6**,** 573-83.

ODENWALD, M. A. & TURNER, J. R. 2017. The intestinal epithelial barrier: a therapeutic target? *Nat Rev Gastroenterol Hepatol,* 14**,** 9-21.

OKADA, T., MILLER, M. J., PARKER, I., KRUMMEL, M. F., NEIGHBORS, M., HARTLEY, S. B., O'GARRA, A., CAHALAN, M. D. & CYSTER, J. G. 2005. Antigen-engaged B cells undergo chemotaxis toward the T zone and form motile conjugates with helper T cells. *PLoS Biol,* 3**,** e150.

OKOYE, I. S., COOMES, S. M., PELLY, V. S., CZIESO, S., PAPAYANNOPOULOS, V., TOLMACHOVA, T., SEABRA, M. C. & WILSON, M. S. 2014. MicroRNA-Containing T-Regulatory-Cell-Derived Exosomes Suppress Pathogenic T Helper 1 Cells. *Immunity,* 41**,** 503.

OSHIMA, K., YASUEDA, T., NISHIO, S. & MATSUDA, T. 2014. MFG-E8: Origin, Structure, Expression, Functions and Regulation. *In:* WANG, P. (ed.) *MFG-E8 and Inflammation.* Dordrecht: Springer Netherlands.

OSTMAN, S., TAUBE, M. & TELEMO, E. 2005. Tolerosome-induced oral tolerance is MHC dependent. *Immunology,* 116**,** 464-76.

PAN, B. T., TENG, K., WU, C., ADAM, M. & JOHNSTONE, R. M. 1985. Electron microscopic evidence for externalization of the transferrin receptor in vesicular form in sheep reticulocytes. *J Cell Biol,* 101**,** 942-8.

PAPE, K. A., CATRON, D. M., ITANO, A. A. & JENKINS, M. K. 2007. The humoral immune response is initiated in lymph nodes by B cells that acquire soluble antigen directly in the follicles. *Immunity,* 26**,** 491-502.

PARK, C. & KEHRL, J. H. 2019. An integrin/MFG-E8 shuttle loads HIV-1 viral-like particles onto follicular dendritic cells in mouse lymph node. *Elife,* 8.

PARK, H. Y., LIGHT, A., LAHOUD, M. H., CAMINSCHI, I., TARLINTON, D. M. & SHORTMAN, K. 2013. Evolution of B cell responses to Clec9A-targeted antigen. *J Immunol,* 191**,** 4919-25.

PARKIN, J. & COHEN, B. 2001. An overview of the immune system. *Lancet,* 357**,** 1777-89.

PAUTHNER, M., HAVENAR-DAUGHTON, C., SOK, D., NKOLOLA, J. P., BASTIDAS, R., BOOPATHY, A. V., CARNATHAN, D. G., CHANDRASHEKAR, A., CIRELLI, K. M., COTTRELL, C. A., EROSHKIN, A. M., GUENAGA, J., KAUSHIK, K., KULP, D. W., LIU, J., MCCOY, L. E., OOM, A. L., OZOROWSKI, G., POST, K. W., SHARMA, S. K., STEICHEN, J. M., DE TAEYE, S. W., TOKATLIAN, T., TORRENTS DE LA PEÑA, A., BUTERA, S. T., LABRANCHE, C. C., MONTEFIORI, D. C., SILVESTRI, G., WILSON, I. A., IRVINE, D. J., SANDERS, R. W., SCHIEF, W. R., WARD, A. B., WYATT, R. T., BAROUCH, D. H., CROTTY, S. & BURTON, D. R. 2017. Elicitation of Robust Tier 2 Neutralizing Antibody Responses in Nonhuman Primates by HIV Envelope Trimer Immunization Using Optimized Approaches. *Immunity,* 46**,** 1073-1088.e6.

PELED, J. U., KUANG, F. L., IGLESIAS-USSEL, M. D., ROA, S., KALIS, S. L., GOODMAN, M. F. & SCHARFF, M. D. 2008. The biochemistry of somatic hypermutation. *Annu Rev Immunol,* 26**,** 481-511.

PENG, Y. & ELKON, K. B. 2011. Autoimmunity in MFG-E8-deficient mice is associated with altered trafficking and enhanced cross-presentation of apoptotic cell antigens. *J Clin Invest,* 121**,** 2221-41.

PIFFOUX, M., SILVA, A. K. A., WILHELM, C., GAZEAU, F. & TARESTE, D. 2018. Modification of Extracellular Vesicles by Fusion with Liposomes for the Design of Personalized Biogenic Drug Delivery Systems. *ACS Nano,* 12**,** 6830-6842.

POLLARD, A. J. & BIJKER, E. M. 2021. A guide to vaccinology: from basic principles to new developments. *Nature Reviews Immunology,* 21**,** 83-100.

POLLARD, A. J. & HILL, A. V. 2011. Antibody repertoire: embracing diversity. *Sci Transl Med,* 3**,** 93ps32.

POUW, R. B. & RICKLIN, D. 2021. Tipping the balance: intricate roles of the complement system in disease and therapy. *Semin Immunopathol,* 43**,** 757-771.

PULENDRAN, B. & AHMED, R. 2011. Immunological mechanisms of vaccination. *Nat Immunol,* 12**,** 509-17.

PULENDRAN, B., SMITH, J. L., CASPARY, G., BRASEL, K., PETTIT, D., MARASKOVSKY, E. & MALISZEWSKI, C. R. 1999. Distinct dendritic cell subsets differentially regulate the class of immune response in vivo. *Proc Natl Acad Sci U S A,* 96**,** 1036-41.

QAZI, K. R., GEHRMANN, U., DOMANGE JORDÖ, E., KARLSSON, M. C. & GABRIELSSON, S. 2009. Antigen-loaded exosomes alone induce Th1-type memory through a B-cell-dependent mechanism. *Blood,* 113**,** 2673-83.

QI, H., CANNONS, J. L., KLAUSCHEN, F., SCHWARTZBERG, P. L. & GERMAIN, R. N. 2008. SAP-controlled T-B cell interactions underlie germinal centre formation. *Nature,* 455**,** 764-9.

QU, C., NGUYEN, V. A., MERAD, M. & RANDOLPH, G. J. 2009. MHC class I/peptide transfer between dendritic cells overcomes poor cross-presentation by monocyte-derived APCs that engulf dying cells. *J Immunol,* 182**,** 3650-9.

QUAST, I., DVORSCEK, A. R., PATTARONI, C., STEINER, T. M., MCKENZIE, C. I., PITT, C., O'DONNELL, K., DING, Z., HILL, D. L., BRINK, R., ROBINSON, M. J., ZOTOS, D. & TARLINTON, D. M. 2022. Interleukin-21, acting beyond the immunological synapse,

independently controls T follicular helper and germinal center B cells. *Immunity,* 55**,** 1414-1430.e5.

QUEREC, T. D., AKONDY, R. S., LEE, E. K., CAO, W., NAKAYA, H. I., TEUWEN, D., PIRANI, A., GERNERT, K., DENG, J., MARZOLF, B., KENNEDY, K., WU, H., BENNOUNA, S., OLUOCH, H., MILLER, J., VENCIO, R. Z., MULLIGAN, M., ADEREM, A., AHMED, R. & PULENDRAN, B. 2009. Systems biology approach predicts immunogenicity of the yellow fever vaccine in humans. *Nat Immunol,* 10**,** 116-125.

RAPOSO, G., NIJMAN, H. W., STOORVOGEL, W., LIEJENDEKKER, R., HARDING, C. V., MELIEF, C. J. & GEUZE, H. J. 1996. B lymphocytes secrete antigen-presenting vesicles. *J Exp Med,* 183**,** 1161-72.

RAPOSO, G. & STOORVOGEL, W. 2013. Extracellular vesicles: exosomes, microvesicles, and friends. *J Cell Biol,* 200**,** 373-83.

RAUSCH, L., FLASKAMP, L., ASHOKKUMAR, A., TREFZER, A., RIED, C., BUCHHOLZ, V. R., OBST, R., STRAUB, T., BROCKER, T. & KRANICH, J. 2023. Phosphatidylserine-positive extracellular vesicles boost effector CD8(+) T cell responses during viral infection. *Proc Natl Acad Sci U S A,* 120**,** e2210047120.

RAUSCH, L., LUTZ, K., SCHIFFERER, M., WINHEIM, E., GRUBER, R., OESTERHAUS, E. F., RINKE, L., HELLMUTH, J. C., SCHERER, C., MUENCHHOFF, M., MANDEL, C., BERGWELT-BAILDON, M., SIMONS, M., STRAUB, T., KRUG, A. B., KRANICH, J. & BROCKER, T. 2021. Binding of phosphatidylserine-positive microparticles by PBMCs classifies disease severity in COVID-19 patients. *J Extracell Vesicles,* 10**,** e12173.

REED, S. G., ORR, M. T. & FOX, C. B. 2013. Key roles of adjuvants in modern vaccines. *Nat Med,* 19**,** 1597-608.

RIALLAND, P., LANKAR, D., RAPOSO, G., BONNEROT, C. & HUBERT, P. 2006. BCR-bound antigen is targeted to exosomes in human follicular lymphoma B-cells. *Biol Cell,* 98**,** 491-501.

ROBBINS, P. D. & MORELLI, A. E. 2014. Regulation of immune responses by extracellular vesicles. *Nat Rev Immunol,* 14**,** 195-208.

ROBINSON, D. G., DING, Y. & JIANG, L. 2016. Unconventional protein secretion in plants: a critical assessment. *Protoplasma,* 253**,** 31-43.

RODDA, L. B., BANNARD, O., LUDEWIG, B., NAGASAWA, T. & CYSTER, J. G. 2015. Phenotypic and Morphological Properties of Germinal Center Dark Zone Cxcl12-Expressing Reticular Cells. *J Immunol,* 195**,** 4781-91.

ROSSAINT, J., KÜHNE, K., SKUPSKI, J., VAN AKEN, H., LOONEY, M. R., HIDALGO, A. & ZARBOCK, A. 2016. Directed transport of neutrophil-derived extracellular vesicles enables platelet-mediated innate immune response. *Nat Commun,* 7**,** 13464.

SANCHO, D., MOURÃO-SÁ, D., JOFFRE, O. P., SCHULZ, O., ROGERS, N. C., PENNINGTON, D. J., CARLYLE, J. R. & REIS E SOUSA, C. 2008. Tumor therapy in mice via antigen targeting to a novel, DC-restricted C-type lectin. *J Clin Invest,* 118**,** 2098-110.

SARAVIA, J., CHAPMAN, N. M. & CHI, H. 2019. Helper T cell differentiation. *Cell Mol Immunol,* 16**,** 634-643.

SAUNDERSON, S. C., DUNN, A. C., CROCKER, P. R. & MCLELLAN, A. D. 2014. CD169 mediates the capture of exosomes in spleen and lymph node. *Blood,* 123**,** 208-16.

SAUNDERSON, S. C., SCHUBERTH, P. C., DUNN, A. C., MILLER, L., HOCK, B. D., MACKAY, P. A., KOCH, N., JACK, R. W. & MCLELLAN, A. D. 2008. Induction of exosome release in primary B cells stimulated via CD40 and the IL-4 receptor. *J Immunol,* 180**,** 8146-52.

SCHUSSEK, S., BERNASCONI, V., MATTSSON, J., WENZEL, U. A., STRÖMBERG, A., GRIBONIKA, I., SCHÖN, K. & LYCKE, N. Y. 2020. The CTA1-DD adjuvant strongly potentiates follicular

dendritic cell function and germinal center formation, which results in improved neonatal immunization. *Mucosal Immunol,* 13**,** 545-557.

SCHWICKERT, T. A., VICTORA, G. D., FOOKSMAN, D. R., KAMPHORST, A. O., MUGNIER, M. R., GITLIN, A. D., DUSTIN, M. L. & NUSSENZWEIG, M. C. 2011. A dynamic T cell-limited checkpoint regulates affinity-dependent B cell entry into the germinal center. *J Exp Med,* 208**,** 1243-52.

SEGAWA, K., KURATA, S. & NAGATA, S. 2016. Human Type IV P-type ATPases That Work as Plasma Membrane Phospholipid Flippases and Their Regulation by Caspase and Calcium. *J Biol Chem,* 291**,** 762-72.

SEGAWA, K., KURATA, S., YANAGIHASHI, Y., BRUMMELKAMP, T. R., MATSUDA, F. & NAGATA, S. 2014. Caspase-mediated cleavage of phospholipid flippase for apoptotic phosphatidylserine exposure. *Science,* 344**,** 1164-8.

SEGURA, E., GUÉRIN, C., HOGG, N., AMIGORENA, S. & THÉRY, C. 2007. CD8+ dendritic cells use LFA-1 to capture MHC-peptide complexes from exosomes in vivo. *J Immunol,* 179**,** 1489-96.

SEGURA, E., NICCO, C., LOMBARD, B., VERON, P., RAPOSO, G., BATTEUX, F., AMIGORENA, S. & THERY, C. 2005. ICAM-1 on exosomes from mature dendritic cells is critical for efficient naive T-cell priming. *Blood,* 106**,** 216-23.

SHI, J., HEEGAARD, C. W., RASMUSSEN, J. T. & GILBERT, G. E. 2004. Lactadherin binds selectively to membranes containing phosphatidyl-L-serine and increased curvature. *Biochim Biophys Acta,* 1667**,** 82-90.

SHI, J., SHI, Y., WAEHRENS, L. N., RASMUSSEN, J. T., HEEGAARD, C. W. & GILBERT, G. E. 2006. Lactadherin detects early phosphatidylserine exposure on immortalized leukemia cells undergoing programmed cell death. *Cytometry A,* 69**,** 1193-201.

SHIH, T. A., MEFFRE, E., ROEDERER, M. & NUSSENZWEIG, M. C. 2002. Role of BCR affinity in T cell dependent antibody responses in vivo. *Nat Immunol,* 3**,** 570-5.

SHINNAKASU, R., INOUE, T., KOMETANI, K., MORIYAMA, S., ADACHI, Y., NAKAYAMA, M., TAKAHASHI, Y., FUKUYAMA, H., OKADA, T. & KUROSAKI, T. 2016. Regulated selection of germinal-center cells into the memory B cell compartment. *Nat Immunol,* 17**,** 861-9.

SKELTON, D., SATAKE, N. & KOHN, D. B. 2001. The enhanced green fluorescent protein (eGFP) is minimally immunogenic in C57BL/6 mice. *Gene Ther,* 8**,** 1813-4.

SKOKOS, D., BOTROS, H. G., DEMEURE, C., MORIN, J., PERONET, R., BIRKENMEIER, G., BOUDALY, S. & MÉCHERI, S. 2003. Mast cell-derived exosomes induce phenotypic and functional maturation of dendritic cells and elicit specific immune responses in vivo. *J Immunol,* 170**,** 3037-45.

SMITH, D. M., SIMON, J. K. & BAKER, J. R., JR. 2013. Applications of nanotechnology for immunology. *Nat Rev Immunol,* 13**,** 592-605.

SMYTH, L. A., RATNASOTHY, K., TSANG, J. Y., BOARDMAN, D., WARLEY, A., LECHLER, R. & LOMBARDI, G. 2013. CD73 expression on extracellular vesicles derived from CD4+ CD25+ Foxp3+ T cells contributes to their regulatory function. *Eur J Immunol,* 43**,** 2430-40.

SUAN, D., KRÄUTLER, N. J., MAAG, J. L. V., BUTT, D., BOURNE, K., HERMES, J. R., AVERY, D. T., YOUNG, C., STATHAM, A., ELLIOTT, M., DINGER, M. E., BASTEN, A., TANGYE, S. G. & BRINK, R. 2017. CCR6 Defines Memory B Cell Precursors in Mouse and Human Germinal Centers, Revealing Light-Zone Location and Predominant Low Antigen Affinity. *Immunity,* 47**,** 1142-1153.e4.

SUN, D., ZHUANG, X., XIANG, X., LIU, Y., ZHANG, S., LIU, C., BARNES, S., GRIZZLE, W., MILLER, D. & ZHANG, H. G. 2010. A novel nanoparticle drug delivery system: the anti-inflammatory activity of curcumin is enhanced when encapsulated in exosomes. *Mol Ther,* 18**,** 1606-14.

SUN, L., SU, Y., JIAO, A., WANG, X. & ZHANG, B. 2023. T cells in health and disease. *Signal Transduct Target Ther,* 8**,** 235.

SUNDLING, C., LAU, A. W. Y., BOURNE, K., YOUNG, C., LAURIANTO, C., HERMES, J. R., MENZIES, R. J., BUTT, D., KRÄUTLER, N. J., ZAHRA, D., SUAN, D. & BRINK, R. 2021. Positive selection of IgG(+) over IgM(+) B cells in the germinal center reaction. *Immunity,* 54**,** 988-1001.e5.

SUNG, B. H., PARENT, C. A. & WEAVER, A. M. 2021. Extracellular vesicles: Critical players during cell migration. *Dev Cell,* 56**,** 1861-1874.

SUTARIA, D. S., JIANG, J., ELGAMAL, O. A., POMEROY, S. M., BADAWI, M., ZHU, X., PAVLOVICZ, R., AZEVEDO-POULY, A. C. P., CHALMERS, J., LI, C., PHELPS, M. A. & SCHMITTGEN, T. D. 2017. Low active loading of cargo into engineered extracellular vesicles results in inefficient miRNA mimic delivery. *J Extracell Vesicles,* 6**,** 1333882.

SUZUKI, J., DENNING, D. P., IMANISHI, E., HORVITZ, H. R. & NAGATA, S. 2013. Xk-related protein 8 and CED-8 promote phosphatidylserine exposure in apoptotic cells. *Science,* 341**,** 403-6.

SUZUKI, J., IMANISHI, E. & NAGATA, S. 2014. Exposure of phosphatidylserine by Xk-related protein family members during apoptosis. *J Biol Chem,* 289**,** 30257-30267.

TAM, H. H., MELO, M. B., KANG, M., PELET, J. M., RUDA, V. M., FOLEY, M. H., HU, J. K., KUMARI, S., CRAMPTON, J., BALDEON, A. D., SANDERS, R. W., MOORE, J. P., CROTTY, S., LANGER, R., ANDERSON, D. G., CHAKRABORTY, A. K. & IRVINE, D. J. 2016. Sustained antigen availability during germinal center initiation enhances antibody responses to vaccination. *Proc Natl Acad Sci U S A,* 113**,** E6639-E6648.

TANG, C., BAGNARA, D., CHIORAZZI, N., SCHARFF, M. D. & MACCARTHY, T. 2020a. AID Overlapping and Polη Hotspots Are Key Features of Evolutionary Variation Within the Human Antibody Heavy Chain (IGHV) Genes. *Front Immunol,* 11**,** 788.

TANG, R., XU, J., ZHANG, B., LIU, J., LIANG, C., HUA, J., MENG, Q., YU, X. & SHI, S. 2020b. Ferroptosis, necroptosis, and pyroptosis in anticancer immunity. *J Hematol Oncol,* 13**,** 110.

TAS, J. M., MESIN, L., PASQUAL, G., TARG, S., JACOBSEN, J. T., MANO, Y. M., CHEN, C. S., WEILL, J. C., REYNAUD, C. A., BROWNE, E. P., MEYER-HERMANN, M. & VICTORA, G. D. 2016. Visualizing antibody affinity maturation in germinal centers. *Science,* 351**,** 1048-54.

TAS, J. M. J., KOO, J. H., LIN, Y. C., XIE, Z., STEICHEN, J. M., JACKSON, A. M., HAUSER, B. M., WANG, X., COTTRELL, C. A., TORRES, J. L., WARNER, J. E., KIRSCH, K. H., WELDON, S. R., GROSCHEL, B., NOGAL, B., OZOROWSKI, G., BANGARU, S., PHELPS, N., ADACHI, Y., ESKANDARZADEH, S., KUBITZ, M., BURTON, D. R., LINGWOOD, D., SCHMIDT, A. G., NAIR, U., WARD, A. B., SCHIEF, W. R. & BATISTA, F. D. 2022. Antibodies from primary humoral responses modulate the recruitment of naive B cells during secondary responses. *Immunity,* 55**,** 1856-1871 e6.

THÉRY, C., DUBAN, L., SEGURA, E., VÉRON, P., LANTZ, O. & AMIGORENA, S. 2002. Indirect activation of naïve CD4+ T cells by dendritic cell-derived exosomes. *Nat Immunol,* 3**,** 1156-62.

TIAN, Y., LI, S., SONG, J., JI, T., ZHU, M., ANDERSON, G. J., WEI, J. & NIE, G. 2014. A doxorubicin delivery platform using engineered natural membrane vesicle exosomes for targeted tumor therapy. *Biomaterials,* 35**,** 2383-90.

TIGHE, H., TAKABAYASHI, K., SCHWARTZ, D., MARSDEN, R., BECK, L., CORBEIL, J., RICHMAN, D. D., EIDEN, J. J., JR., SPIEGELBERG, H. L. & RAZ, E. 2000a. Conjugation of protein to immunostimulatory DNA results in a rapid, long-lasting and potent induction of cell-mediated and humoral immunity. *Eur J Immunol,* 30**,** 1939-47.

TIGHE, H., TAKABAYASHI, K., SCHWARTZ, D., VAN NEST, G., TUCK, S., EIDEN, J. J., KAGEY-SOBOTKA, A., CRETICOS, P. S., LICHTENSTEIN, L. M., SPIEGELBERG, H. L. & RAZ, E. 2000b. Conjugation of immunostimulatory DNA to the short ragweed allergen amb a 1 enhances its immunogenicity and reduces its allergenicity. *J Allergy Clin Immunol,* 106**,** 124-34.

TIMÁR, C. I., LORINCZ, A. M., CSÉPÁNYI-KÖMI, R., VÁLYI-NAGY, A., NAGY, G., BUZÁS, E. I., IVÁNYI, Z., KITTEL, A., POWELL, D. W., MCLEISH, K. R. & LIGETI, E. 2013. Antibacterial effect of microvesicles released from human neutrophilic granulocytes. *Blood,* 121**,** 510-8.

TOKATLIAN, T., READ, B. J., JONES, C. A., KULP, D. W., MENIS, S., CHANG, J. Y. H., STEICHEN, J. M., KUMARI, S., ALLEN, J. D., DANE, E. L., LIGUORI, A., SANGESLAND, M., LINGWOOD, D., CRISPIN, M., SCHIEF, W. R. & IRVINE, D. J. 2019. Innate immune recognition of glycans targets HIV nanoparticle immunogens to germinal centers. *Science,* 363**,** 649-654.

TORRALBA, D., BAIXAULI, F., VILLARROYA-BELTRI, C., FERNÁNDEZ-DELGADO, I., LATORRE-PELLICER, A., ACÍN-PÉREZ, R., MARTÍN-CÓFRECES, N. B., JASO-TAMAME Á, L., IBORRA, S., JORGE, I., GONZÁLEZ-ASEGUINOLAZA, G., GARAUDE, J., VICENTE-MANZANARES, M., ENRÍQUEZ, J. A., MITTELBRUNN, M. & SÁNCHEZ-MADRID, F. 2018. Priming of dendritic cells by DNA-containing extracellular vesicles from activated T cells through antigen-driven contacts. *Nat Commun,* 9**,** 2658.

TRAJKOVIC, K., HSU, C., CHIANTIA, S., RAJENDRAN, L., WENZEL, D., WIELAND, F., SCHWILLE, P., BRÜGGER, B. & SIMONS, M. 2008. Ceramide triggers budding of exosome vesicles into multivesicular endosomes. *Science,* 319**,** 1244-7.

TRAUTZ, B., WIEDEMANN, H., LÜCHTENBORG, C., PIERINI, V., KRANICH, J., GLASS, B., KRÄUSSLICH, H. G., BROCKER, T., PIZZATO, M., RUGGIERI, A., BRÜGGER, B. & FACKLER, O. T. 2017. The host-cell restriction factor SERINC5 restricts HIV-1 infectivity without altering the lipid composition and organization of viral particles. *J Biol Chem,* 292**,** 13702-13713.

TRICARICO, C., CLANCY, J. & D'SOUZA-SCHOREY, C. 2017. Biology and biogenesis of shed microvesicles. *Small GTPases,* 8**,** 220-232.

VAN NIEL, G., D'ANGELO, G. & RAPOSO, G. 2018. Shedding light on the cell biology of extracellular vesicles. *Nat Rev Mol Cell Biol,* 19**,** 213-228.

VIANT, C., WEYMAR, G. H. J., ESCOLANO, A., CHEN, S., HARTWEGER, H., CIPOLLA, M., GAZUMYAN, A. & NUSSENZWEIG, M. C. 2020a. Antibody Affinity Shapes the Choice between Memory and Germinal Center B Cell Fates. *Cell,* 183**,** 1298-1311 e11.

VIANT, C., WEYMAR, G. H. J., ESCOLANO, A., CHEN, S., HARTWEGER, H., CIPOLLA, M., GAZUMYAN, A. & NUSSENZWEIG, M. C. 2020b. Antibody Affinity Shapes the Choice between Memory and Germinal Center B Cell Fates. *Cell,* 183**,** 1298-1311.e11.

VICTORA, G. D. & NUSSENZWEIG, M. C. 2012. Germinal centers. *Annu Rev Immunol,* 30**,** 429-57.

VICTORA, G. D. & NUSSENZWEIG, M. C. 2022. Germinal Centers. *Annu Rev Immunol,* 40**,** 413-442.

VINUESA, C. G., LINTERMAN, M. A., YU, D. & MACLENNAN, I. C. 2016. Follicular Helper T Cells. *Annu Rev Immunol,* 34**,** 335-68.

VOLCKMAR, J., GEREKE, M., EBENSEN, T., RIESE, P., PHILIPSEN, L., LIENENKLAUS, S., WOHLLEBER, D., KLOPFLEISCH, R., STEGEMANN-KONISZEWSKI, S., MÜLLER, A. J., GRUBER, A. D., KNOLLE, P., GUZMAN, C. A. & BRUDER, D. 2017. Targeted antigen delivery to dendritic cells elicits robust antiviral T cell-mediated immunity in the liver. *Sci Rep,* 7**,** 43985.

WAKIM, L. M. & BEVAN, M. J. 2011. Cross-dressed dendritic cells drive memory CD8+ T-cell activation after viral infection. *Nature,* 471**,** 629-32.

WANG, H. B. & WELLER, P. F. 2008. Pivotal advance: eosinophils mediate early alum adjuvant-elicited B cell priming and IgM production. *J Leukoc Biol,* 83**,** 817-21.

WANG, Q., YU, J., KADUNGURE, T., BEYENE, J., ZHANG, H. & LU, Q. 2018. ARMMs as a versatile platform for intracellular delivery of macromolecules. *Nat Commun,* 9**,** 960.

WANG, X., RODDA, L. B., BANNARD, O. & CYSTER, J. G. 2014. Integrin-mediated interactions between B cells and follicular dendritic cells influence germinal center B cell fitness. *J Immunol,* 192**,** 4601-9.

WATANABE, T., TOTSUKA, R., MIYATANI, S., KURATA, S., SATO, S., KATOH, I., KOBAYASHI, S. & IKAWA, Y. 2005. Production of the long and short forms of MFG-E8 by epidermal keratinocytes. *Cell Tissue Res,* 321**,** 185-93.

WEINSTEIN, J. S., HERMAN, E. I., LAINEZ, B., LICONA-LIMÓN, P., ESPLUGUES, E., FLAVELL, R. & CRAFT, J. 2016. TFH cells progressively differentiate to regulate the germinal center response. *Nature Immunology,* 17**,** 1197-1205.

WESSELS, M. R., BUTKO, P., MA, M., WARREN, H. B., LAGE, A. L. & CARROLL, M. C. 1995. Studies of group B streptococcal infection in mice deficient in complement component C3 or C4 demonstrate an essential role for complement in both innate and acquired immunity. *Proc Natl Acad Sci U S A,* 92**,** 11490-4.

WILEY, S. R., RAMAN, V. S., DESBIEN, A., BAILOR, H. R., BHARDWAJ, R., SHAKRI, A. R., REED, S. G., CHITNIS, C. E. & CARTER, D. 2011. Targeting TLRs expands the antibody repertoire in response to a malaria vaccine. *Sci Transl Med,* 3**,** 93ra69.

WITMER-PACK, M. D., SWIGGARD, W. J., MIRZA, A., INABA, K. & STEINMAN, R. M. 1995. Tissue distribution of the DEC-205 protein that is detected by the monoclonal antibody NLDC-145. II. Expression in situ in lymphoid and nonlymphoid tissues. *Cell Immunol,* 163**,** 157-62.

WONG, R., BELK, J. A., GOVERO, J., UHRLAUB, J. L., REINARTZ, D., ZHAO, H., ERRICO, J. M., D'SOUZA, L., RIPPERGER, T. J., NIKOLICH-ZUGICH, J., SHLOMCHIK, M. J., SATPATHY, A. T., FREMONT, D. H., DIAMOND, M. S. & BHATTACHARYA, D. 2020. Affinity-Restricted Memory B Cells Dominate Recall Responses to Heterologous Flaviviruses. *Immunity,* 53**,** 1078-1094.e7.

XU, Z., ZAN, H., PONE, E. J., MAI, T. & CASALI, P. 2012. Immunoglobulin class-switch DNA recombination: induction, targeting and beyond. *Nat Rev Immunol,* 12**,** 517-31.

YAARI, G. & KLEINSTEIN, S. H. 2015. Practical guidelines for B-cell receptor repertoire sequencing analysis. *Genome Med,* 7**,** 121.

YAARI, G., UDUMAN, M. & KLEINSTEIN, S. H. 2012. Quantifying selection in high-throughput Immunoglobulin sequencing data sets. *Nucleic Acids Res,* 40**,** e134.

YANG, Z., ROBINSON, M. J., CHEN, X., SMITH, G. A., TAUNTON, J., LIU, W. & ALLEN, C. D. 2016. Regulation of B cell fate by chronic activity of the IgE B cell receptor. *Elife,* 5.

YANG, Z., SULLIVAN, B. M. & ALLEN, C. D. 2012. Fluorescent in vivo detection reveals that IgE(+) B cells are restrained by an intrinsic cell fate predisposition. *Immunity,* 36**,** 857-72.

YATES, A. G., PINK, R. C., ERDBRUGGER, U., SILJANDER, P. R., DELLAR, E. R., PANTAZI, P., AKBAR, N., COOKE, W. R., VATISH, M., DIAS-NETO, E., ANTHONY, D. C. & COUCH, Y. 2022a. In sickness and in health: The functional role of extracellular vesicles in physiology and pathology in vivo: Part I: Health and Normal Physiology: Part I: Health and Normal Physiology. *J Extracell Vesicles,* 11**,** e12151.

YATES, A. G., PINK, R. C., ERDBRUGGER, U., SILJANDER, P. R., DELLAR, E. R., PANTAZI, P., AKBAR, N., COOKE, W. R., VATISH, M., DIAS-NETO, E., ANTHONY, D. C. & COUCH, Y. 2022b. In sickness and in health: The functional role of extracellular vesicles in physiology and pathology in vivo: Part II: Pathology: Part II: Pathology. *J Extracell Vesicles,* 11**,** e12190.

ZHANG, Y., GARCIA-IBANEZ, L., ULBRICHT, C., LOK, L. S. C., PIKE, J. A., MUELLER-WINKLER, J., DENNISON, T. W., FERDINAND, J. R., BURNETT, C. J. M., YAM-PUC, J. C., ZHANG, L., ALFARO, R. M., TAKAHAMA, Y., OHIGASHI, I., BROWN, G., KUROSAKI, T., TYBULEWICZ, V. L. J., ROT, A., HAUSER, A. E., CLATWORTHY, M. R. & TOELLNER, K. M. 2022. Recycling of memory B cells between germinal center and lymph node subcapsular sinus supports affinity maturation to antigenic drift. *Nat Commun,* 13**,** 2460.

ZHANG, Y., TECH, L., GEORGE, L. A., ACS, A., DURRETT, R. E., HESS, H., WALKER, L. S. K., TARLINTON, D. M., FLETCHER, A. L., HAUSER, A. E. & TOELLNER, K. M. 2018. Plasma cell output from germinal centers is regulated by signals from Tfh and stromal cells. *J Exp Med,* 215**,** 1227-1243.

ZHAO, T., CAI, Y., JIANG, Y., HE, X., WEI, Y., YU, Y. & TIAN, X. 2023. Vaccine adjuvants: mechanisms and platforms. *Signal Transduct Target Ther,* 8**,** 283.

ZHOU, J., TAGAYA, Y., TOLOUEI-SEMNANI, R., SCHLOM, J. & SABZEVARI, H. 2005. Physiological relevance of antigen presentasome (APS), an acquired MHC/costimulatory complex, in the sustained activation of CD4+ T cells in the absence of APCs. *Blood,* 105**,** 3238-46.

ZITVOGEL, L., REGNAULT, A., LOZIER, A., WOLFERS, J., FLAMENT, C., TENZA, D., RICCIARDI-CASTAGNOLI, P., RAPOSO, G. & AMIGORENA, S. 1998. Eradication of established murine tumors using a novel cell-free vaccine: dendritic cell-derived exosomes. *Nat Med,* 4**,** 594-600.

10. Acknowledgements

Doing a PhD is a long and difficult journey, now the finishing line is just around the corner, it's time to review the journey, to give it a comment and also to myself. Looking back my five-year experience in Munich, I have grown, learnt new knowledge, become more confident and more determined. For me, the meaning of doing a PhD is not just exploring the unknown field of science, it's also a self-questioning process, to reveal what I really want and most importantly, to be honest to the true heart.

During this journey, there are many great people who had supported me and helped me overcome the difficulties. Soon it will be the time to say goodbye, there are so many things to remember and so many words to say. In the end of the thesis, I would like to squeeze my great thanks and gratitude to these people in this small text.

First of all, I would like to thank my supervisor Prof. Dr. Thomas Brocker for giving me the opportunity and abundant funding to complete my project, and also the precise scientific suggestions that helped me work in the correct direction and make progresses. Additionally, I would like to thank him for his liberal that give me flexible of time and space to make mistakes, to learn and to explore what I am interested and curious about.

Then I would like to thank my second supervisor PD. Dr. Jan Kranich, who had meticulously planned this project and always responsive to my questions and helped me go through the difficulties I met during the PhD. Besides, I really appreciate his character and not being a "stereotype PI". He has a very young but interesting soul, and he is willing to be friends with students. He is the person that you can discuss serious scientific question in the last minute, but joke around in the next minute. Although due to the huge culture difference, I am still not completely adapted to making jokes with my supervisor, but thanks to him, my PhD journey is much less stressful. After completion of this thesis, I would like to thank him again for patiently correcting my grammar and spelling mistakes in almost every sentence, I hope he still has the courage and willing to take foreign students.

Next, I would like to thank Mrs. Christine Ried for organizing everything in order. She is the real Doraemon in the lab and I could always get what I need from her. She is also the one who has taught me the most experimental skills, and helped me finish those long and big experiments. I would also thank her for her efficiency that always helped me order and pick up reagents immediately, although her effort was sometimes ruined by DHL and strikes in public transportations. Besides, I would thank her for the cookies and cakes she prepared for birthdays and other events. She is so versatile that every time in the party, her dishes were always my first target.

After that, I would like to thank Dr. Eva Sofía Sánchez Quant, Dr. Yujuan Gui and Dr. Lisa Richter for helping me establish the sequencing protocol and giving me really useful guidance on data analysis. I would also thank Tijana Kandic, Christine Ried, Beatrice Rauter and Dr. Pallavi Pranita for spending days and nights to produce the Mfge8-EGFP that I have used a lot in this project. Additionally, I would like to thank the SFB 1054 coordinator Dr. Elizabeth Schroeder Reiter, she is always responsible and considerate, she talks to student regularly, get to known what stage we are and what difficulties we have, she provided me with very useful suggestions, reading material and workshops that not only helped me finish the PhD, but also good for the future career.

Last but not least, I would like to thank my family and friends Sergio Gómez, Pallavi Kadam, Elaine Wong, Dr. Timsse Raj and Batuhan Akcabozan for giving me support, sharing useful information and exploring the city and restaurants with me. Besides, I would like to thank my colleagues and the CPM (Core Facility Party Management) members: Lavinia Flaskamp, Monica Prechtl, Franziska Prummer and Annkathrin Scheck, who managed different type of theme parties. From them, I felt the vibrant lives, the infinite passion and hope for the future. They gave more color to my PhD journey, and I wish all of them have bright future and happy life!